NOTE TO USERS

Performance of Patch-Repair of Corroded Concrete Deck Slabs

Mohammad Saifuzzaman

December 2004

Department of Civil Engineering and Applied Mechanics
McGill University
Montreal, Canada

A thesis submitted to the
Faculty of Graduate Studies and Research
in partial fulfilment of the requirements for the degree of
Master of Engineering

Your file Votre référence
ISBN: 0-494-12643-4
Our file Notre référence
ISBN: 0-494-12643-4

Abstract

Durability of reinforced concrete infrastructure is severely affected by corrosion of reinforcing steel. Conventional patch repair techniques are unable to stop this corrosion due to electrochemical incompatibility between the "repaired" concrete and the original "chloride-infested" concrete. This research was undertaken to compare the performance of different patch repair strategies of corroded concrete bridge deck slabs, proposed by different industrial partners, with respect to the conventional patch repair.

The results show that the potential difference between the "repaired-patch" concrete and the "existing" concrete accelerates local corrosion around the patch, and gradually progresses towards the repaired zone. Beneficial effect of sacrificial anodes and corrosion inhibitors in a KCl and a NaCl environment, are evaluated at the beginning of the repair, however, their effectiveness decreases with time. Corrosion penetration rate obtained from Tafel Test, overestimated the actual rebar mass loss, indicating the need for more research in this area.

It is recommended that for new construction, concrete must have low diffusivity to avoid premature deterioration, and for repair, electrochemical protection systems such as cathodic protection, embedded sacrificial anode, corrosion inhibitor, and chloride extraction should be considered to increase the service life of the repaired system. Surface coatings such as zinc, epoxy, sealer or membrane can be used as additional line of defence. In addition, the existing cracks must be treated, and the bridge deck drainage system and expansion joints must be designed properly to avoid ingress of chloride-contaminated water into the concrete.

The results of this study can be potentially quite useful for the concrete repair industry as well as for future research to mitigate corrosion.

Résumé

La durabilité de l'infrastructure de béton armé est sévèrement affectée par la corrosion de l'acier d'armature. La technique conventionnelle de réparation des nids-de-poule n'est pas capable d'arrêter cette corrosion à cause de l'incompatibilité électrochimique entre le béton « réparé » et le béton original infesté par les chlorures. Cette recherche a été réalisée afin de comparer avec la méthode conventionnelle, la performance des différentes stratégies des réparations des nids-de-poule des tabliers des ponts en béton armé corrodés. Ces stratégies ont été proposées par les partenaires de l'industrie.

Les résultats montrent que la différence de potentiel entre le béton armé « réparé » des nids-de-poule et le béton armé existant, accélérait la corrosion locale aux alentours des nids-de-poule et qu'elle avancée graduellement vers la zone réparée. Les effets bénéfiques de l'anode sacrificielle et des inhibiteurs dans deux environnement: l'un de KCl et l'autre de NaCl, ont été évalués au début de la « réparation ». Le taux de pénétration de la corrosion obtenu avec le test Tafel surestime la perte de masse de la barre. Ceci nous indique le besoin de recherche additionnelle dans ce domaine.

On recommande que pour les nouvelles constructions le béton ait une faible diffusivité afin d'éviter sa détérioration prématurée. En ce qui a trait à la « réparation » pour allonger la vie en service de celle-ci, on doit considérer un système de protection électrochimique tel que la protection cathodique, l'anode sacrificielle encastré, les inhibiteurs de la corrosion et l'extraction des chlorures. Le recouvrement de la surface avec le zinc, l'époxy: scellant ou membrane peut être utilisé comme une ligne de défense additionnelle. De plus les fissures existantes devraient être traitées. Le système de drainage du tablier et les joints d'expansion devraient être conçus de manière appropriée afin d'empêcher l'entrée d'eau contaminée par les chlorures, dans le béton.

Les résultats de cette étude s'avèrent potentiellement utiles aussi bien pour l'industrie de la réparation du béton que pour la recherche qui vise le traitement de la corrosion.

Acknowledgements

This work has been carried out at the Department of Civil Engineering and Applied Mechanics at McGill University in Montreal, Canada. I wish to express my deepest gratitude to my excellent teacher and project supervisor, Professor M. Saeed Mirza, for his valuable suggestions, constant encouragement and continuous support through the research program and in the development of this thesis.

I would like to express my gratefulness to Mr. Paul Jeffs, President, PJ Materials Consultants Ltd., Mr. Ron Grieve, Tekron Services Inc., and Mr. Nourredine Kadoum, President, CPI Corrosion Ltd. for their collaboration and technical support to this project.

Considerable assistance was provided by the staff of the Department of Civil Engineering and Applied Mechanics and School of Architecture to finish the experimental program smoothly. I would like to thank to all of the staff, especially Mr. Ron Sheppard and Mr. Marek Przykorski for their on-going assistance.

I also extend my thanks to all of my friends for their continuous support during the experiment, especially to Mr. R. Humberto Pizarro-C for his contribution in translating the Abstract in French.

Finally, I would like to thank my mother, wife and our son for their love, support and patience during my research program.

Table of Contents

List of Figures

List of Tables

Chapter 1
Introduction

1.1 Background

Infrastructure is an umbrella of all public works. It creates the foundation for a healthy economy and a high standard of living. It ensures modern day conveniences and supports a climate favorable to jobs and employment growth. Highways, roads, bridges, airports, and mass transit systems anchor our economy and lifestyle. Water supply systems, wastewater treatment plants and sewer systems secure public health. But with each traffic jam, airport delay, water main break, or sewer overflow decreases the quality of life of citizens. Therefore, appropriate timely measures should be taken to ensure that the infrastructure is safe and serviceable for modern day life.

The cost of Canada's infrastructure is estimated between three and five trillion dollars and because of lack of funding and related political decisions leading to deferred maintenance, the current infrastructure deficit is well over $100 billion (Amleh, 2000). It is frightening that if the present deterioration and degradation is not halted and if the appropriate repair and upgrading programs are not undertaken now or in the near future, this estimate of $100 billion could easily increase to $200 to $300 billion over next five to ten years, and to well over $500 to $600 billion in the next twenty years (Mirza, 1998). It is noted that the condition of infrastructure has a direct impact on Canada's productivity, international competitiveness, and socio-economic developments. Therefore, it should be ensured that Canada continues to be a better country to live in, and that Canadian politicians, engineers and taxpayers assume the responsibility to mitigate this crisis successfully.

The major components of infrastructure are highway or roadway bridges. In Canada, approximately 80,000 of bridges link different highways and roadways (Leyne, 2004). According to McGill-FCM (Federation of Canadian Municipalities) survey (1996), the

rehabilitation needs for the bridges in Canada is about $0.7 billion annually. According to the US Department of Transportation, 230,000 out of more than 580,000 bridges, i.e. about 40% of the bridges are structurally deficient or functionally obsolete, and 25% are more than 50 years old, while 5% are more than 80 years old. According to the Report Card for America's Infrastructure released by the ASCE (2003), the overall grading of bridges in USA is "C"; no change of train has been observed from 2001 to 2003. Reinforced concrete is the primary construction material for these bridges, and followed by steel. Corrosion problems associated with these bridges particularly located in the cold climate region, or in the marine environment, are the major cause of deterioration.

Reinforced concrete, a combination of concrete and steel, is a relatively inexpensive composite material that is widely used in the construction industry. It is one of the oldest building materials, and was invented by Joseph Monier in 1849. Traditionally, it was considered to be a life-long durable manmade rock. But time has revealed the limitation of man's creation, which is manifested in the widespread corrosion of reinforcing steel (Leyne, 2004). Corrosion of reinforced concrete was first recognized early in the twentieth century, but it has become worse in recent decades with extensive use of de-icing salts on the highways and bridge decks (Amleh, 2000). According to the result of a five-year scientific study released by Environment Canada, the National Environmental Protection Agency, in a typical year, approximately 5 million tonnes of road salt are applied in Canada for de-icing, anti-icing and dust suppression.

Naturally, concrete provides an oxidized protective (passive) layer on the reinforcing steel during hydration. If it can be ensured that this impervious, dense, protective layer is maintained on the entire surface of the reinforcement, there is no danger of corrosion taking place. However, when salt (chloride ions) or carbon dioxide penetrate the concrete and reach the steel bar, this protective layer breaks and corrosion commences. Corrosion increases the volume of the iron in the steel bar up to ten times of its original volume due to the formation of hydrate oxides (Heckroodt, 2002). This expansion of steel results in development of 35 MPa (5000 psi) pressure on the encasing concrete (Amleh, 2000), which

causes cracking and spalling of the concrete cover and exposes the rebar to initiate further corrosion. Thus, corrosion progressively increases the deterioration without showing any major sign of distress, gradually reduces the cross section of the rebar, and decreases the ductility of the reinforced concrete structure.

Most of the deterioration in concrete bridge decks, parking garage slabs and marine structures has been caused by chloride-induced corrosion. This deterioration is influenced by several factors: environmental severity, unsuitable materials, inadequate construction practices and specifications, and in some cases improper design. Concrete cover acts as a primary barrier to retard the aggressive agents, e.g., chloride ions, carbon dioxide, etc. from reaching the steel bars, thereby delaying the corrosion process. Considerable research has been undertaken to study the corrosion mechanism and to reduce / stop the corrosion of reinforcing steel in concrete, as a result of the development of low permeability high performance concrete and different corrosion protection techniques (e.g., cathodic protection) but very little research has been addressed the reduction or stopping of corrosion in reinforced concrete structures, which are suffering from corrosion. An alarming number of repaired and rehabilitated concrete structures have suffered from significant corrosion deterioration earlier than their expected service life, in some cases only a few year after the original repairs (Emmons and Vaysburd, 2003). Repeated repair and rehabilitation costs of some structures have already exceeded their original construction costs. Yet the annual expenditure for repair and rehabilitation of concrete structures has exceeded 50% of the total construction costs (Beaudoin et al., 1997). Therefore, research should be undertaken to develop a scientific approach of long lasting repair techniques to upgrade the deteriorated structures in a safe and serviceable condition up to their targeted service lives.

1.2 Research Significance

A study on the influence of chloride-free new concrete on the chloride-contaminated surrounding concrete is very important for understanding how this incompatibility develops further the corrosion around the patch, and also inside the patch. Development of scientific

correlation between the electrochemical incompatibility of old and new concrete and the corrosion of reinforcing steel in concrete needs urgent attention.

Different kinds of corrosion protection systems such as sacrificial anode, discrete anode and impressed current cathodic protection systems, coatings, and treatments are commercially available. Few companies have undertaken some research programs for their own interest to market their products with specifications and application procedures. But most of the treatments are developed to provide an additional corrosion protection to the new concrete from different aggressive agents and very few techniques are available for restoring the existing corroded concrete structures. Some research has been performed at different universities and organizations to develop some sustainable patch repair techniques. However, there are no scientific guidelines available for long-lasting patch repair of corroded concrete deck slab or structure. Therefore, focused research is needed to develop durable patch repair techniques and to stop the corrosion of steel in a deteriorated concrete structure from the aggressive environment, otherwise it would continue to deteriorate in an accelerated manner, and it may not be possible to repair the structure, which may have to be replaced at a much higher cost.

Most of the design and construction industry is more interested in replacing corrosion-damaged structures rather than restoring it, because of the smaller effort to design a new structure using the familiar design codes. Occasionally, they recommend to the owners to replace the structure because they can provide a guarantee for the service life of their newly designed structures. However, when time comes for designing a repair and rehabilitation projects, they are unable to handle it scientifically, besides being uncertain about the project service life. No scientific design methodology or design code is available for designing the patch repair of corrosion-damaged concrete deck slab, or structure. Therefore, it is urgent to continue this research to establish a sustainable patch repair technique for corroded concrete deck slab and to enhance the safety and serviceability of the transportation system.

1.3 Summary of Related Research

This section covers the summary of related topics that have been published in different literature, journals, books or web. Significant numbers of papers are found on nondestructive test for corrosion monitoring, numerical model of corrosion mechanism, corrosion protection of steel in concrete for new construction, etc. but very few papers exist on detailed corrosion protection guideline for repairing of existing corroded reinforced concrete structure. Special attention is given here to highlight the research associated with chloride-induced corrosion mechanism, electrochemical incompatibility between existing chloride-contaminated concrete and new chloride-free repair concrete.

Cleland, Long, and Yeoh (1997) at Queen's University of Belfast addressed corrosion of reinforcing steel in concrete repair. They identified that the patch repairs consist of three zones: (1) the repaired area, (2) the unrepaired adjacent area, and (3) the interface between these two areas. The interface between the repaired and unrepaired zone is noted as the critical zone, and the chloride-contaminated concrete adjacent to the repaired zone can actually promote the corrosion. The objective of the project was to compare the performance of five repair mortars. Each reinforced concrete slab consisted of a patch at the middle that was filled with certain repair mortar, and selected slabs had a coating on the exposed steel. Only one layer of 10 mm diameter steel bars was used, which is not realistically comparable to the field condition; however, it is an excellent preliminary study to investigate the effectiveness and compatibility of the patch repairs.

Similar experiments were performed by Beaudette (2001) to repair test slabs with embedded sacrificial galvanic anodes. Three type of 610 mm long and 305 mm wide and 60 mm thick slabs were cast in two halves: the first half was chloride-contaminated with 3% salt solution (by weight of cement) and the other half was uncontaminated concrete, thus creating a situation for patch accelerated corrosion. Three 10M bar were placed longitudinally at a depth of 36 mm from the bottom @ 76 mm center to center. A sacrificial galvanic anode was placed in the uncontaminated concrete part along its interior edge between the two bars. First type of slab was cast with a galvanic anode, second type was

cast with a presoaked galvanic anode, and third the type was cast without any anode. Corrosion potential measurement showed that the potential difference associated with patch-accelerated corrosion was reduced, or eliminated by the presence of sacrificial anode. The measurement of corroded areas of steel bars embedded into the test slabs showed that the galvanic anode can reduce up to 85% of corrosion compared with the bars which were not protected. In addition to the area of corrosion being reduced, severity of corrosion had been minimized to the point where nearly no pitting could be found on the protected bars. Based on the surface area results, it took seven times longer for a bar in a patch protected with a galvanic anode to reach the same degree of corrosion as an unprotected bar. In practice, patches are surrounded by the contaminated concrete but in this experiment contaminated and uncontaminated concretes are placed side by side for simplicity, which deviates from the field condition; however, it is a very effective example of patch repair technique. Nonetheless, more research needed to develop different kind of patch repair technique with specific guidelines.

El Maaddawy and Soudki (2003), at the University of Waterloo, investigated the effectiveness of accelerated corrosion technique and impressed current technique to simulate corrosion accurately and realistically. A summary of the important details of some of the previous accelerated corrosion tests involving applied current, current density, cathode type, and corrosion environment (i.e. percentage of the salt solution and immersion conditions) was presented in the report. Specifically, the effect of variable impressed current density was examined. It was discovered that at relatively high degree of corrosion, increasing the current density resulted in significant increases in the concrete strain measurements. It was suggested that this was due to some diffusion of corrosion products in the short corrosion time, resulting in a higher concentration of corrosion products around the steel rebars causing a higher strain. Finally, it was concluded that varying the current density level to get different degrees of corrosion might have other effects, which might mislead the interpretation of the test results. Therefore, the implications of such a phenomenon need to be examined in more detail.

Law and Cairns (2003) of Heriot-Watt University, and Millard and Bungey (2003) of Liverpool University evaluated the corrosion loss of steel reinforcing bars in concrete using linear polarization resistance (LPR) measurements. In this experiment, the actual and predicted weight loss data for a number of mild steel bars contained in Ordinary Portland Cement (OPC) concrete, subjected to three different environment regimes, were monitored using potentiostaticaly controlled linear polarization resistance measurements. The three sets of reinforced concrete specimens were subjected to (a) chloride-induced corrosion, (b) carbonation-induced corrosion, and (c) a control environment with no corrosion. Each set of specimens was exposed to a daily regime of wetting and drying in a controlled environment for 1700 days. Two sets of tests were conducted at around 1200 days and 1700 days. Prior to casting, the mild steel bars were cleaned and weighed individually. The mass loss for each bar due to corrosion was recorded at the end of the period of exposure. Instantaneous corrosion measurements by linear polarization resistance technique were taken on each bar at regular intervals for the duration of the exposure time. These resistance measurements were then integrated to evaluate a predicted mass loss of the steel rebars. The conclusions of these experiments are:

1. The corrosion rates for chloride exposure and carbonation exposure specimens show a distinct variation. Chloride exposure specimens display a significantly higher maximum corrosion rate and higher degree of scatter in the results.
2. The LPR corrosion rate measurements can used to predict the mass of steel lost when either chloride or carbonation-induced corrosion is occurring.
3. The predicted mass-loss of steel from LPR measurements gives an overestimate of the mass-loss of steel determined from weighing of the actual specimens.
4. The mean ratio of LPR mass-loss with actual mass-loss for all specimens is 2.1:1, which corresponds to a mean overestimate of 110% for the total mass of steel lost.
5. The mean overestimate for chloride-exposed specimens was 204%, and it was 56% for carbonated specimens.
6. The results indicate that the external environment may influence the accuracy of the LPR measurements.

7. Environmental effects on corrosion rate can be considered by increasing the number of LPR measurements.

These informative observations can be helpful for future research, and can also be helpful to predict mass-loss of reinforcing steel due to corrosion.

But one question, which needs to be considered by the researchers, is how accurately these laboratory tests results reflect the "real" world conditions. Li (2000) from the University of Dundee, sums up this concern that "Current research in chloride-induced reinforcing steel corrosion, both analytical and experimental, is focussed on the corrosion process (initiation and propagation) without service loads, not under natural salt spray and simultaneous service loads, or not on full-size structural members. This does not represent the real world of chloride-affected reinforced concrete in service". Therefore, a model or tool needs to be developed to bridge between the laboratory results and the actual field conditions.

Daniel of Transport Québec (1997) checked the performance of corrosion inhibitors to reduce / stop the corrosion of steel in concrete. Different kinds of chemical additives (corrosion inhibitors) were used according to their specified guidelines. Following the ASTM G 109-92: "Test Method for Determining the Effect of Chemical Admixtures on the Corrosion of Embedded Steel Reinforcement and Concrete Exposed to Chloride Environments", corrosion current density, polarization resistance, and corrosion rate were measured. Based on the analysis of the results, it was recommended that use of corrosion inhibitors does not prevent corrosion, but retards the corrosion process. The tests that were performed do not allow to estimate the increase in service life attributable to the use of inhibitors. All of the additives have random side effects on parameters, such as curing time, air content, and development of resistance. Finally it was concluded that the High Performance Concrete (HPC) proved to be the most efficient for preventing corrosion in steel.

A complete report on protection for steel corrosion is available in "Steel Corrosion in Concrete" by Bentur, Berke, and Diamond (1997), which includes details of high-performance concretes, corrosion inhibitors, surface sealers and membranes, coatings of reinforcing bars, and electrochemical protection. These protection systems are described mostly for application on new construction. Malhotra et al. (2000) concentrated on testing the effectiveness of incorporating fly ash (or silica fume and blast furnace slag) into a cement mix as a means of reducing the permeability of the concrete and thus reducing corrosion. Other researchers, such as Erdogdu, Bremner and Kondratova (2001), have questioned the effectiveness of epoxy coatings of steel rebars (Leyne, 2004).

1.4 Previous Related Research at McGill University

Palumbo (1991), and Farah (1993) experimented with two detailed investigations, dealing with the development of accelerated electrochemical corrosion of reinforced concrete. A test set-up and a detailed procedure for accelerated corrosion testing using lollipop specimens were developed. Complete corrosion period of most specimens did not exceed 45 days. The effects of concrete cover thickness, deformed steel bars with and without an epoxy coating, and the effectiveness of the surface sealants were studied.

Palumbo (1991) summarized that:

1. Operating potential values of reinforced concrete versus a saturated calomel reference electrode (SCE) lower than zero millivolt may indicate the potential for corrosion activity.
2. An electrical current reading of three milliampere and above signifies corrosion activity at the level of the reinforcing steel.
3. A minimum [concrete] cover of 38 mm over the reinforcing steel should be specified to ensure that the concrete would offer the corrosion protection in the design requirements. Furthermore, for concrete exposed to severe chloride attack, a minimum clear cover thickness of 51 mm is recommended.
4. An increased concrete cover thickness is no substitute for poor quality concrete cover.

Farah (1993) also reviewed that:

1. The negative operating potential values versus a saturated calomel reference electrode (SCE) indicate a sign of corrosion.
2. A current value of four milliamperes and above signifies corrosion activity at the level of reinforcing steel. Higher value of current flow indicates an advanced stage of corrosion.
3. The minimum [concrete] clear cover depth required to protect the steel from corrosion attack in normal steel is 37 mm.
4. The concrete surface sealing penetrates the concrete and fills its pores forming a protective layer that prevents the embedded steel from chloride ingress.
5. Application of the sealant on the specimens after it started to corrode is a good solution to stop the progression of the corrosion attack.
6. A minimum [concrete] cover of 27 mm is recommended for the specimens with seal protection to ensure that the service life of the structure is prolonged.
7. A higher quality concrete cover is more effective in the protection of the steel reinforcement than a more permeable concrete cover of greater thickness.

Fazio (1996) investigated on the flexural behavior of reinforced concrete beams subjected to an accelerated corrosion regime. The beams were tested with different levels of corrosion. The report concluded that:

1. The flexural capacity of the simply supported beams subjected to two third point loads is slightly reduced with the progress of the corrosion process. The crack development is modified at later corrosion stages.
2. The stress distribution is concentrated in the vicinity of the center of the beam.
3. The number of cracks decreases, but the crack widths increase with an increasing level of corrosion. The strain in the concrete and steel is also decreased along the length of the beam.
4. The performance at the steel-concrete interface changes and the formation of primary and internal cracks is influenced.

5. The chloride ion content of the concrete increases with time and tends to reach a saturation point. The presence of cracks increases the diffusion of the free chloride ions permitting the ions to travel faster along the cracks instead of the concrete pores.

Amleh (1996) examined the influence of corrosion of reinforcing bars on bond between steel and concrete. The bond strength was studied through both transverse and longitudinal splitting cracks. Relative bond effectiveness of a corroded 20M deformed bar embedded at the center of a 1000 mm by 100 mm diameter cylindrical concrete specimen, was determined from the crack spacing. Different stages of the steel reinforcement corrosion were established to study their relative bond behavior, ranging from no corrosion at all to complete corrosion at the steel-concrete interface. The findings of this experiment were:

1. The bond strength decreases rapidly with an increase in the corrosion level, especially in the case of any severe localized corrosion. It has been found that the first level of corrosion, which is 4% weight loss due to corrosion, resulted in a 9% decrease of the nominal bond stress, while the sixth level of corrosion with a 17.5% weight loss (the case of severe localized corrosion) due to corrosion, resulted in a 92% loss of the nominal bond stress.
2. The bond behavior is influenced by the deterioration of the reinforcing bar ribs, and by the reduced adhesion and cohesion of the reinforcing bar due to the widening of the longitudinal splitting crack resulting from corrosion.

Amleh (2000) further studied the bond deterioration of reinforcing steel in concrete due to corrosion. The basic objective of this research was to study the influence of increasing levels of corrosion on the progressive deterioration of bond between the steel bars and the concrete, and to determine the extent to which the water / cementitious material ratio influence the corrosion of the reinforcement as a function of the chloride ion penetration phenomenon. The outcome of this research was:

1. The development of a standardized accelerated electrochemical corrosion testing procedure with the objective of "completely" corroding the bar in a period of 15-20 weeks.
2. The high volume of fly ash is very effective in delaying the corrosion process as compared to that of the normal Portland cement.
3. The bond performance of the steel bars embedded in the normal Portland cement concrete mixtures with a low water-cement ratio, e.g., 0.32 in this investigation, was found to be superior than that with concrete mixture with larger water-cement ratios.

McGill has a wide range of research experience in the field of corrosion of reinforcing steel in concrete. Only few of them are summarized above. Presently, the research team is concentrated on the developing of sustainable patch repair techniques for corroded concrete deck slab, along with the development of tools for design for durability against corrosion of steel rebars embedded in concrete.

1.5 Scopes and Objectives of the Present Research Program

Dickson Bridge in Montreal was constructed in 1959. The bridge was 366m long and 27m wide. A 150mm thick reinforced concrete deck was supported over reinforced concrete girder with spans of 12 to 18m, except for the central three spans over the CN rail tracks, where the deck was supported on steel plate girders. Because of the influence of severe environmental conditions, poor materials and construction quality, the bridge was abandoned after a service life of 35 years Amleh (2000). After several different electrochemical, chemical, physical and mechanical investigations, it was decided by the City of Montreal to demolish the bridge. Before the bridge was demolished, McGill University along with some industrial partners approached the City to let them use the bridge for research purposes. Consequently, a collaborative research project was undertaken to assess the corrosion-induced damage in the concrete deck and to identify the causes of the deterioration.

Part of the investigations was to determine in detail why the bridge deteriorated so rapidly. Amleh (2000) reported that one of the possible causes of deterioration of the bridge deck was the loss of bond resistance at the steel-concrete interface due to excessive corrosion of steel reinforcement. Different laboratory tests were performed to determine the loss of bond using the samples made with the same concrete mixture used for the Dickson Bridge. Different mechanisms of rebar corrosion were also examined in the field and relationships were established between the laboratory and field results.

Continuation of this research, another project was initiated between McGill University, PJ Consultants, and CPI Corrosion. The project was implemented in two phases, which were performed individually by Leyne (2004) and the author, respectively. The major objectives of this program are:

1. To study the corrosion process in different kind of repaired reinforced concrete slabs in the laboratory, test slabs were constructed to model the deterioration of the demolished Dickson Bridge
2. To examine the electrochemical compatibility between the repaired new concrete and the unrepaired "old" concrete for different restoration techniques
3. To determine the effectiveness of different surface coating to reduce the chloride ingress into the concrete
4. To establish the relationship between different type of repair techniques and the ongoing corrosion activity using half-cell potential monitoring
5. To establish visual records of the extracted bars of different slabs repaired by different strategies by digital photography
6. To calculate average mass loss of each bar and compare the results with different strategies of repair.

At the beginning of the research program, it was decided to repair the selected segments of the original bridge deck using different repair techniques before its demolition and to investigate the performance of the repair. However, the City did not agree to postpone the

demolition of the bridge for political reasons. Consequently, the research team decided to continue the investigation in the laboratory. Accordingly, fifteen bridge deck specimens were specially designed and constructed using the concrete mixture, which had been used for the deck of the Dickson Bridge. The specimens were exposed to a unique corrosive environment, subjected to different repair strategies, and monitored in accordance with the outlined objectives of the research program.

1.6 Outline of the Report

The report is divided into six chapters as follows:

Chapter One – Introduction, addresses the goals of the research program, highlighting the reinforcement corrosion problems in concrete bridges. A summary of the related research is also described in this chapter.

Chapter Two – Corrosion of Steel in Concrete, provides a brief description of corrosion of steel in new and repaired concrete, and it includes a discussion of the different corrosion mechanisms, theory of electrochemical thermodynamics and kinetics of corrosion, different factors influencing corrosion, and mechanism of macrocell formation.

Chapter Three – Manifestation and Restoration of Corrosion Damaged Reinforced Concrete Structure, illustrates the manifestation of reinforcement corrosion, concrete deterioration diagnostic table, condition surveys of the reinforcement corrosion, and finally different strategies of reinforced concrete structures.

Chapter Four – Experimental Methodology, describes the detailed experimental methodology of the project, which covers overview of the experiment, specimen geometry, material properties, test procedures of the two phases including exposure description, patch repair procedures, and different techniques of corrosion activity monitoring.

Chapter Five – Results and Discussion, presents the calculation procedures, data interpretation and presentation, and observation and discussion of the different test results found from different corrosion monitoring tests, such as the half-cell potential measurement, chloride content determination, mass loss measurement, and corrosion penetration rate measurement. This chapter also explains any possible grounding effects and the age effects of the electrolyte on the half-cell readings or not.

Chapter Six – Conclusions and Recommendations, summarizes all of the results, observations, and discussions of the results found from the experimental program, and also presents recommendations for future researches.

Appendix–A presents the monthly average half-cell potential vs. time results for each of the slab, Appendix–B presents the visual records of all bottom bars for each slab, Appendix–C presents the visual records of all top bars for each slab, and Appendix–D presents mass loss chart for all top mesh bars of the fifteen slabs.

Chapter 2
Corrosion of Steel in Concrete

2.1 Introduction

Corrosion is defined as the spontaneous destruction of substance such as metals and mineral building materials by surrounding media, which are usually moisture, oxygen, carbon dioxide, chloride ions (saline-water or / and deicing-salt), etc. Generally, it begins at the surface of the material and then spread into the interior, is caused by chemical and electrochemical reactions.

The natural source of iron is ores, mostly in the form of iron oxide. To extract iron from its ore involves considerable amount of heat energy. According to thermodynamics, iron has a tendency to back to its original oxidized form and release this energy. Therefore, corrosion can be defined to explain this destructive process.

2.2 Corrosion of Steel in New Concrete

When cement is being hydrated, or more to be exact, when calcium silicate is being hydrated, calcium hydroxide [$Ca(OH)_2$] is formed. This calcium hydroxide is partly dissolved in the water within the pore [supersaturated $Ca(OH)_2$ solution], and partly participated in the form of calcium hydroxide crystals, which are embedded within the hydrated cement. This is the reason why most concretes have a pH value in excess of 12, therefore, they are strongly basic. In such a basic environment steel is made passive, i.e., it is protected from corrosion by means of an impervious protective layer of iron oxides. If it can be ensured that this impervious, dense, protective layer is maintained on the entire surface of the reinforcement, then there is no danger of corrosion taking place.

However, if the environment inside the concrete is changed, the protective layer can deteriorate and corrosion process can get initiated. The protective layer is unstable at pH

lower than 11.5 (Richardson, 2002), due to carbonation or leaching, which lowers pH. Sources of chloride ions are seawater, or use of deicing salts on road surface in winter, certain types of aggregates (especially from desert climates) and $CaCl_2$ used earlier as an accelerator (Lindvall, 2001). Therefore, two major phenomenon concerns with the corrosion of steel in concrete, one is carbonation and other is chloride ingress into the concrete, which are stated below in brief.

2.2.1 Corrosion Mechanism in Carbonated Concrete

Carbonation is a process when carbon dioxide from the air reacts with calcium hydroxide, $Ca(OH)_2$. Carbonation occurs when carbon dioxide dissolves in the pore solution of cement paste, producing carbonate ions, CO_3^{2-}, which reacts with calcium hydroxide, $Ca(OH)_2$, to produce calcium carbonate, $CaCO_3$. The carbonation process is described by the following simplified equations (Möller, 1994 and Lindvall, 2001):

$$CO_2 + Ca(OH)_2 \leftrightarrow CaCO_3 + H_2O$$

The basic reaction between carbonate ions and calcium ions in the pore solution, can be described by the following equation:

$$Ca^{2+} + HCO_3^- + OH^- \leftrightarrow CaCO_3 + H_2O$$

The dissolution of carbon dioxide, CO_2, in the pore solution is described by the following equation:

$$CO_2 + H_2O \rightarrow 2H^+ + CO_3^{2-}$$

Furthermore the carbonate ions react with other positive ions, e.g. alkali ions. These reactions are described in the following chemical equations:

$$Na^+ + HCO_3^- \leftrightarrow NaHCO_3$$

$$K^+ + HCO_3^- \leftrightarrow KHCO_3$$

Thus the carbonation has an important influence in changing pH of the concrete from about 13-14 to a value of about 9. When all the $Ca(OH)_2$ has become carbonated pH is reduced to 8.3 (Neville, 1995). Furthermore, carbonation changes the moisture conditions in the concrete, due to a decreasing sorptivity (Dias, 2000).

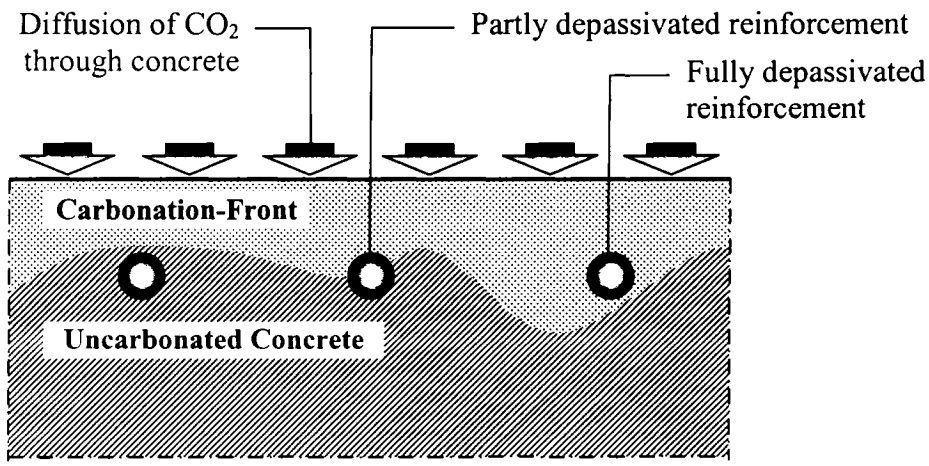

Figure 2.1: Progress of Carbonation-Front to the Reinforcement
(Adopted: Richardson, 2001)

During the carbonation process, carbon dioxide reacts first with the concrete at the surface. Then it passes the carbonated zone and reacts with the next layer of non-carbonated concrete. This gives a carbonation-front (Figure 2.1), which penetrates gradually into the concrete, lowering its pH. The penetration depth associated with this decrease in pH is called carbonation depth. When the carbonation front reaches the reinforcement, and H_2O and O_2 are available to create favorable condition, corrosion initiates.

If the passive film breaks down, iron oxidizes to form ferrous ions (Fe^{2+}) with the following half-cell reaction:

$$Fe_2 \rightarrow Fe^{2+} + 4e^- \qquad \text{[Anodic reaction]}$$

The ferrous ions pass into the pore solution and the electrons flow through the conducting reinforcement to the cathode where they are adsorbed by the electrolyte. The cathodic reaction produces hydroxyl ions (OH^-), in the presence of oxygen and moisture, as follows:

$$2H_2O + O_2 + 4e^- \rightarrow 4OH^- \quad \text{[Cathodic reaction]}$$

The hydroxyl ions move from the cathodic site through the moist concrete, the electrolyte, towards the anodic site where ferrous hydroxide [$Fe(OH)_2$] is formed. The anodic reactions can be represented as follows:

$$2Fe^{2+} + 4OH^- \rightarrow 2Fe(OH)_2$$

The ferrous hydroxide is unstable in the presence of oxygen and therefore the reaction may proceeds to form rust (Figure 2.2) according to the following equations:

$$Fe(OH)_2 + H_2O + \tfrac{1}{2}O_2 \rightarrow 2Fe(OH)_3 \quad \text{[Formation of ferric hydroxide]}$$

$$Fe(OH)_3 \rightarrow Fe_2O_3.H_2O + H_2O \quad \text{[Formation of rust]}$$

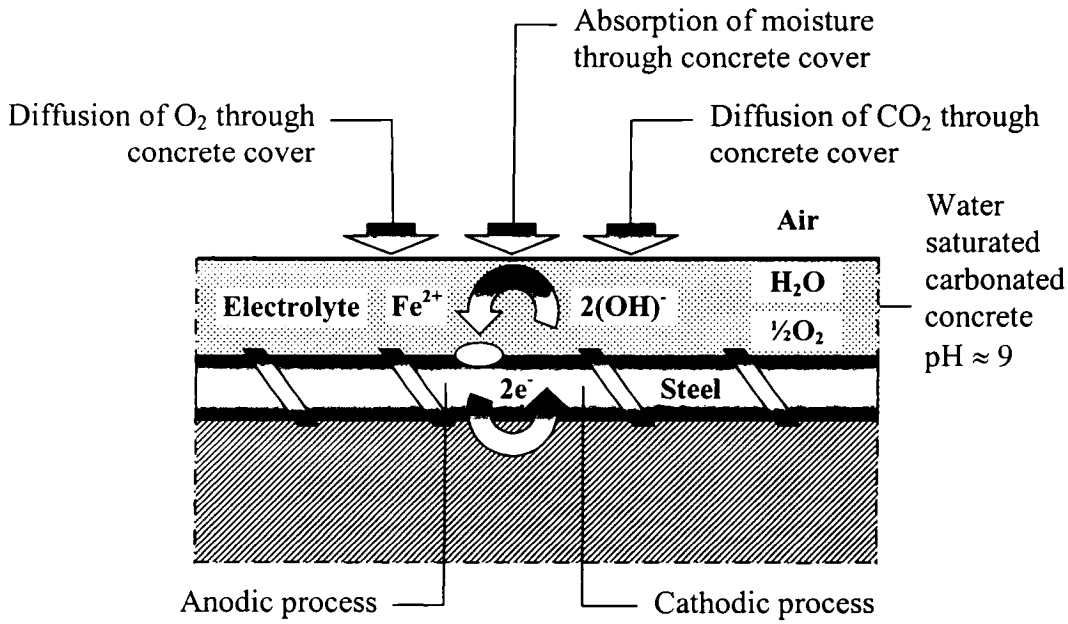

Figure 2.2: Simplified Model of Corrosion of Reinforcement in Concrete due to Carbonation
(Adopted: CEB, 1992)

Further advances of the carbonation front increase the "depassivated" area. Widespread corrosion may then follow with the development of cracking along the lines of the reinforcement.

2.2.2 Corrosion Mechanism in Chloride-Rich Concrete

Corrosion of reinforcement due to chloride ions is the most significant threat to the reinforced concrete infrastructure exposed to chloride-rich environment. Chloride-induced corrosion is generally focused on a small area, which forms a pit surrounded by "uncorroded" reinforcement. The process is illustrated in Figure 2.3. This can lead to rapid loss of cross-section and critically reduce the load bearing capacity of the reinforced concrete member, besides decreasing its ductility significantly. Chloride penetration into concrete is governed by a number of chemical and physical processes, such as ion diffusion, capillary suction and convection.

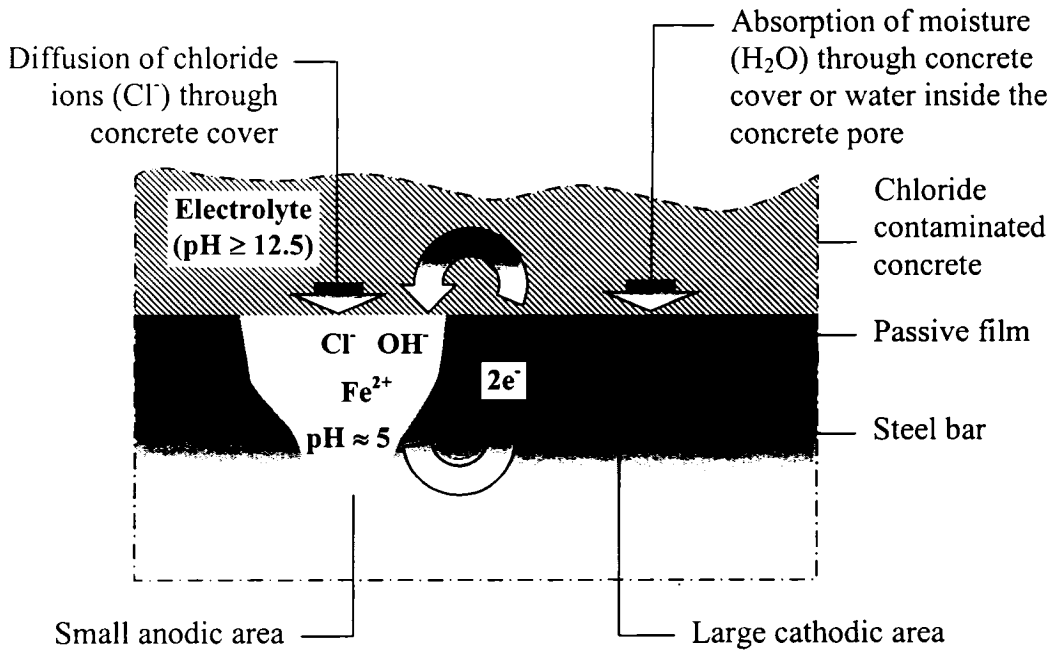

Figure 2.3: Simplified Model of Pitting Corrosion of Reinforcement in Concrete due to Chloride Ions
(Adopted: CEB, 1992)

Corrosion is related to the flow of electrons. An element or compound that loses electrons is said to be oxidised and one that gains electrons is said to be reduced. When metal oxides are formed the metal atoms lose outer electrons. The metal atoms are oxidised and the

oxygen is reduced. In concrete subjected to high chloride levels, the process first involves the oxidation of iron to ferrous ions (Fe^{2+}):

$$2Fe \rightarrow 2\ Fe^{2+} + 4e^{-}$$

If chloride ions are present, they trigger and accelerate the dissoultion of the passive layer on the steel. The chloride-attack starts at the weak spots of the metal surface, where the pH is low or where some defect in the concrete or steel is present. In these weak spots, anodes are formed, which attract chloride ions and pitting corrosion start. The cation combines with chloride ions to form chloride or oxichloride compounds ($FeCl_2$ and FeOCl), for example:

$$2Fe^{2+} + 4Cl^{-} \rightarrow 2FeCl_2$$

The process then becomes self propagating, due to creation of anodic conditions and the recycling of chloride ions. This occurs through the hydrolysis of the chloride compounds, for example:

$$2FeCl_2 + 4H_2O \rightarrow 2Fe(OH)_2 + 4HCl$$

Alternatively,

$$2FeCl_2 + 4H_2O \rightarrow 2Fe(OH)_2 + 4H^{+} + 4Cl^{-}$$

and,

$$2FeOCl + 2H_2O \rightarrow 2Fe(OH)_2 + 2Cl^{-}$$

Consequently, recycling of the liberated chloride ions accelerate the corrosion process. Corrosion product consists of hydrogen chloride, hydrogen (H^{+}), or hydronium ions (H_3O^{+}), which creates an acidic environment. The increased acidity also encourages further oxidation of the iron.

As mentioned earlier, a division is made in general corrosion (carbonation induced) and pitting corrosion (chloride induced). In general corrosion the steel surfaces of the rebars are corroded uniformly, with approximately the same loss of thickness at the areas of the anode and the cathode. In pitting corrosion, corrosion takes place in pit, where chloride ions penetrate the passive oxidized layer. The pitting corrosion has large cathodic areas and a very small anodic area (the pit). The corrosion rate in pitting corrosion can be significantly

higher compared to the corrosion rate in general corrosion, and thus in pitting corrosion the rebars can be rapidly corroded. Furthermore, pitting corrosion may not give signs of an on going corrosion process, such as cracking and spalling, since the process is concentrated in a very small area and the corrosion products are soluble in the local acid pit.

2.2.3 Electrochemical Thermodynamics of Corrosion

The corrosion phenomenon depends on the ability of electrons to transfer across the interface between the metal and the electrolyte, and vice versa. This parameter is described as the 'driving force', or the 'electrode potential' of a particular metal in a particular electrolyte. Thus, in reinforce concrete, the process is driven by the potential difference between the reinforcement and the cover concrete. The potential difference develops at the interface of the reinforcement and the concrete because of the tendency of the metal ions to dissolve and the difference in the environment (metal and concrete) on either side of the surface. An excess of positive charge builds up near the interface.

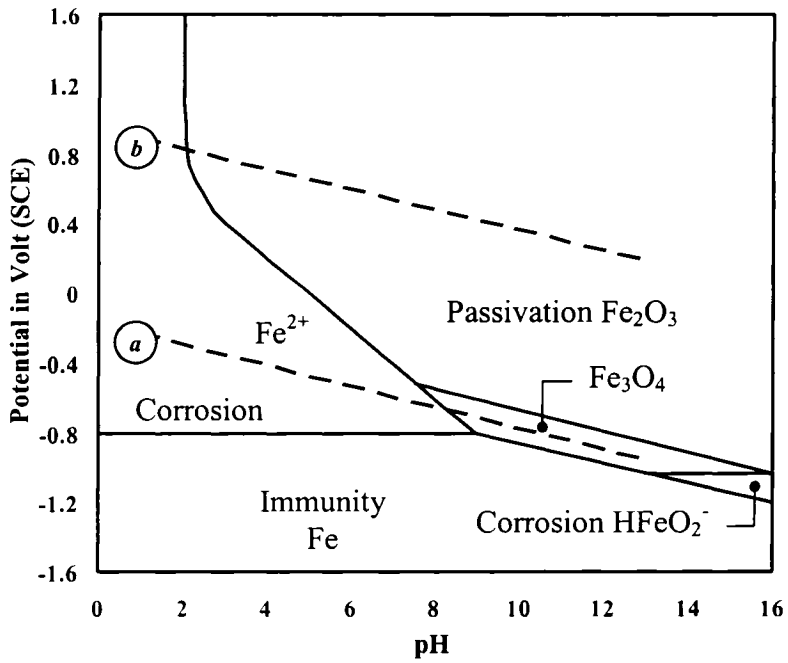

Figure 2.4: Potential vs. pH Diagram (Stability of Iron and Iron Oxide)
(Pourbaix, 1966)

The potential cannot be measured directly and therefore, it measured with respect to a reference electrode. Electrical potentials are measured in the field on the existing structure by a half-cell potential measurement device. Normally, reference electrodes are saturated hydrogen electrode (SHE), saturated calomel electrode (SCE) and saturated silver / silver chloride electrode (SSE).

The driving force in corrosion is the potential as shown in Figure 2.4, where a potential vs. pH diagram for stability of iron and iron oxides in water at +25°C is presented. Pourbaix (1966) developed this diagram to describe corrosion thermodynamically. In Figure 2.4, the potential in a given environment represents the balance between the cathodic reactions, the anodic reactions and any external current. The line "a" and "b" denotes the equilibrium potential for hydrogen evaluation and oxygen reduction.

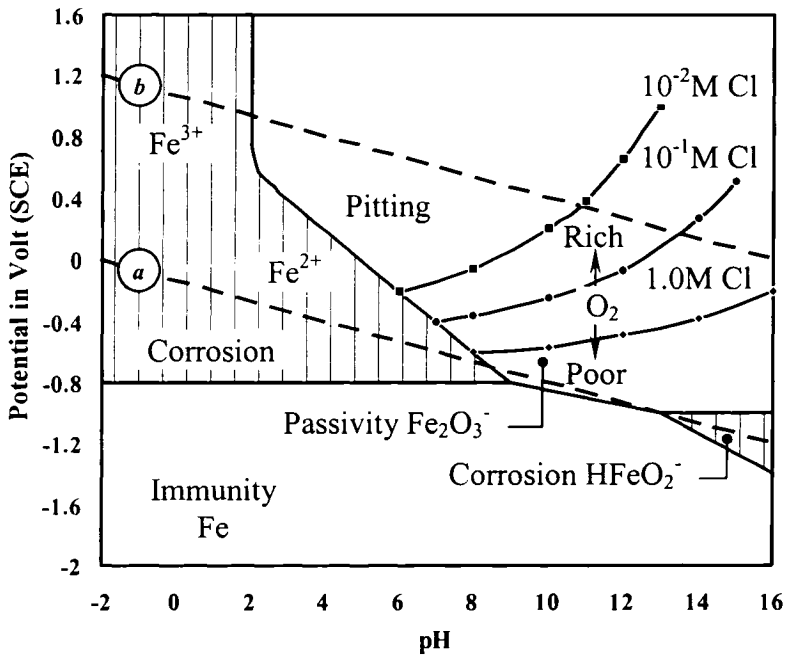

Figure 2.5: Potential vs. pH diagram for Black Steel in Aqueous Solution
(Sandberg, 1998 and Lindvall, 2001)

Sandberg (1998) modified Pourbaix diagram to represent general corrosion and pitting corrosion together (Figure 2.5). If the pH is above about 11.5 and no chlorides are present, the oxide is deposited as a thin protective film, which keeps the corrosion rate so low that it can be considered to be insignificant. This protective film is termed the "passive layer" and is primarily a dense oxide, but it also contains components from the cement paste and the pore water. When the "passive layer" is present, the reinforcement is said to be in a passive condition. Furthermore, the corrosion rate is to a large extent a function of the moisture conditions within the concrete (Lindvall, 2001).

Scully (1990) highlights two limitations of using "Pourbaix diagram" for prediction of corrosion behavior. The first limitation is that the diagrams are derived from known reactions between pure metals and pure water. In reality, water responsible for corrosion often consists of dissolved salts and impurities exists in metals, both of which result in additional reactions not presented in the diagram. The second limitation is that the Pourbaix diagram is based on thermodynamic data and takes no consideration of kinetics of the reactions.

2.2.4 Electrochemical Kinetics of Corrosion

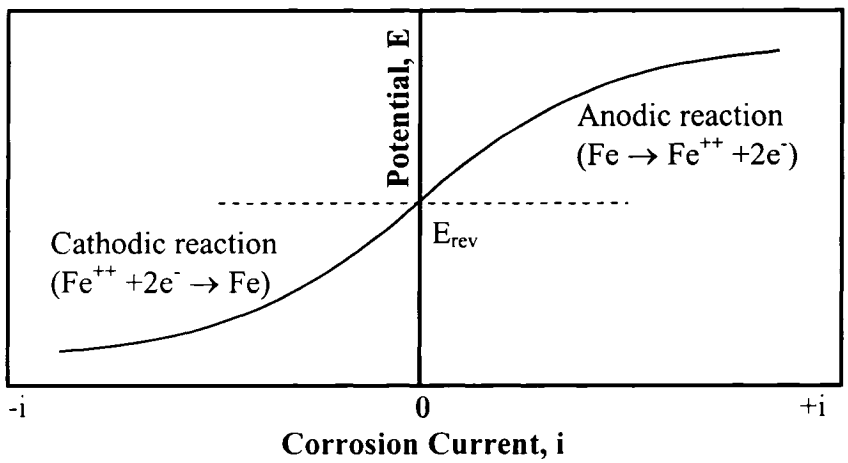

Figure 2.6: Polarization Curve Showing the Reversible Potential
(Richardson, 2001)

All thermodynamic information fails to provide rate of corrosion, the most significant parameter for the engineers. Bentur et al. (1997) demonstrated the Evans' Diagrams to explain the corrosion rate of steel in concrete by considering 'polarization curves'.

These curves graph the relationship between electrical potential and corrosion current. A polarization curve may be generated by experimenting with two electrodes. A potential difference is applied between the two electrodes and the current flow is monitored. The anodic and cathodic potentials are different in values and opposite in signs but there exists a common potential at which the reactions are balanced. This balanced potential is termed as 'reversible potential', E_{rev}. The more polarized the potentials from the reversible potential, the higher is the corrosion current observed (Figure 2.6).

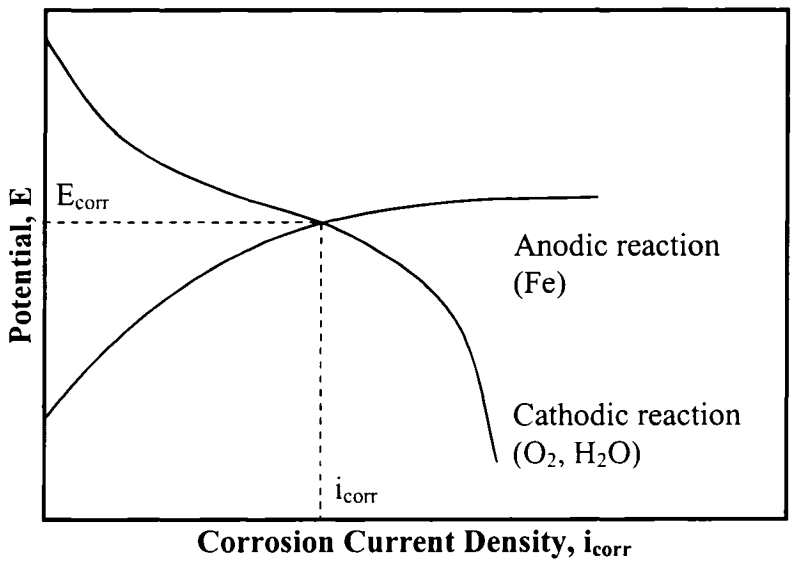

Figure 2.7: Evans' Diagram Showing Corrosion Potential and Corrosion Current Density Adopted by Corroding Metal
(Richardson, 2001)

A common electrode potential is generated between the steel and concrete which is intermediate between the individual anodic and cathodic systems. The corrosion process occurs at the potential where the rates of anodic and cathodic reaction are equal. It is very

informative, therefore, the relationship of potential and current is plotted in a manner that shows where equilibrium of current occurs. This is achieved by plotting curves on a common axis that is ignoring the sign of the current. Such a plot is known as Evans' Diagram. The potential at which the metal corrodes is determined by the point of intersection of the curves (Figure 2.7). It is the value of electrode potential detectable when the metal is corroding freely. The corresponding current may also be assessed. Thus the potential (E_{corr}) and the corresponding corrosion current (i_{corr}) may be determined by considering the kinetics of the anodic and cathodic reactions in a given situation to calculate the corrosion rate.

2.2.5 Factors Influencing Corrosion

Corrosion activity is influenced by several factors including oxygen supply, relative humidity, temperature, crack width, concrete cover thickness, etc., which are summarized briefly in the following sections –

2.2.5.1 Availability of Oxygen

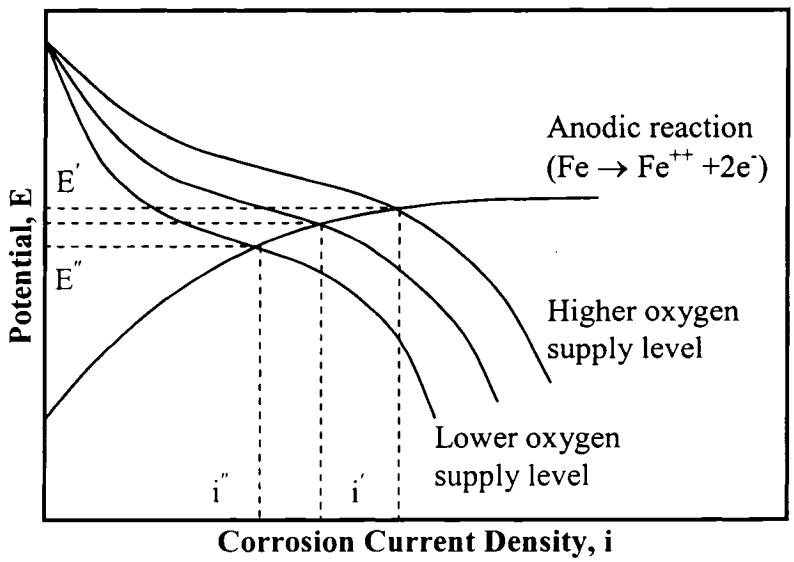

Figure 2.8: Evans' Diagram Showing the Influence of Oxygen Supply in Concrete on Steel Corrosion
(Richardson, 2001)

The passive film may be broken down through carbonation or chloride ingress. The rate of corrosion will then depend on the rate at which oxygen may penetrate the cover. This is illustrated in Figure 2.8. The oxygen supply to the reinforcement is a function of permeability of the cover. Good quality concrete with low permeability can resist oxygen supply. Equally, a condition in which the concrete is saturated may not lead to corrosion even in permeable concretes. This is due to the restriction of oxygen ingress because gaseous diffusion is very slow through the saturated pores and therefore, there may be little dissolved oxygen in the water. Figure 2.8 noted that the cathodic reaction curve becomes steeper as the oxygen supply diminishes leading to a reduced corrosion current as expected.

2.2.5.2 Availability of Chloride Ions

As mentioned earlier, the chloride ions are the governing factor to produce pitting corrosion of steel in concrete. Chloride ions may be present in concrete during manufacturing or they may penetrate into the concrete from some external source. Specific source of chloride ions include accelerating admixtures that contain calcium chloride, salt-contaminated aggregates, seawater, and most importantly deliberately applied deicing salts (Fazio, 1999).

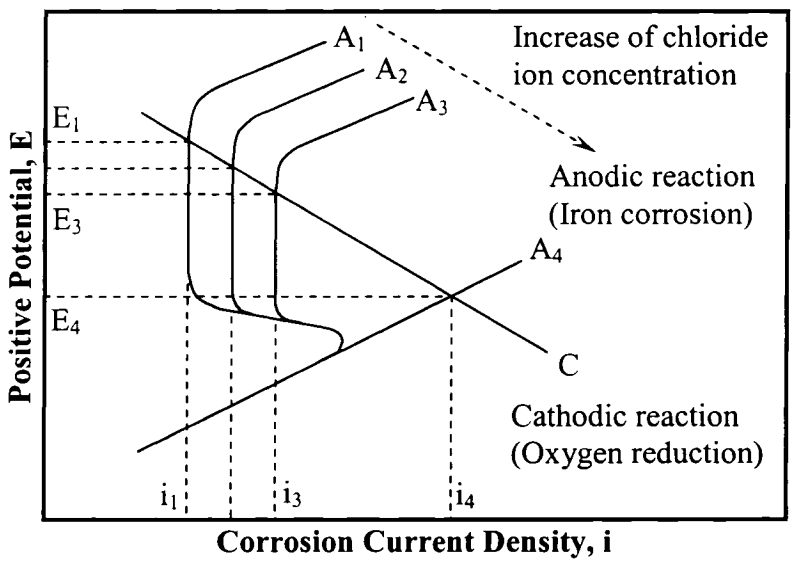

Figure 2.9: Evans' Diagram Showing the Effect of Chloride Ions in Concrete on Steel Corrosion
(Beaudoin et al, 1997)

It is clear from Figure 2.9 that as chloride concentration increases, the positive potential decreases and the corrosion current density increases dramatically, resulting in a large increase in corrosion penetration at the specific depassivated region of the steel bar.

2.2.5.3 Influence of Relative Humidity

A corrosion cell cannot occur if the concrete is too dry to serve as an electrolyte or too wet to allow ingress of oxygen. Sufficiently dry conditions are typical inside the buildings and corrosion does not occur due to the lower probability of reinforcement depassivation through carbonation. Corrosion activity is most vigorous at relative humidity values above 80% as illustrated in Figure 2.10, using data from Andrade et al. (1986) and Parrott (1994).

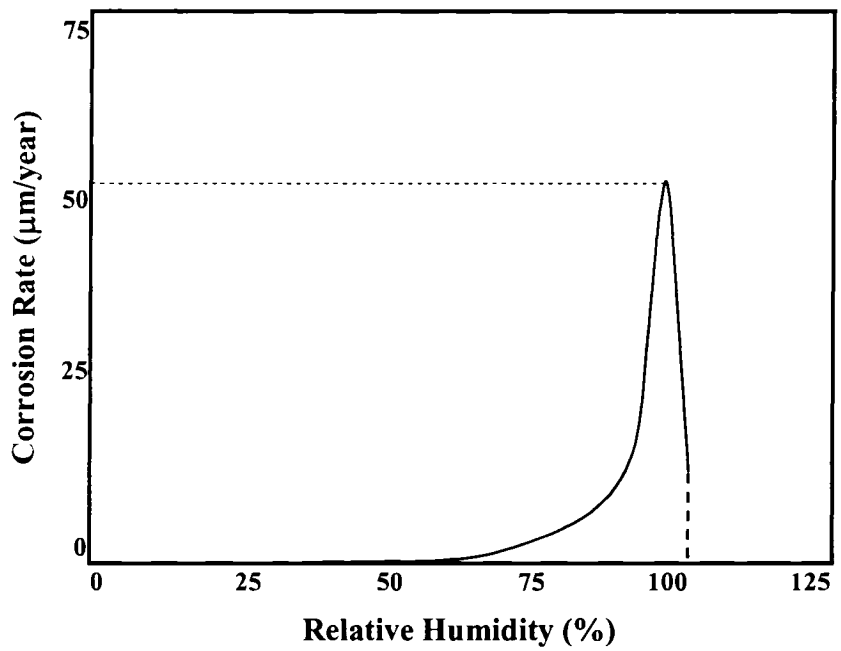

Figure 2.10: Influence of Relative Humidity on Corrosion Rate
(Richardson, 2001)

Figure also shows that relative humidity less than 60% does not support development of any corrosion activity due to carbonation. Also corrosion activity reduces as the relative humidity approaches saturation, since the effect of permeability reduction would become dominant (Richardson, 2001).

2.2.5.4 Influence of Temperature

The rate of corrosion increases with increasing temperature. The effect is not significant in cold humid climates but it could be in hot humid climates. Browne (1988) reported that an increase in temperature from 20°C to 40°C could increase the rate of corrosion by a factor of five.

2.2.5.5 Influence of Cracking

Both carbon dioxide and chloride ions may penetrate to the steel surface through cracks some order of magnitudes faster than through "uncracked" concrete. The time taken for depassivation depends on the crack width; however, the times involved are negligible compared with the lifetime of a reinforced concrete structure. A relationship between depassivation time and crack width is shown in Figure 2.11. The scatter of the figure depends on the environment, the cover and the nature of any deposits on the concrete surface. In the case of normal crack widths at the concrete surface up to 0.4mm, self-healing as a result of calcium, dirt and rust deposits within the cracks can frequently be observed (CEB, 1992); however, it has been a subject of debate in the context of acceptable limits for crack width (Richardson, 2001).

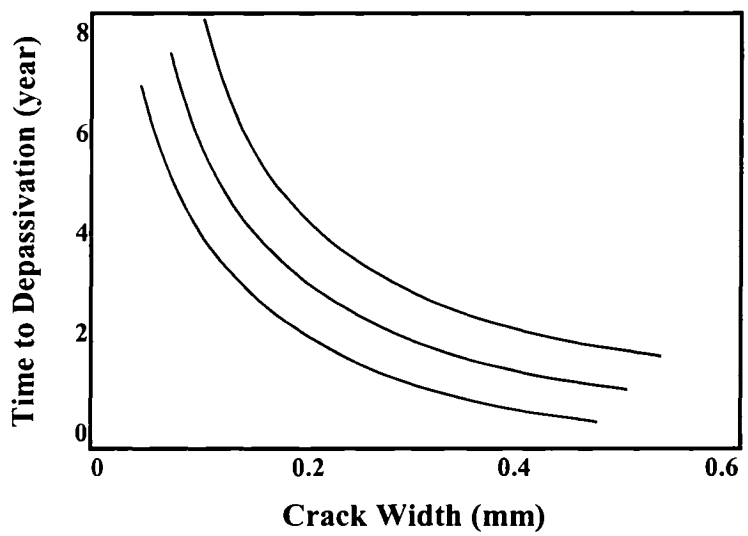

Figure 2.11: Relationship Between Depassivation Time and Crack Width
(Richardson, 2001)

The thickness of concrete cover is of major importance with respect to the influence of cracks. The crack widths, if they are smaller than 0.4 mm, are less important, however, the live cracks parallel to the reinforcement represent a much higher corrosion risk than dormant perpendicular cracks.

If carbonation or chloride ions reach the reinforcement, depassivation of the reinforcement may occur to initiate macrocell corrosion. The steel in the cracked region act anodically, while the cathodic process takes place in the uncracked areas beside the cracks (Figure 2.12). In this process the crack widths are of minor importance after depassivation, because the cathodic process is the main rate-determining factor.

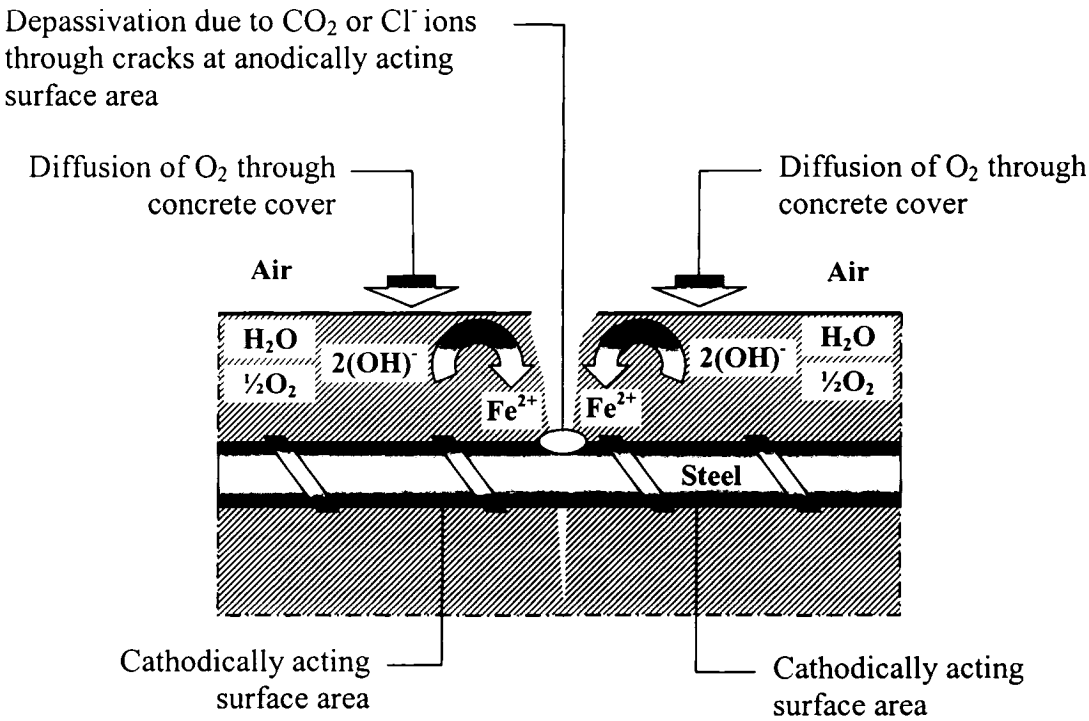

Figure 2.12: Corrosion of Reinforcement in concrete Cracks
(Adopted: CEB, 1992)

Rust has a substantially higher volume than the iron in the steel from which it is formed – theoretically up to more than six times, depending upon availability of oxygen. This leads

to splitting forces that may cause cracking and spalling. Thus cracking accelerates corrosion and corrosion accelerates further cracking, which may lead to sudden failure, if longitudinal cracking along the bars occurs in the region of the bar anchorage. In the case of low availability of oxygen, corrosion processes proceed slowly and rust products may diffuse into the voids and pores of the porous concrete without causing cracking and spalling. In such rare cases, serious corrosion may develop on the reinforcement without any visible warning, and a sudden failure may occur.

2.2.5.6 Influence of Thickness of Concrete Cover

Carbonation and chloride ions penetrate towards the interior concrete at a lower rate than in the outer layer. For an approximate estimation, square-root time function can be used to calculate the carbonation depth, and Crank's error function (solution of Fick's 2nd law of diffusion) can be used to calculate chloride penetration depth. In case of square root function, it means that if the concrete cover is halved, the critical state for incipient danger of corrosion will be reached in less than a quarter of the time. An example is shown in Figure 2.13 that for the nominal concrete cover, carbonation reaches the surface of the reinforcement after 100 years. If the cover is reduced to half of the nominal thickness, the carbonation penetration occurs in only 25 years.

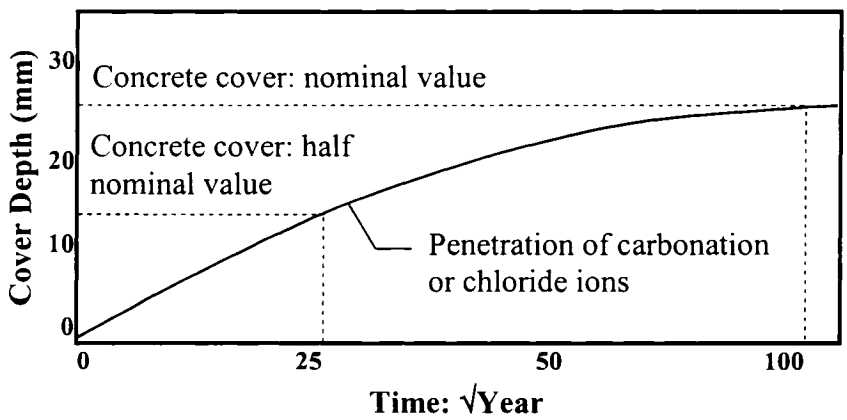

Figure 2.13: Effect of Concrete Cover Thickness on Penetration of Carbonation and Chloride Ions
(CEB, 1992)

Therefore, the depth of the concrete cover has an important role to protect the steel embedded in concrete from corrosion. The corrosion initiation (depassivation) time increases with an increase in the concrete cover thickness, and its quality in terms of permeability.

2.2.5.7 Influence of Permeability of Concrete

The durability of concrete is essentially influenced by the ingress of ions or molecules in the form of liquids or gases through the material (concrete). The passage of these potentially aggressive agencies is influenced primarily by the permeability of the concrete. Permeability is a material property, which represents the quantity of migration of ions, molecules or fluids through the concrete. The migration includes the distinct mechanisms of capillary action, flow under a pressure gradient and flow under a concentration gradient. These mechanisms are characterized by sorptivity, permeability, and diffusivity, respectively.

The permeability of concrete is a function of the pore structure, the degree of interconnection of the pore structure and its moisture content. Thus, the permeability of concrete is predominantly influenced by the permeability of cement paste, especially the quality of paste in the cover concrete and at the interface with the aggregate particles. The following factors influence the permeability of concrete:

2.2.5.7.1 Influence of W/C Ratio on Permeability

The water/cement (W/C) ratio of concrete influences the permeability of concrete decisively, particularly when the W/C ratio exceeds 0.6, the permeability increases considerably with the W/C ratio, due to an increase in the capillary porosity. Figure 2.14 shows how the water permeability depends on the W/C ratio and the degree of hydration. In principle, the same basic influence of W/C ratio holds true for gas and ion permeability.

2.2.5.7.2 Influence of Curing on Permeability

If the concrete is insufficiently cured (i.e. if the concrete surface dries early), the permeability of the surface layer of the concrete may be increased by five to ten times than the sufficiently cured concrete. The depth of the influenced layer depends on the grade of drying; however, it is often equal to or thicker than the concrete cover. Wind and high temperatures are very dangerous as far as early drying out of the concrete surface is concerned.

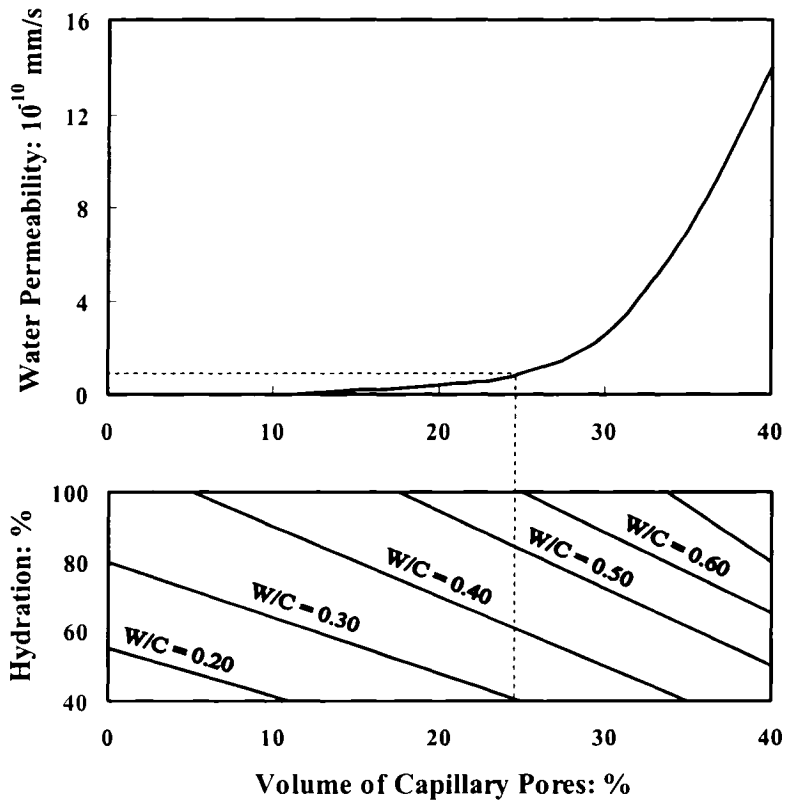

Figure 2.14: Influence of W/C Ratio on Permeability
(CEB, 1992)

Curing measures taken after the first drying out of the concrete are normally useless, because the hardening hardly continues after having been interrupted once. Therefore, curing measures must begin immediately after concreting and they must not to be interrupted.

2.2.5.7.3 Influence of Compaction on Permeability

Poor compaction or gravel pockets tend to increase the permeability of concrete to such an extent that protection of the reinforcement no longer exists. Therefore, proper compaction must be achieved to decrease the permeability of the concrete.

2.2.5.7.4 Influence of Cement Content on Permeability

With an increase in the cement content, the binding capacity of the concrete both for carbon dioxide and chloride ions is increased (Figure 2.15). However, over the normal range of cement contents, the penetration rates of carbonation and chloride ions are influenced to a considerably lower extent by the cement content than by the W/C ratio, the quality of compaction, and curing. Nevertheless, the amount of cement is important in connection with the workability and to a certain extent with the curing sensitivity.

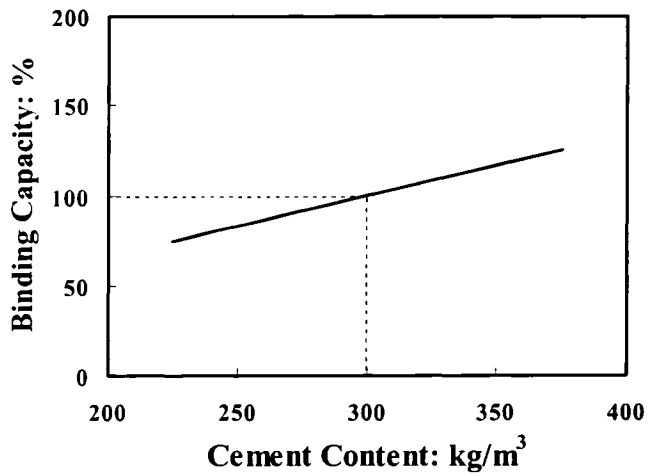

Figure 2.15: Influence of Cement Content on Binding Capacity
(CEB, 1992)

Normally, cement content in the range of 300 kg/m^3 is sufficient to achieve concrete with sufficiently low permeability and adequate durability if the W/C ratio is kept below 0.5–0.6, depending on the environmental conditions (the presence or absence of chlorides) and an adequate curing (CEB, 1992).

2.2.5.7.5 Influence of Cement Type / Cement Supplement on Permeability

Generally, the most common composite and blended cements with natural pozzolanas, blast-furnace slag or fly ash have in common the properties of

(a) Slow hardening at an early age

(b) Distinct hardening later on.

This means that composite and blended cements are more curing-sensitive than Portland cements.

If the later hardening is ensured by adequate curing, a lower permeability of concrete can be achieved by using composite or blended cements rather than Portland cements. This helps to improve the resistance of concrete against chloride penetration.

Whatever the type of cement, inadequate curing can lead to a poor quality (in terms of permeability and binding capacity) of the concrete cover. The sensitivity to curing is especially pronounced if cements with high percentages of blending agents (i.e. in excess of 50% slag, 15% fly ash, or 8% silica fume) are used (Figure 2.16).

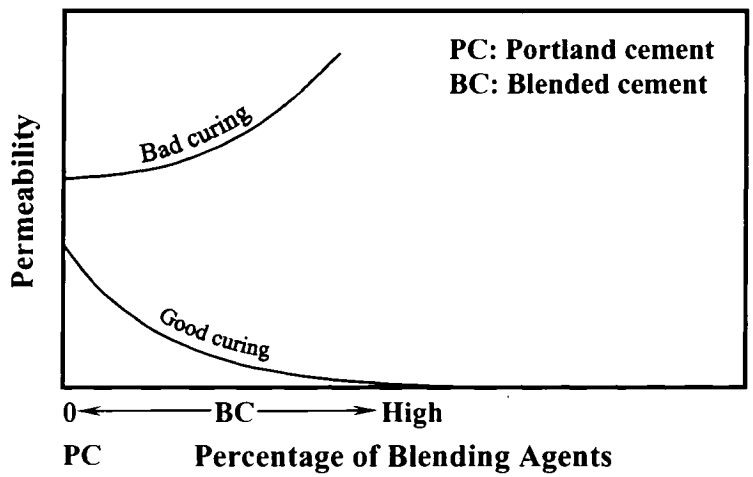

Figure 2.16: Influence of Type of Cement on Permeability
(CEB, 1992)

2.2.5.7.6 Influence of Formwork on Permeability

The exterior shell of the concrete or the cover with a thickness of about 40 to 50 mm, is responsible for eliminating or significantly reducing the ingress of carbon dioxide and chloride ions into the concrete, and thus increase considerably the time to the onset of corrosion. During compaction by an immersion vibrator, water and air bubble moves around the outer shell of the concrete near the formwork. This water and air are normally trapped near the traditional formwork and thus increases the water-cement ratio and therefore the permeability of the concrete cover.

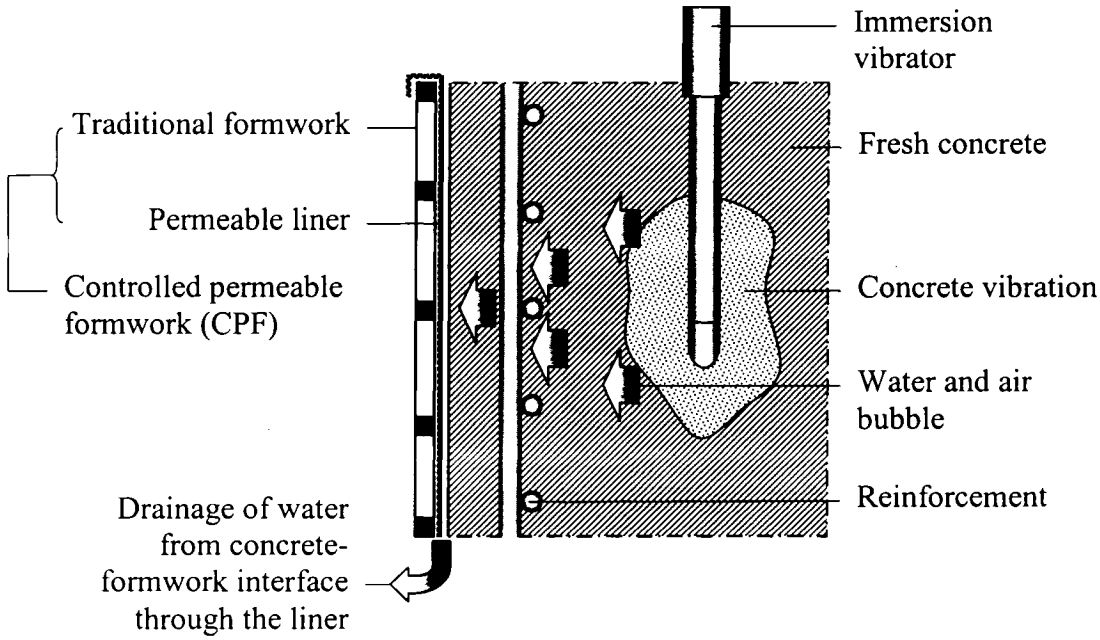

Figure 2.17: Controlled Permeable Formwork (CPF)
(Adopted: Basheer et al., 1993)

Laboratory and field studies have shown that the use of controlled permeability formwork (CPF) can produce high quality durable surface concrete (Wilson ,1994, Price and Widdows, 1991, Basheer et al., 1993). The CPF systems normally consist of a specially designed permeable liner attached to the surface of the traditional formwork (Figure 2.17). This membrane consists of many macropores, which act as filter and retain the fine material

in the concrete, however, they permit some of the water in the concrete and the air to pass through the liner and the backing material.

The drainage of water at the concrete-formwork interface reduces the water-cement ratio significantly in the outer 15 to 20 mm of the concrete (Figure 2.18). This improves the surface aesthetics, eliminates blowholes, provides greater consistency, increases abrasion resistance and it considerably improves the concrete resistance to freezing and thawing cycles. Also, the permeability of the concrete to gas and water is decreased significantly, reducing ingress of both carbon dioxide and chloride ions thereby reducing the risk of corrosion, and increasing the service life of the structure.

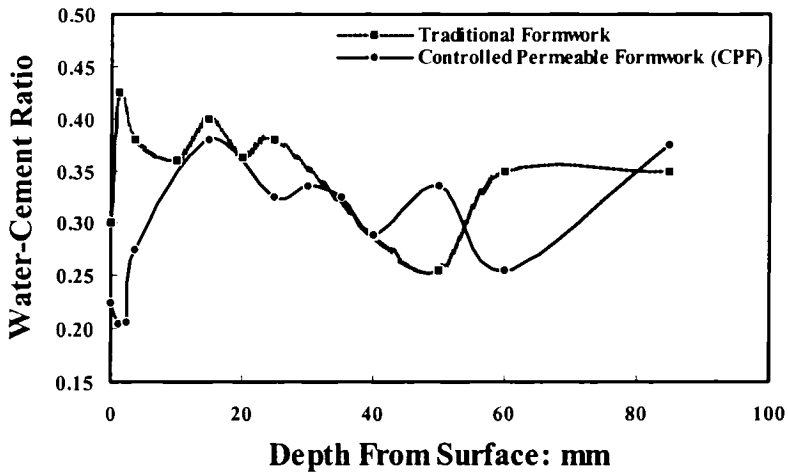

Figure 2.18: Variation of W/C Ratio with the Distance from Concrete Surface Due to Different Formwork
(Wilson, 1994)

2.3 Corrosion of Steel in Repaired Concrete

Repaired concrete has different characteristic compared to the new concrete due to their electrochemical incompatibility, which reflects on the corrosion mechanism; corrosion mechanism in repaired concrete is not entirely identical with that in the new concrete. However, the basic information regarding corrosion of steel in new concrete is also

applicable for repaired concrete. The following section is discussed on the additional information on the corrosion of steel in repaired concrete.

2.3.1 Influence of Macrocell Formation

Corrosion of steel in concrete occurs due to formation of microcells or macrocells (Elsener, 2002). Microcells form when anodes and cathodes develop adjacent to each other. Generally, microcells are responsible for producing uniform corrosion. Such corrosion is found typically in carbonated concrete or concrete with a very high chloride content. Macrocells are defined by clearly distinct cathodic and anodic areas, as manifested in pitting corrosion, where the anode is very small in comparison to the amount of surrounding passive steel (Leyne, 2004). This type of corrosion is very dangerous leading to high rates of local corrosion and loss of cross-section that are not easily detectable.

Since the concrete quality in a structure varies and the environmental conditions differ from one area to the next, corrosion damage tends to be in locally limited regions (Raupach, 1996). It is now understood that the removal of these relatively small areas of deteriorated concrete, and their replacement with new concrete, a traditional patch repair, regardless of the quality of repair concrete can also lead to the formation of macrocells (Emmons and Vaysburd, 2003). The formation of macrocells after local patch repairs can be attributed to electrochemical incompatibility between the repaired and "unrepaired" phases.

2.3.2 Influence of Electrochemical Incompatibility

"Compatibility can be defined as a balance of physical, chemical, and electrochemical properties and dimensions between a repair material and the existing substrate that will ensure that the repair can withstand all the stresses induced by volume changes and chemical and electrochemical effects without distress and deterioration over a designated period of time (Morgan, 1996)" (Leyne, 2004).

Therefore, a repair may be considered to be incompatible due to physical, chemical, dimensional, or electrochemical imbalances. Therefore, not all types of imbalances result in corrosion of the steel reinforcement. The formation of macrocells due to patch repairs is a result of the electrochemical incompatibility, although the factors leading to such incompatibility necessarily include physical, chemical, and dimensional factors.

The term electrochemical incompatibility provides a new meaning to reinforced concrete repair, and is described clearly by Beaudoin et al. (1997). Normally, the idea of electrochemical incompatibility would refer to the imbalance of electrochemical potentials when two metals come in contact, which acts as a driving force of corrosion. In this case, the least noble metal would be subject to corrosion. In case of patch repair, electrochemical incompatibility refers to electrochemical potential imbalance on reinforcing steel bar due to the dissimilar environments, caused by the patch repair due to the dissimilar properties such as density, porosity, permeability, moisture and oxygen content, non-uniformity or non-continuity of reinforcement coatings between the repair and unrepaired regions. Thus the electrochemical imbalance causes corrosion due to the formation of macrocell between the dissimilar environments of the repaired and unrepaired concrete. Two examples, adapted from Beaudoin et al. (1997) and Raupach (1996), are described below to illustrate in more detail the various forms of these macrocell corrosions.

2.3.2.1 Macrocell Corrosion due to Chloride Contaminated Concrete

The electrochemical imbalance is observed when chloride-free patch concrete is surrounded by chloride contaminated non-patch concrete. A qualitative Evans' diagram is shown in Figure 2.19 with three clear anodic regions: active, passive, and trans-passive. The line A_1 represents the typical Tafel line for passive steel in the repaired patch region, whereas the line A_2 represents depassivated steel in the existing chloride contaminated non-patch concrete. The difference between the electrochemical potential of patch (repaired) region, E_P and non-patch (un-repaired) region, E_{NP} represents the electrochemical incompatibility, and leads to produce macrocell corrosion due to variation of chloride concentration (Beaudoin et al., 1997).

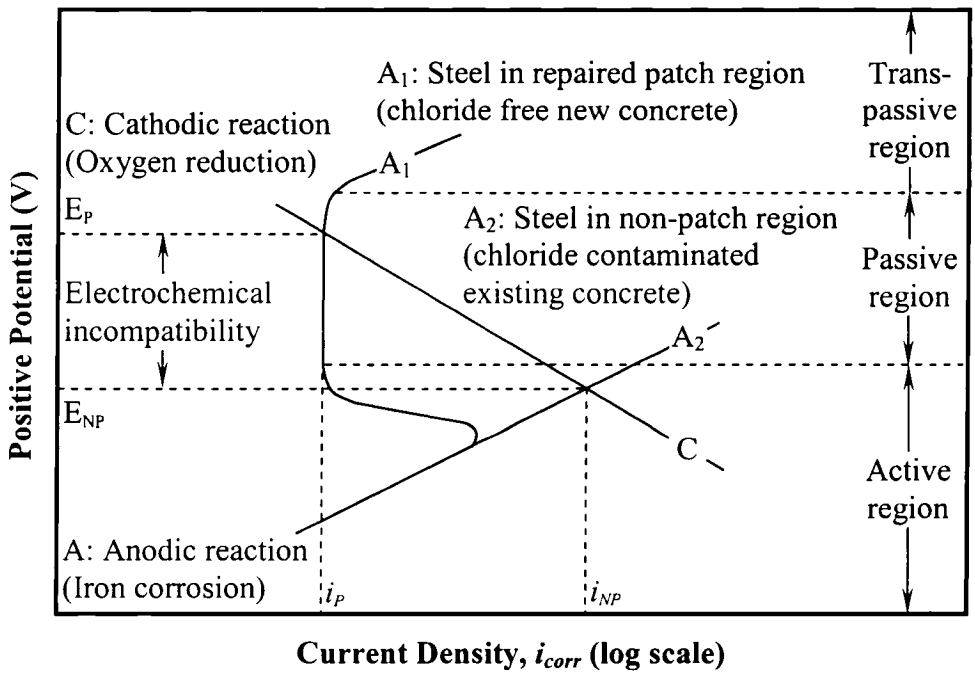

Figure 2.19: Electrochemical Imbalance between Chloride-free Patch Concrete and Chloride Contaminated Non-Patch Concrete
(Beaudoin et al., 1997)

2.3.2.2 Macrocell Corrosion due to Dense and Porous Concrete

Beaudoin et al. (1997) also illustrated the mechanism of formation macrocell corrosion due to availability of oxygen in densely repaired patch concrete and porous existing concrete. In Figure 2.20, line C_1 represents the oxygen reduction line for steel in the existing non-patch concrete, which has a relatively high oxygen concentration due to its porous structure, and therefore, it results in a high corrosion potential, E_{NP}. Line C_2 represents the oxygen reduction line for steel in densely repaired patch concrete, which due to the lower oxygen concentration results in a lower corrosion potential, E_P. Because of the difference in oxygen concentrations, an electrochemical imbalance occurs resulting in an oxygen corrosion macrocell. The steel in the non-patch (existing) concrete acts as a cathode due to the high levels of oxygen and the patch steel in densely repaired region becomes an anode. When oxygen levels are extremely low in the repaired zone, the line C_3, the value of the corrosion current density, i_P' in the repaired zone is much higher than that of in the existing porous

concrete (i_{NP}). Therefore, densely repaired patch concrete accelerates the corrosion instead of reducing it.

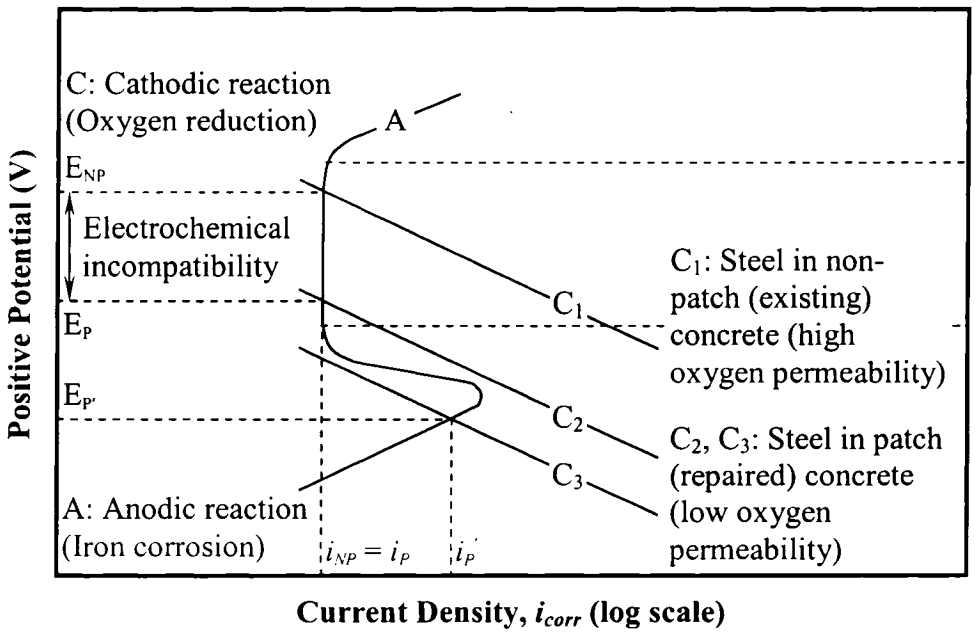

Figure 2.20: Electrochemical Imbalance between Dense Patch Concrete and Porous Non-Patch Concrete
(Beaudoin et al., 1997)

Chapter 3

Manifestation and Restoration of Corrosion Damaged Reinforced Concrete Structure

3.1 Introduction

The dominant cause for failure of concrete structures is corrosion of the embedded reinforcing steel. The failure of concrete structures can be recognized either exclusively to the failure of a material component (cement, aggregate or reinforcement), or exclusively due to the failure of the system (structural or design failure). For completeness, some tables and figures from Heckroodt (2002) and Vector Corrosion Technology (2003) are reported here. Different kind of concrete deteriorations are summarized in Table 3.1.

3.2 Manifestation of Reinforcement Corrosion

Corrosion increases in volume of steel bars up to ten times of its original volume due to the formation of hydrate oxides (Heckroodt, 2002). This expansion of steel results in mechanical disruption of the encasing concrete.

Reinforcement corrosion is particularly destructive. Some times, this damage may occur rapidly and the repairs may be quite expensive. There are two major consequences of reinforcement corrosion:

1. Cracking and spalling of the cover concrete as a result of the formation of corrosion products
2. A reduction of the cross-sectional area of the rebar by pitting corrosion (specially more destructive in prestressed concrete structure).

Unfortunately, most of the reinforced concrete structures exhibit cracking and spalling have gone beyond the point where simple and cost effective measures can be taken to restore the structure to its original condition.

Table 3.1: Concrete Deterioration Diagnostics
(Heckroodt, 2002)

Type of Deterioration and Causes	Visual Appearance of Deterioration	Confirmatory Testing
Reinforcement Corrosion: exposure to normal climatic conditions with wetting and drying cycles.	Large area of rust stains, cracking along pattern of reinforcement, spalling and delamination of cover concrete.	Cover depth of rebar, Carbonation and chloride testing, Exploratory coring, and Electrochemical testing.
Alkali-Aggregate Reaction: concrete made with reactive aggregates.	Expansive map cracking, restrained cracking following the line of reinforcement, white silica gel at cracks.	Core analysis for gel and rimming of aggregates, Petrographic analysis, and Aggregate testing.
Drying Shrinkage/Creep: initially very rapid drying, long-term wetting and drying cycles.	Deep parallel cracking, pattern reflects reinforcement positions	Concrete core analysis, Loading and structural analysis, and Aggregate and binder analysis.
Chemical Attack: exposure to aggressive water (e.g. domestic and industrial effluents)	Deterioration of surface, salt deposits on surface, cracking caused by internal expansive reactions.	Chemical analysis of concrete, Core examination for depth of attack and internal distress.
Soft-water Attack: exposure to moving fresh water (slightly acidic) in conduits.	Surface leaching of the hydrated cement paste concrete, exposed aggregate, no salt deposits.	Chemical analysis of water, Core examination for leaching, Aggregate and binder analysis.
Fire Damage: exposure to open fires for a long duration causes damage.	Surface discoloration, concrete spalling, buckling, loss of strength, microcracking.	Core examination for color variations and steel conditions, Petrographic analysis.
Structural Damage: structure subject to overload.	Major cracking and localized crushing, excessive deformations and deflections of structural members.	Loading and structural analysis, Core testing for compressive strength and elastic modulus.

Table 3.2: Conditions and Features of Reinforcement Corrosion

(Heckroodt, 2002)

Type of Corrosion	Environment and Causative Conditions	Significant Features of Deterioration
Carbonation-induced	• Unsaturated concrete • Polluted environment • Low concrete cover depth to steel • Permeable concrete cover	• General corrosion with multiple pitting occurrences along rebars • Moderate corrosion rates except when wet and dry faces are near each other • Corrosion damage easily noticed (surface stains, cracking, spalling); generally only affects aesthetics • Requires a different repair approach from chloride-induced corrosion; repairs are generally successful
Chloride-induced	• Deicing salt • Marine environments • Industrial chemicals • Admixed chlorides (old structures)	• Distinct intense anode and cathode region • Rapid and severe localized pitting corrosion and damage to surrounding concrete • Corrosion damage affecting structural integrity may be far advanced before being noticed (surface stains, cracking, spalling) • More destructive and difficult to treat than carbonation-induced corrosion
Chemically induced	• Sulphate in ground water • Use of fertilizers • Industrial waste • Sewage treatment works	• Corrosion generally associated with near saturated conditions • Concrete deterioration occurring together with corrosion
Artificially-induced	• Bimetallic corrosion • Partial sealing of corrosion • High temperature (>200°C)	• Generally very localized intense corrosion due to well-defined anode-cathode region
Stray current	• DC power supplies • Railway systems • Industrial waste	• General corrosion of rebar exposed to moist conditions • Corrosion not confined to low cover depth • Large crack width possible
Secondary forms	• Primary cracking due to alkali-aggregate reaction, structural cracking	• Corrosion localized in regions where cracks intersects the rebars

Table 3.3: Manifestation of Reinforcement Corrosion
(Heckroodt, 2002)

Factor	Influence
Geometry of the element	Large diameter bars at low covers allow easy spalling
Cover depth	Deep concrete cover may prevent full oxidation of corrosion product
Moisture condition	Conductive electrolytes encourage formation of well-defined macrocells to produce corrosion
Age of structure	Rust stains progress to cracking, and spalling accelerates further corrosion
Rebar spacing	Closely spaced bars may encourage delamination and produce further corrosion
Crack distribution	Cracks may provide low resistance paths to the reinforcement to produce corrosion
Service stress	Corrosion may be accelerated in highly stressed zones
Quality of concrete	Severity of damage depends on the concrete quality. Low permeable and high resistance concrete provides more protection against corrosion

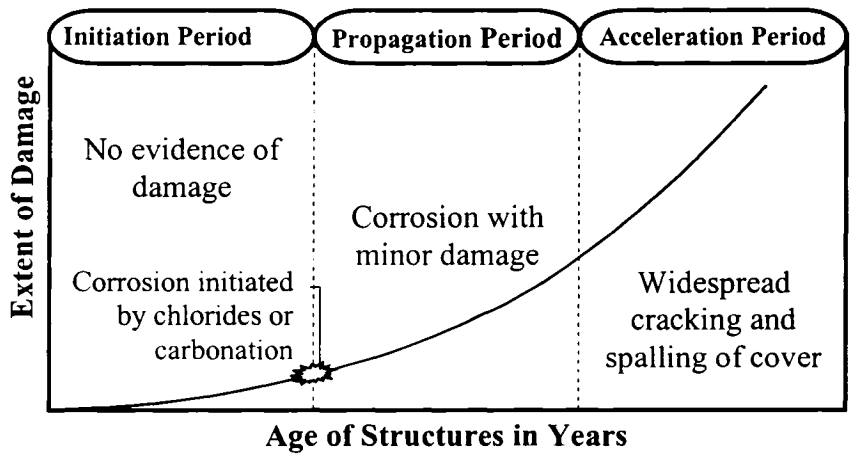

Figure 3.1: Three-Stage of Corrosion Damage
(Heckroodt, 2002)

The features of reinforcement corrosion induced by different conditions are summarized in Table 3.2 and the factors that influence the manifestation of reinforcement corrosion are listed in Table 3.3. Figure 3.1 illustrates a typical three stages of corrosion development profile in reinforced concrete structures.

3.3 Condition Surveys of Reinforcement Corrosion

Condition surveys are an important strategy for identifying and quantifying the state of corrosion of a structure over time. Before repair options are considered, a detailed corrosion or condition survey should be undertaken to identify the exact cause and extent of deterioration. The results of such surveys may determine the most appropriate repair strategy. The various survey techniques are summarized in Table 3.4.

3.3.1 Visual Assessments

Items, which should be included in a checklist for a visual assessment of concrete degradation, are listed in Table 3.5. Visual assessment of deterioration may come too late for cost-effective repairs because damage due to corrosion of reinforcement often appears at the surface after significant deterioration has occurred.

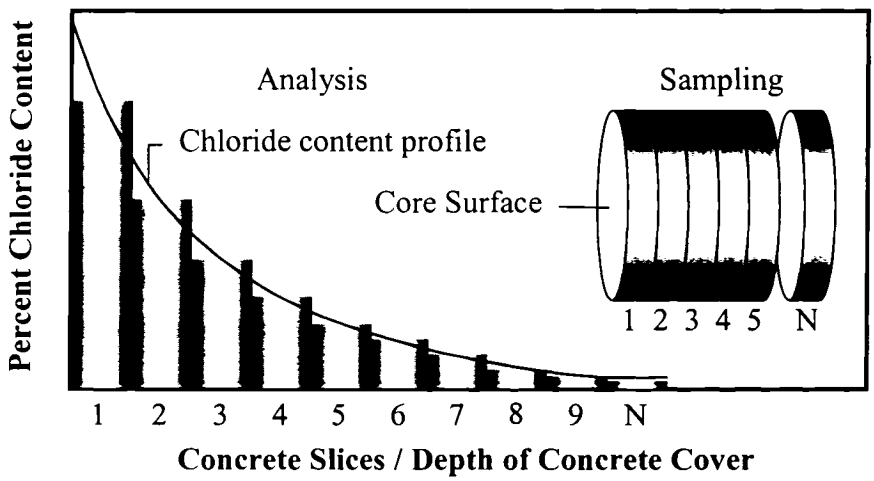

Figure 3.2: Determination of Chloride Content Profile

Table 3.4: List of Condition Surveys of Reinforcement Corrosion

(Heckroodt, 2002)

Surveys	Comments
Visual: use of comprehensive checklist	• Corrosion during early stages is not normally visible • Visual survey is the first action of any detailed investigation
Delamination: hammer or chain drag	• Often underestimates full extent of delamination and internal cracking
Cover Surveys: use alternating magnetic field to locate the position of steel in concrete	Unreliable when: • Rebar closely spaced, different types / size, at deep cover • Site-specific calibrations not done • Other magnetic material nearby (windows, bolts, conduits)
Chloride Testing: chemical analysis	• Chlorides in aggregate give misleading results • Chlorides in cracks, or defects difficult to determine
Carbonation Depth: chemical analysis (pH indicator)	• Slightly underestimates carbonation depth • Difficult to distinguish color change caused by pH indicator in dark-colored concrete • Indicator ineffective at very high pH levels (e.g. after electrochemical re-alkalization) • Testing must be done only on very freshly exposed concrete surfaces (before atmospheric carbonation occurs)
Rebar Potentials: potentiometer (voltmeter) using copper / copper sulphate reference electrode	• Not recommended for carbonation induced corrosion • Interpretation is a specialist task • Delamination could disrupt potential field and thus produce false readings • Environmental effects (temperature, humidity) influence potentials • No direct correlation between rebar potential and corrosion rates • Stray currents influence measured potentials
Resistivity: Wenner probes and resistivity meter	• Carbonation and wetting fronts affect measurements • Concrete with high resistance results in unstable readings • Rebar directly below probes influences readings
Corrosion Rate: linear polarization resistance	• Sophisticated technique, requires expertise to operate • Environmental and material conditions have large influence on measurements and single readings may not reliable

Table 3.5: Visual Assessment of Structural Failure: Items for Checklist
(Heckroodt, 2002)

Item	Details
Background:	
• Identification	• Reference, number, location
• Environment	• Severity and type of location
• History	• Age, design data, repair
Original Condition:	
• Surface condition	• Honeycombing, bleeding, voids, pop-outs
• Early cracking	• Plastic settlement or plastic shrinkage
• Concrete quality	• Surface hardness, density, voids, color
• Rebar cover	• Covermeter survey, mechanical breakout
• Structural effects	• Overloading, dynamic effects, structural cracking
Present Condition:	
• Surface damage	• Abrasion, staining, chemical attack, spalling, leaching
• Staining	• Rebar corrosion, alkali-aggregate reaction gel, efflorescence, salts
• Cracking	• Width, pattern, location, causes of cracking
• Joint deficiencies	• Joint spalling, vertical and lateral movements, seal damage
• Carbonation	• Indicator test on cores, or mechanical breakouts
• Delamination	• Size, frequency, severity of delamination
• Previous repairs	• Integrity of repairs, signs of damage near repair locations

3.3.2 Chloride Content Determination

Chlorides exist in concrete as both bound and free ions, however, only free chlorides directly affect corrosion. Accurate measurement of free water-soluble chlorides is very difficult, and chlorides are, therefore, most commonly determined as acid soluble or total chlorides in accordance with the appropriate national standard.

Chloride sampling and determination of chloride content in concrete are illustrated in Figure 3.2 and are usually performed in the following manner:

1. Concrete samples are extracted as either core or drilled powder sample

2. Depth increments are chosen depending on the cover to the steel rebar and the likely level of chloride contamination (increments are typically between 5 and 25 mm)
3. Dry powder samples are digested in dilute nitric acid to release all chlorides
4. Chlorides are analyzed using potentiometric titration or the Volard method
5. Chloride contents should preferably be expressed as a percentage by mass of the cement
6. Chloride profiles may be drawn such that chloride concentrations may be interpolated or extrapolated for any depth.
7. Future chloride levels can be estimated using Fick's second law of diffusion.

3.3.3 Carbonation Depth Measurement

Carbonation depth is measured by spraying a phenolphthalein indicator solution (1% by mass of ethanol/water solution) on a freshly fractured concrete surface. Phenolphthalein remains clear where concrete is carbonated but turns pink /purple where concrete is still strongly alkaline (pH > 9.0). Carbonation moves through concrete as a distinct front and reduces the natural alkalinity of concrete from a pH in excess of 12.5 to approximately 8.3. Steel starts to depassivate when the alkalinity is reduced below pH value of 10.5.

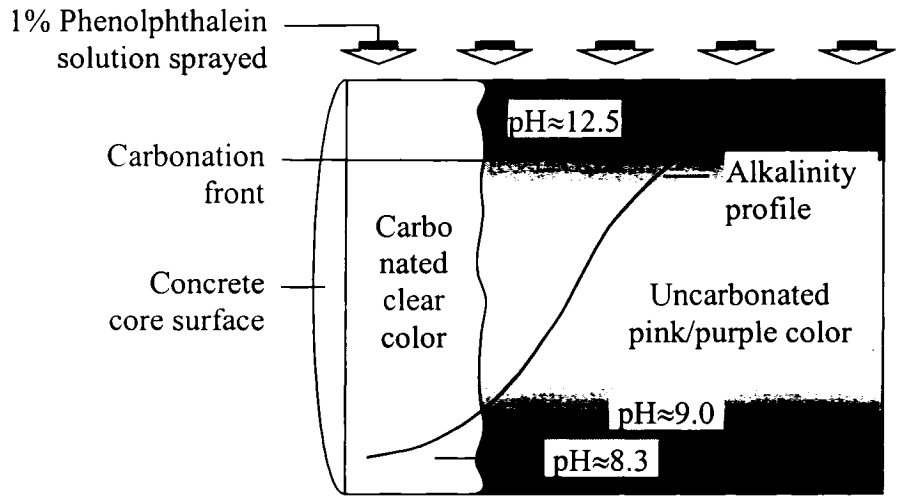

Figure 3.3: Progress of Carbonation Front on a Longitudinally Sliced Concrete Core
(Heckroodt, 2002)

The progress of the carbonation front is shown in Figure 3.3. For prediction purposes, the rate of carbonation is approximately proportional to the square root of time.

3.3.4 Rebar Potential Measurement

Chloride-induced corrosion of steel is associated with anodic and cathodic reaction along the rebar with consequent changes in the electropotential of the steel rebars. It is possible to measure these rebar potentials at different points and plot the results in the form of a contour map. Measurement of rebar potentials determines the thermodynamic risk of corrosion instead of evaluating the kinetics of the reaction, therefore, it cannot reflect the rate of corrosion. Rebar potentials are normally determined in accordance with ASTM C876: 1991 using a copper/copper sulphate reference electrode connected to a hand-held voltmeter. The qualitative risk of corrosion based on rebar potentials is shown in Table 3.6. This technique is not recommended for carbonation-induced corrosion where clearly defined anodic regions are absent.

Table 3.6: Qualitative Risk of Chloride-Induced Corrosion
(Heckroodt, 2002)

Rebar Potential (-mV $Cu/CuSO_4$)	Qualitative Risk of Corrosion
< 200	Low
200–350	Uncertain
> 350	High

The procedure for undertaking a rebar potential survey is as follows:

1. Mark a grid pattern in the area of measurement (not more than 500 mm center to center)
2. Make an electrical connection to clean steel by coring or breaking out concrete
3. Use a multimeter to check that the steel is electrically continuous over the survey area
4. Wet the concrete surface with tap water if the concrete appears to be dry

5. Take the readings either manually or by using a data logger
6. Check some data on site to ensure that it correlates with the visual signs of corrosion.

Rebar potential measurements are relatively quick to perform. Absolute values are often of lower importance than the differences between values measured on a structure. A shift of several hundred millivolts over a short distance of 300–500 mm often indicates a high risk of corrosion.

3.3.5 Concrete Resistivity Measurement

Concrete resistivity controls the rate at which steel corrodes in the concrete, once favorable conditions exist for corrosion. Resistivity is dependent on the moisture condition of the concrete, permeability and interconnectivity of the pore structure, and the concentration of ionic species in the pore water of concrete.

1. Poor quality, saturated concrete has low resistivity (< 10 kΩ-cm)
2. High quality, dry concrete has high resistivity (> 25 kΩ-cm).

Table 3.7: Likely Corrosion Rate Based on Concrete Resistivity
(Heckroodt, 2002)

Concrete Resistivity (kΩ-cm)	Likely Corrosion Rate for Given Corrosive Conditions
< 12	High
12–20	Moderate
> 20	Low

Resistivity measurements are simple to perform on site and are performed with a Wenner probe connected to a portable resistivity meter. The outer two probes send an alternating current through the concrete, while the inner two probes measure the potential difference in the concrete. Once the concrete resistivity is known, a rough assessment of likely corrosion

rates can be made as shown in Table 3.7. This assessment assumes that the conditions are favorable for corrosion.

3.3.6 Corrosion Rate Measurement

Corrosion rate measurements are the only reliable method of measuring actual corrosion activity in reinforced concrete. Numbers of sophisticated corrosion monitoring systems are available based on linear polarization resistance (LPR) principles. Corrosion rate measurements on field structures are most commonly under using galvanostatic LPR techniques with a guard-ring type sensor to confine the area of steel under test. Table 3.8 shows a qualitative guide for the assessment of corrosion rates in structures.

Table 3.8: Qualitative Assessment of Corrosion Rate Measurement
(Heckroodt, 2002)

Corrosion Rate ($\mu A/cm^2$)	Qualitative Assessment of Corrosion Rate
> 10	High
1.0–10	Moderate
0.2–1.0	Low
< 0.2	Passive

3.4 Repair Strategies of Reinforced Concrete Structures

Repair of reinforced concrete structures needs to be undertaken in a rational manner to guarantee success. Repair options must be considered in terms of cost-effectiveness, technically feasibility and reliability. Engineers must understand all relevant material, structural and environmental issues associated with concrete repairs to make intelligent choices.

Following factors should be considered for selecting suitable and cost-effective repair:

1. Level of deterioration

2. Specific conditions of the structure
3. Environmental conditions

Therefore, high-quality repairs require a through investigation of the causes of deterioration, appropriate repair specifications and high quality execution of the repair work. This can only be achieved when independent experts carryout structural investigations, engineers with specialist repair expertise draw up specifications and competent contractors undertake repairs. The various repair options are compared in Table 3.9.

Table 3.9: Different Reinforced Concrete Repair Strategies
(Heckroodt, 2002)

Strategies	Comments
Patching: removal of all cracked and delaminated concrete and cleaning of all corroded reinforcement, application of protective coatings to steel and repairing with mortar or micro-concrete	• Popular due to low cost and temporary aesthetic improvement • Limited success against chloride-induced corrosion
Barrier Coating: these systems attempt to seal the surface of the concrete, restricting the flow of oxygen to the cathode, thus stifling corrosion	• Not suitable for large concrete structures, because large amounts of oxygen are already present in the system • Generally ineffective due to the presence of defects underneath the new coating • Likely to promote the formation of differential aeration cells, further accelerating the corrosion potential
Hydrophobic Coating: (penetrating pore liner, e.g. silane and siloxane) surface capillary channels are lined with a hydrophobic coating, which repels water during wetting but allows water vapor movement during drying	• Reduces the moisture content, and thereby electrolytically stifles the corrosion reaction • Suitability for marine structures is questionable due to the high ambient humidity, effect of capillary suction and presence of high salt concentrations, all of which interfere with drying • Application to a new construction is effective for about 10-15 years

Table 3.9: Different Reinforced Concrete Repair Strategies (Continued)

Strategies	Comments
Electrochemical Techniques: restore the passivated condition of the steel by the temporary application of a strong electric field to the cover concrete region	• **Re-alkalization:** nondestructively restoring the alkalinity of carbonated concrete, treatment can be completed in less than two weeks • **Electrochemical Chloride Removal (ECR):** a more time-consuming and complex technique; its suitability must be carefully assessed
Cathodic Protection: the electrical potential of the embedded reinforcement is artificially increased either by an impresses external current or by a sacrificial anode system, thus decreasing the corrosion rate of the steel	• **Sacrificial Anode System:** most effective in submerged structures (saturated concrete with low resistivity) and temperature above 20°C • **Impressed Current:** anode system designed for long life (20-50 years) • Cathode systems require electrically continuous reinforcement and uniformly conductive, delamination-free concrete cover
Migrating Corrosion Inhibitor: organic-based materials (e.g. amino-alcohol) suppress corrosion by being absorbed onto the steel surface and displacing corrosion ions, such as chlorides, interfering with the anodic dissolution of iron and simultaneously disrupting the reduction of oxygen at the cathode	• Effectiveness of inhibitor controlled by environmental, material and structural factors • Migrating inhibitors penetrate by vapor diffusion. Movement is fairly rapid through partially saturated concrete, but penetration is poor in near-saturated concretes (e.g. partially submerged marine structures with high moisture and salt levels) • Control of chloride-induced corrosion is largely dependent on the chloride levels at the reinforcement • Effectiveness of inhibitors is enhanced when they are used in combination with hydrophobic coatings
Delamination/Reconstruction: only viable if deterioration of the total structure is very advanced	• Corrosion damage is generally confined to the near-surface regions of a structure and surveyors must guard against overestimation of damage

3.4.1 Patch Repairs

The approach to repairing damaged concrete structures depends on whether the corrosion is carbonation induced or chloride induced. Important aspects of traditional patch repair procedures are to:

1. Fully expose all corroded reinforcement by removing all cracked and delaminated concrete
2. Thoroughly clean the corroded reinforcement and apply a protective coating to the steel surface (e.g. anti-corrosion epoxy coating or zinc-rich primer coating)
3. Coat or seal the entire concrete surface to reduce the moisture levels in the concrete.

Patch repair has limited success against chloride-induced corrosion as the surrounding concrete may be contaminated with chloride and therefore, the reinforcement is still susceptible to corrosion. The patched area of new repair material often causes the formation of incipient anodes adjacent to the repairs as shown in Figure 3.4.

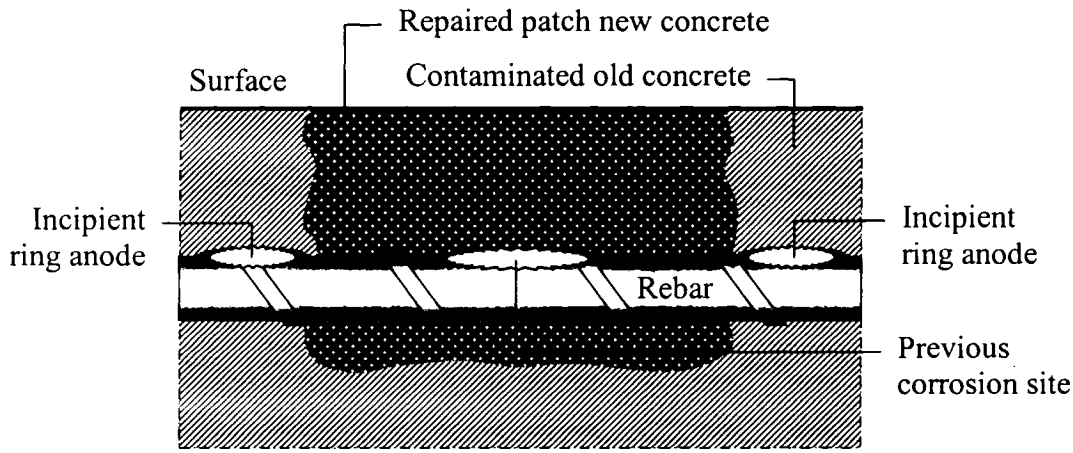

Figure 3.4: Formation of Incipient Ring Anode after Patch Repairs
(Adopted: Heckroodt, 2002)

These new corrosion sites not only affect the structure but often also undermine the repair, leading to accelerate ion of patch repair, failures in as little as two years. Consequently, it is necessary to remove all chloride-contaminated concrete in the vicinity of the reinforcement.

Complete removal of chloride-contaminated concrete should successfully halt corrosion by restoring passivating conditions to the reinforcement. Mechanical removal of cover concrete is usually done with a pneumatic hammer, hydrojetting or abrading machines. This form of repair is most successful when treating areas of localized low cover, before significant chloride penetration has occurred. If the corrosion damage has become fairly widespread, it is considered to be expensive to mechanically remove the chloride-contaminated concrete from depths well beyond the reinforcement. Electrochemical repair technique shows better performance to restore this type of damage.

3.4.2 Electrochemical Repair Techniques

It is not always feasible or ideal to remove and repair large sections of chloride-contaminated concrete. Electrochemical repair techniques are known as the potentially more efficient and ideal solution to repair the large chloride contaminated concrete sections. Furthermore, conventional repairs such as patch repairing, surface treatments, and reinforcement coatings can end up being low-cost solutions that may last over only a short term. As discussed earlier, conventional repairs can also be problematic if the new concrete overlays trap some remaining chloride ions, moisture and oxygen in the old concrete and actually initiate new corrosion. If a patch repair is not electrochemically compatible, and no additional repair measures are taken such as electrochemical techniques, corrosion may start in the surrounding areas. Some electrochemical repair techniques are stated below.

3.4.2.1 Realkalization

The electrochemical treatment consists of placing an anode system and sodium carbonate electrolyte on the concrete surface and applying high current density (typically $1 A/m^2$). The electrical field generates hydroxyl ions at the reinforcement and draws alkalis into the concrete. Table 3.10 and Figure 3.5 shows the general technical specifications and the basic principles of electrochemical realkalization techniques.

Table 3.10: General Technical Specifications for Realkalization and Chloride Extraction
(Vector Corrosion Technology, 2003)

Items	Technical Specification for Realkalization	Technical Specification for Chloride Extraction
Anode	Metallic mesh temporarily mounted on concrete surface	Metallic mesh temporarily mounted on concrete surface
Cathode	Existing steel reinforcement	Existing steel reinforcement
Electrolyte	Sodium carbonate solution	Fresh water (calcium hydroxide may be added)
Current density	1 A/m^2 of concrete surface	1 A/m^2 of concrete surface
Treatment Time	Three to seven days	Four to twelve weeks
Applied Voltage	Between 10 to 40 Volt (DC)	Between 10 to 40 Volt (DC)

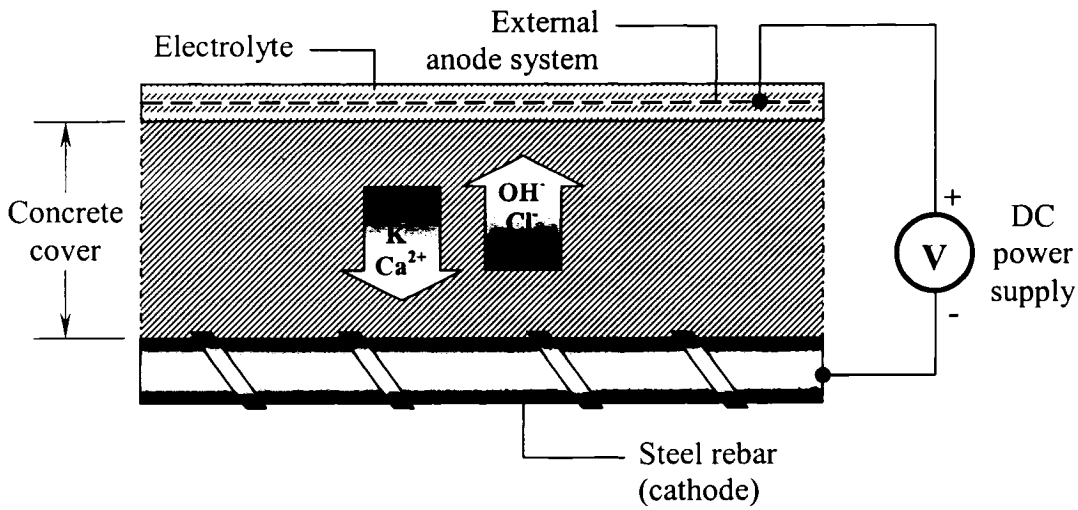

Figure 3.5: Electrochemical Realkalization / Chloride Removal Technique
(Heckroodt, 2002)

3.4.2.2 Electrochemical Chloride Removal (ECR)

Chloride removal is induced by applying a direct current between the reinforcement and an electrode that is placed temporarily onto the outside of the concrete. The impressed current

creates an electric field in the concrete that causes negatively charged ions to migrate from the reinforcement to the external anode. The technique decreases the potential of the reinforcement, increases the hydroxyl ion concentration and decreases the chloride concentration around the steel, thereby restoring passivating conditions. Table 3.10 and Figure 3.5 show the general technical specifications and the basic principles of electrochemical chloride removal (ECR) technique.

The effectiveness of ECR depends on several factors:

1. The extent of chloride contamination in the concrete
2. The structural configuration, including the depth and spacing of the reinforcement
3. The applied current density and the time of application
4. The pore solution conductivity and the resistance of the cover concrete
5. The presence of cracks, delamination and defects causing uneven chloride removal.

ECR typically takes four to twelve weeks to run at current densities within the normal range of 1-2 A/m^2. In some circumstances, chloride beyond the reinforcement may be forced deeper into the concrete during the process. There is a risk that chloride left in the concrete may diffuse back to the reinforcement and cause further corrosion with time.

The feasibility of using ECR depends on a number of factors:

1. The presence of major cracking, delamination and defects that require repair before ECR
2. Large variations in reinforcement cover cause differential chloride extraction and possible short-circuiting
3. Reactive aggregates require special precautions to avoid possible alkali-silica reaction (lithium salts should be used in these cases)
4. Prestressed concrete structures may be susceptible to hydrogen embrittlement after ECR (special precautions are needed to reduce this risk)
5. Temporary power supplies of significant capacity are required during the application of ECR.

3.4.3 Cathodic Protection Systems

Cathodic protection (CP) systems have an excellent record in the corrosion control of steel and reinforced concrete structures. If a third electrode is connected to the steel with a potential more negative than that of the corroding steel, then the rebar becomes cathodic in comparison to the new electrode and reinforcement corrosion is prevented. There are two basic forms of cathodic protection, which are illustrated in Figure 3.6 and 3.7, sacrificial anodes and impressed current method.

3.4.3.1 Sacrificial Anodes CP System

In sacrificial anode CP systems, the anode consists of metals higher than steel in the electrochemical series (e.g. zinc). By short-circuiting the sacrificial metal to the corroding steel bar, effectively a new corrosion cell is developed. The sacrificial metal becomes the anode relative to the steel and corrodes, hence the named sacrificial anode.

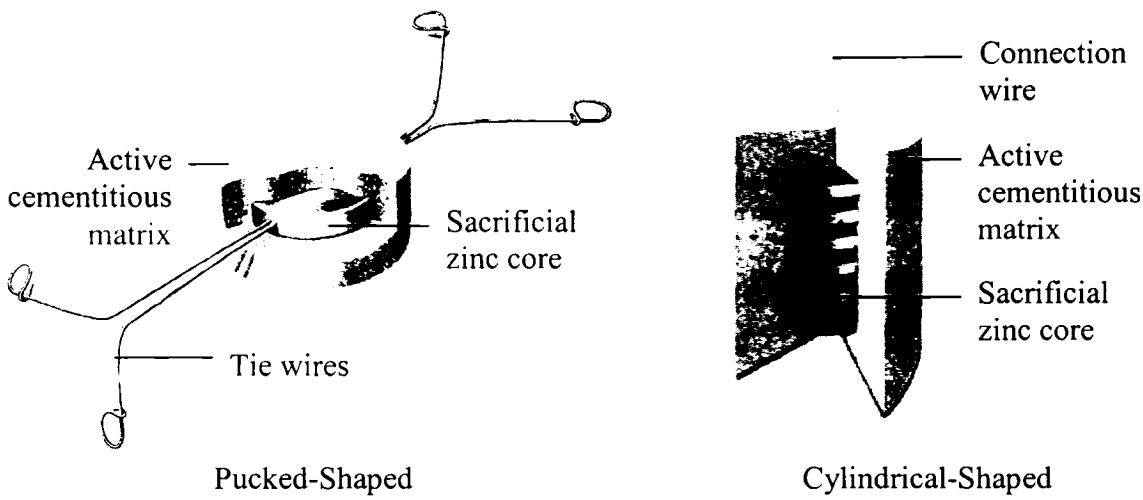

Figure 3.6: Different Sacrificial Anodes
(Vector Corrosion Technology, 2003)

The disadvantage of this technique is that it is only temporary because finally the anode corrodes completely. Furthermore, the protective efficiency of the sacrificial anode is never 100%, which means that the sacrificial metal always corrodes partly and independently of

the steel reinforcement (Scully, 1990). The mechanisms involved in this form of cathodic protection with an external sheet metal, are in fact similar to that of the galvanized steel (coated with zinc primer). Different forms of sacrificial anode systems are also being developed, apart from the standard sheet anode, which take the form of smaller zinc elements that can actually be embedded in the concrete (Figure 3.6).

3.4.3.2 Impressed Current CP System

Impressed current CP systems use an external electrical power source to supply electrons from the anode to the cathode. The anode is placed near the surface of the concrete cover and is connected to the reinforcement through a transformer rectifier that supplies the impressed current (Figure 3. 7). Anodes may be conductive overlays, titanium mesh within a sprayed concrete overlay, discrete anodes or conductive paint systems.

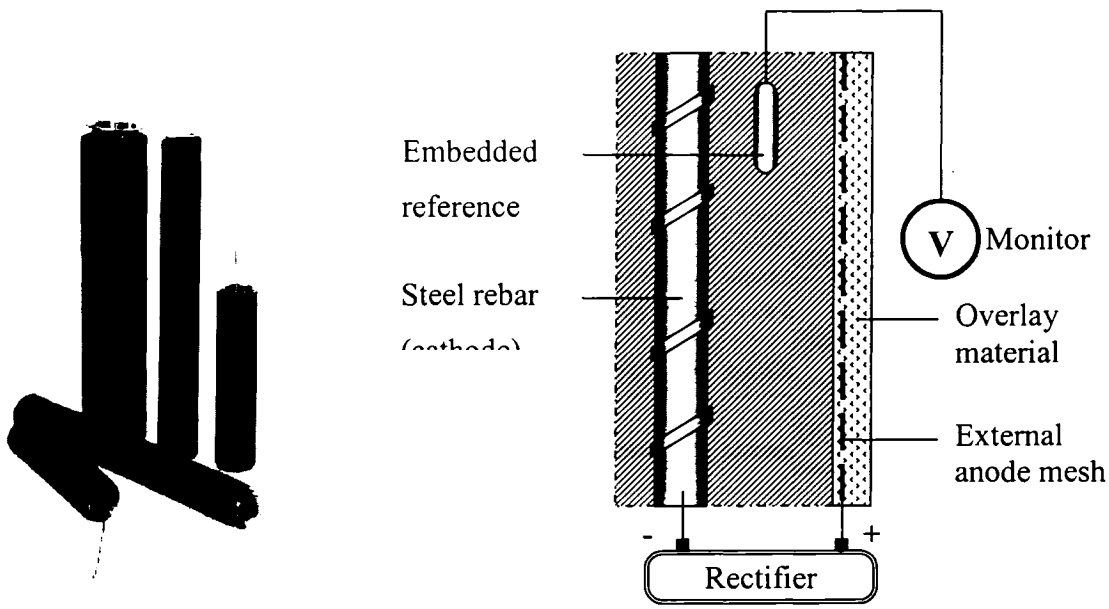

Discrete Anode

Anode with a Concrete Overlay

Figure 3.7: Typical Impressed Current Cathodic Protection System
(Vector Corrosion Technology, 2003, and Heckroodt, 2002)

CP repair of concrete structures requires a thorough corrosion survey by a specialist and design needs to be undertaken by a corrosion expert. Reliable CP systems are fully

controlled and monitored by a series of embedded sensors in order to ensure optimum performance. It is essential since any under-or overprotection of the reinforcement may be potentially harmful to operation of the CP system. Therefore, continuous monitoring of CP system is usually performed from a remote station.

3.4.4 Demolition or Reconstruction

This option should only be considered to be a last resort since the total cost (capital costs plus loss of service and temporary works) is usually well in excess of any repair costs. Engineer who have limited repair experience or lack of confidence in new repair systems often prefer demolition and reconstruction. Nevertheless, it is crucial that the lessons are learnt from the old structure when designing the replacement.

Chapter 4

Experimental Methodology

4.1 Overview

The basic philosophy of this experimental program was to establish relationship between different strategies of patch repair of corroded concrete deck slab with respect to two control specimens. Fifteen test slabs were constructed with the same geometrical configuration, including two control specimens. Different protective barriers were adopted for patch repair of different slab to mitigate corrosion. However, no protective barrier was used for control specimens. One of the control specimens was ponded with standard sodium chloride (NaCl) solution and other with potassium chloride (KCl) solution to accelerate corrosion. The main focus was to find how certain protective barrier result in compatibility between the chloride contaminated concrete and the uncontaminated new patch concrete, which will ensure effectiveness of corrosion mitigation.

4.2 Specimen Geometry

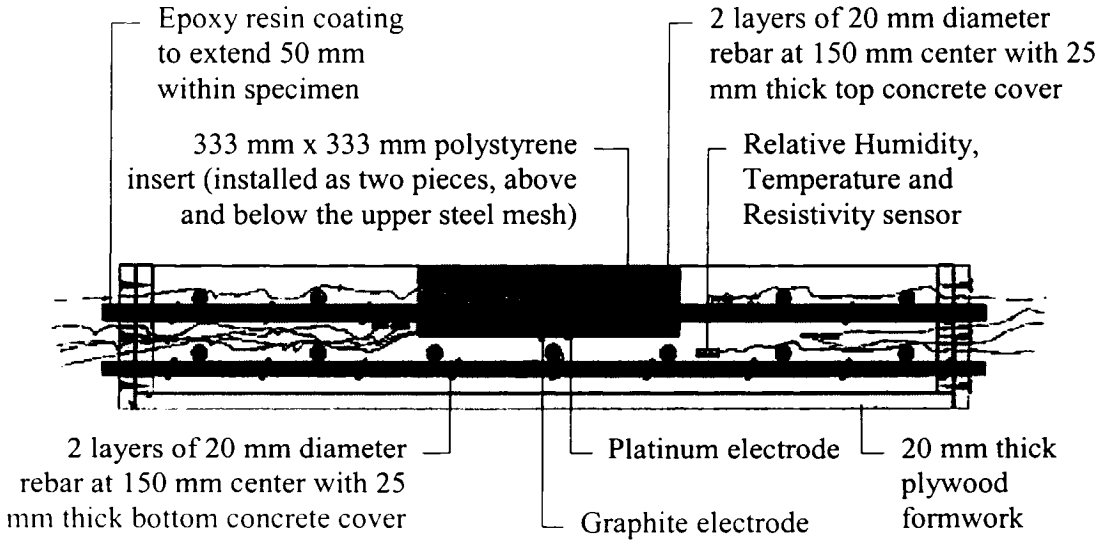

Figure 4.1: Cross-Section Details of a Typical Specimen
(Adopted: Leyne, 2004)

Each slab was 1000 mm long, 1000 mm wide and 200 mm deep. A uniform patch of 333 mm x 333 mm x 100 mm was created by placing two pieces of styrofoam during casting in the upper central part of the slab. Seven No. 20 deformed bars (19.5 mm diameter) were placed at 150 mm center to center in both directions in both layers. The properties of the steel reinforcing bars are shown in Table 4.4. A 25mm concrete clear cover was maintained over both top and bottom faces of the slab.

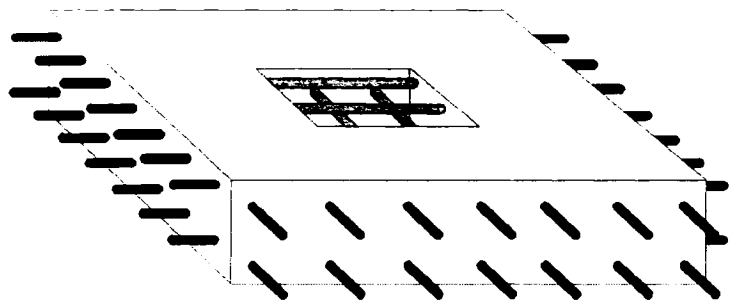

Figure 4.2: 3D View of a Typical Specimen
(Leyne, 2004)

All bars were extended on an average of 75 mm on each side of the slab. Figure 4.1 and 4.2 show the detailed cross-section and a three-dimensional view of a typical specimen.

4.3 Material Properties

Table 4.1: Concrete Mixture used for Casting of the Test Slabs
(Leyne, 2004)

Item	Quantity
Water	240 kg/m^3
Cement	450 kg/m^3
Limestone Coarse Aggregate (6-12 mm)	720 kg/m^3
St. Gabriel de Brandon Sand	1020 kg/m^3
Air Entraining Agent	300 ml/m^3

The Dickson Bridge in Montreal, was constructed in 1959 and demolished in 1989~1999 due to its severe deterioration (Leyne, 2004). To investigate the performance of different restoration techniques of this deteriorated deck slab, fifteen test slabs were cast in the laboratory using the same concrete mixture as was used for the construction of the deck of the bridge. Table 4.1 shows the mixture details, which was delivered by Lafarge Canada Inc.

Table 4.2: Concrete Mixture used for Construction of the Deck of Dickson Bridge
(Leyne, 2004)

Item	Quantity
Water	160 kg/m^3
Cement	320 kg/m^3
Fine Aggregate (Feldspatic Sand)	750 kg/m^3
Coarse Aggregate (Limestone) ¼"	800 kg/m^3
Coarse Aggregate (Limestone) ½"	216 kg/m^3
Total Coarse Aggregate	1016 kg/m^3
Air Entraining Agent	32 ml/m^3

The concrete mixture used for construction of the deck of Dickson Bridge is shown in Table 4.2 and its characteristics in Table 4.3.

Table 4.3: Characteristics of Dickson Bridge Deck Mixture used in the Present Investigation
(Leyne, 2004)

Item	Quantity
Water Cement (W/C) Ratio	0.5
28 days Compressive Strength	28 MPa
Air Content	5-6 %

Table 4.4: Properties of No. 20 Reinforcing Bars
(Leyne, 2004)

Nominal diameter	19.5 mm
Nominal yield strength	400 MPa
Modulus of elasticity	200 GPa

4.4 Test Procedure

The experimental program was implemented in two phases.

The Phase-I consisted of -

1. Construction of fifteen test slabs according to previously described geometry and concrete mixture design
2. Curing, ponding the "non-patch" region of each slab at a depth of 30mm using 15% salt solution, 3 days wetting and 4 days drying cycle, for a period of 5 months approximately
3. Initial ponding, repairing the patch region of different slabs using different restoration techniques
4. Continuing similar corrosion acceleration procedure to corrode the reinforcement of patch and "non-patch" region of each slab
5. Monitoring the corrosion activity of each slab including the half-cell potential, corrosion rate, crack pattern, macro-cell current flow, and relative humidity, resistivity and temperature
6. Coring of samples from patch and "non-patch" regions of each slab for chloride content test
7. Demolition of slabs S06, S08, S10, and S13 for visual inspection of corrosion of rebars.

Phase-II consisted of –

1. Determination of chloride content of the concrete powder obtained from the specified depth of patch and "non-patch" region of each slab
2. Demolition of remaining 11 slabs and extraction of the rebars
3. Establishment of visual records of the extracted bars by digital photography

4. Cleaning of rebars to remove concrete residue and rust using sand blasting
5. Calculation of average mass loss of each bar and comparing the results with different strategies of repair
6. Measurement of half-cell potential readings of slabs S02 and S05, keeping the slabs on metal frames, and then on wooden blocks to verify the influence of any grounding effect on the half-cell readings
7. Measurement of half-cell potential readings of the same slabs, filling new copper sulphate ($CuSO_4$) solution in the electrode, and then taking the reading after two weeks to check the effect of the age of the solution on the readings

4.4.1 Phase-I

Phase-I of this project was implemented by Leyne (2004). A brief description of this phase is included here for completeness.

4.4.1.1 Specimen Construction

Concrete specimens were cast in specially designed wooden moulds shown in Figure 4.3. Fourteen holes were drilled in each side of the mould, according to Figure 4.3.

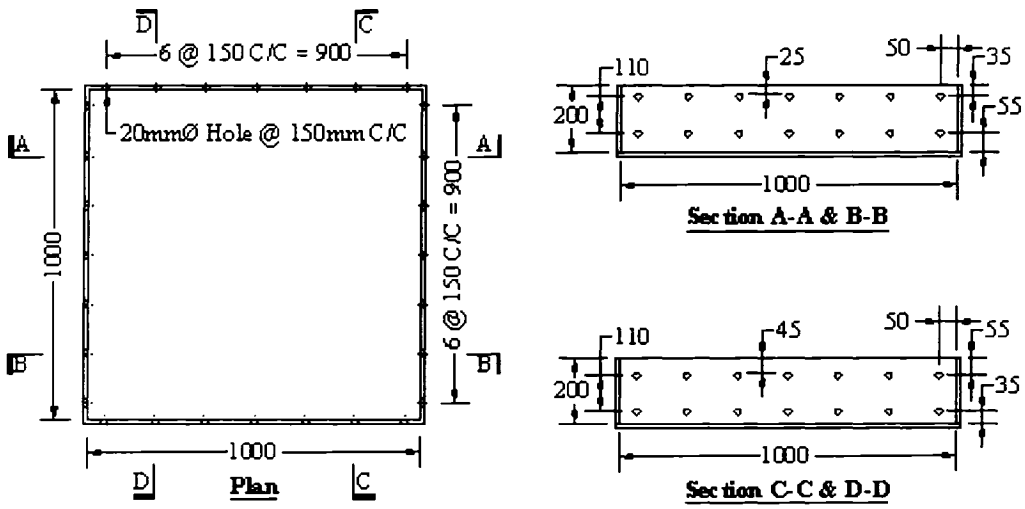

Figure 4.3: Dimension Details of a Typical Mould

All 20 mm diameter steel bars were extended beyond the holes by 75 mm from the inner face of the mould. A length of 125 mm at each end of each bar was coated with epoxy resin so that 50 mm of coated portion would remain inside the concrete. The objective of coating the ends of the bars was to protect the interface between the steel bars and the surface of the concrete specimen from corrosion. Two pieces of styrofoams were placed on the upper and lower face of the top mesh of the bars to develop a 333 mm x 333 mm x 100 mm patch in the upper central part of the slab during casting. Proper care had been taken to place the concrete underneath the styrofoam. The specimens were moist-cured in the moulds for 48 hours, when the formwork was removed and the sides of all specimens were coated with an epoxy resin to prevent any moisture from escaping from inside the concrete. Styrofoam from the patch area was also removed. The specimens were placed on especially constructed steel frames for the long-term testing in the laboratory. Grid lines were drown on top of each slab to identify 49 nodal points for half-cell potential measurements.

Different sensors, installed during the casting, were connected with the data acquisition system and computer to monitor the relative humidity, resistivity, and temperature.

4.4.1.2 Wetting and Drying Cycles

Before starting wetting and drying cycles, a simulated concrete pore solution [composition of 0.14M NaOH, 0.23M KOH, and 0.002M $Ca(OH)_2$] with a pH of 13.4 was prepared to fill the patch region (Leyne, 2004). The objective of using pore solution was to create an artificial alkaline environment around the patch steel. The function of the pore solution was to reduce any electrochemical differences between the patch region and the surrounding area, and to eliminate any possibility of macrocell corrosion that could result in the exposed patch, and the remaining steel acting cathodically, which would be opposite to the goal of the conditioning period (Leyne, 2004).

A 60 mm high and 25 mm thick styrofoam was glued with silicon sealing around the outer edge and patch edge of each slab to pond the salt solution. The "non-patch" steel of each slab was corroded in an accelerated manner using 15% (by mass of water) salt solution, and

3-days wetting and 4-days drying cycle, for a period of five-months. To eliminate any change in the concentration, the salt concentration was checked weekly and adjusted to the required percentage. Constant solution depth of 30mm was also maintained.

All slabs, except for slabs S10 and S11 were ponded with NaCl solution. However, slab S10 and S11 were ponded with KCl solution. The KCl was used specifically to test concrete additives of one of the commercial partners, used in the restoration stage, which was believed to be potentially valuable for corrosion mitigation in the potash industry.

4.4.1.3 Patch Repair

When corrosion in "non-patch" region of each slab was actively detected by half-cell potential measurement after 5 months of wetting and drying cycle, repair phase was commenced with the removal of the pore solution from all of the patch regions. Corrosion activity monitoring is discussed in detail in Section 4.4.1.4. Patch steels of slab S02 were treated with epoxy primer, S03 and S07 were treated with zinc primer, and S11, S12 and S13 were treated with corrosion inhibitor grout (CI-G). An embedded sacrificial anode was installed at a corner of the patch region of slab S08. Following the mixture design of Table 4.5, required $0.011 m^3$ of concrete to be prepared for each slab. Patches were then filled in succession with the prepared mixture except for slabs S11, S12, and S13.

Table 4.5: Concrete Mixture for Patch Repair
(Leyne, 2004)

Water	144 kg/m^3
Cement	320 kg/m^3
Coarse Aggregate (Stone)	1280 kg/m^3
Fine Aggregate (Sand)	785 kg/m^3

Six millilitres of corrosion inhibitor admixture / superplasticizer (CI-A) was added in each concrete mixture for patches of slabs S11, S12, and S13, as part of their specific restoration strategies. Then the patches were filled with the new mixture. After repairing of all patches,

and hardening of the patch concrete, surface coatings were applied on the top of the selected slabs.

Before applying coating on slabs S04, S05, S06, and S07, 20 mm diameter and 50 mm high plastic tubes were glued to the concrete surface at each grid point of the slabs to allow the half-cell electrode to be brought in contact with the concrete surface. Coatings were then applied around the tubes. Concrete top surface of slabs S04 and S05 were treated with penetrating sealer and epoxy coating respectively, slabs S06, S07 and S09 were treated with breathable membrane, slab S13 was coated with corrosion inhibitor surface treatment (CI-S), and slab S14 was treated with both zinc sheet anode and epoxy coating. Zinc sheet of slab S14 also needed to cut at each grid point for similar reason. After all of the repairs were completed, the slabs were corroded again using a similar acceleration procedure for next fifteen months, and different electrochemical and other tests were performed to monitor the corrosion activity of each slab. Different designations and treatments of patch repair are presented in Table 4.6.

Table 4.6: Specimen Designation and Treatment
(Leyne, 2004)

Slab No.	Designation	"Patch" Steel Treatment	"Patch" Concrete Mixture	Concrete Top Surface Treatment	Ponding Solution	Comments
S01	Control A	None	Standard	None	NaCl	Standard control mixture
S02	Epoxy Primer	Epoxy	Standard	None	NaCl	Evaluation of effect of epoxy steel primer compared to S01
S03	Zinc Primer	Zinc	Standard	None	NaCl	Evaluation of effect of zinc steel primer compared to S01
S04	Penetrating Sealer	None	Standard	Sealer	NaCl	Evaluation of effect of breathable surface sealer compared to S01
S05	Epoxy Coating	None	Standard	Epoxy	NaCl	Evaluation of effect of impermeable barrier compared to S01
S06	Membrane	None	Standard	Membrane	NaCl	Evaluation of effect of breathable membrane compared to S01
S07	Membrane and Zinc Primer	Zinc	Standard	Membrane	NaCl	Evaluation of effect of breathable membrane in conjunction with zinc primer
S08	Embedded Anode	None	Standard	None	NaCl	Evaluation of effect of embedded anode system compared to S01
S09	Membrane	None	Standard	Membrane	NaCl	Evaluation of effect of breathable membrane compared to S01
S10	Control B	None	Standard	None	KCl	Comparison between NaCl and KCl ponding
S11	Inhibitor	Inhibitor	Inhibitor	None	KCl	Evaluation of effect of integrally mixed inhibitor compared to S10
S12	Inhibitor	Inhibitor	Inhibitor	None	NaCl	Evaluation of effect of integrally mixed inhibitor compared to S01
S13	Inhibitor and Surface Coating	Inhibitor	Inhibitor	Inhibitor	NaCl	Evaluation of effect of integrally mixed inhibitor and surface treatment compared to S01
S14	Zinc Sheet Top	None	Standard	Zinc Sheet and Epoxy	NaCl	Evaluation of effect of zinc sheet on top surface compared to S01
S15	Zinc Sheet Bottom	None	Standard	None	NaCl	Evaluation of effect of zinc sheet on bottom surface compared to S01

4.4.1.3.1 Treatment Details

In this section treatment of different slabs are presented in details.

Slab S01: This slab was treated as reference slab-1, and designated by **Control A**. Therefore, no additional protective barrier against corrosion was adopted. It was repaired with standard patch mixture concrete (Table 4.5) and ponded with NaCl solution.

Slab S02: Patch steels were painted with **Epoxy Primer**. After that it was repaired with standard patch mixture concrete (Table 4.5) and ponded with NaCl solution.

Slab S03: Patch steels were painted with **Zinc Primer**. After that it was repaired with standard patch mixture concrete (Table 4.5) and ponded with NaCl solution.

Slab S04: After repairing the patch with standard patch mixture concrete (Table 4.5), and hardening, standard silane-based **Penetrating Surface Sealer** was painted on the concrete surface with an ordinary paintbrush. This type of surface treatment is not meant to be a waterproofing system. It is based on the principles of water-repellence through the pores. For this reason, it is expected to allow a degree of **moisture both in and out** of the slab. The slab was then ponded with NaCl solution.

Slab S05: After repairing the patch with standard patch mixture concrete (Table 4.5), and hardening, standard **Epoxy Surface Coating** was applied. The coating was mixed in the laboratory and painted on the surface of the slab. This type of surface treatment is meant to be an impermeable system. In other words, it is a "non-breathable" coating, which is **not expected to allow moisture in or out** of the slab. The slab was then ponded with NaCl solution.

Slab S06: After repairing the patch with standard patch mixture concrete (Table 4.5), and hardening, **Traffic-Bearing Waterproofing Membrane** was applied. The liquid elastomeric coating was applied or painted on the slab. First, the surface was coated with a

standard concrete primer, and then within 24 hours the polyurethane base coat was applied, followed by the polyurethane topcoat or wearing surface. Silica (quartz) sand was immediately spread onto the wet surface coating, and when dry, all excess aggregate was removed and the surface was re-coated with the polyurethane topcoat. This type of surface treatment is designed to be a "breathable" system, allowing **moisture out but not into the slab**. The slab was then ponded with NaCl solution.

Slab S07: In this repair strategy, two barriers were combined together, **Traffic-Bearing Waterproofing Membrane** for concrete top surface treatment and **Zinc Primer** for patch steel coating. Patch steel and concrete top surface were treated following the procedure of slabs S03 and S06, respectively. The slab was then ponded with NaCl solution.

Slab S08: Before casting the patch with standard patch mixture concrete (Table 4.5), **Sacrificial Embedded Anode** was installed in the patch region. The galvanic embedded anode was designed as a small puck-shaped anode, 64 mm diameter by 27 mm height, with a sacrificial zinc core surrounded by cementitious mortar. The anode was fastened to the exposed top steel mat, in one corner of the simulated repair area, as close as possible to the edge of the surrounding contaminated concrete. It was then connected to the reinforcing steel through an externally mounted switch, so that it could be effectively turned on or off to enable comparisons of data, and also to allow manual control of the anode. The slab was then ponded with NaCl solution.

Slab S09: Similar to treatment of slab S06 i.e., **Traffic-Bearing Waterproofing Membrane** was applied on this slab except no plastic tubes were glued on the each grid point of the slab. The slab was then ponded with NaCl solution.

Slab S10: This slab was also treated as the reference slab-2, designated as **Control B**. Therefore, no additional protective barrier against corrosion was adopted. It was also repaired with same standard patch mixture concrete (Table 4.5), but it was ponded with KCl solution.

Slab S11: For this slab **Corrosion Inhibitor System with KCl Ponding** was assigned. This system was designed as a unique migratory corrosion inhibitor system, and was made up and applied as three components. The first component was a surface treatment (CI-S), which was brush-applied to the exposed concrete that was to receive the patch repair concrete (i.e. the inside of the patch zone), however, no top surface treatment was applied. This corrosion inhibitor product was designed to penetrate and migrate throughout the concrete structure. The second component was a passivating grout (CI-G) that was applied to the exposed reinforcement in the patch. Finally, the third component was a liquid concrete admixture (CI-A), a corrosion inhibiting superplasticizer that was added to the standard patch mixture concrete (Table 4.5).

Slab S12: Similar treatment as for slab S11, but different exposure environment was created i.e. **Corrosion Inhibitor System with NaCl Ponding** was adopted.

Slab S13: Similar treatment as for slab S12 i.e. **Corrosion Inhibitor System with NaCl Ponding** was applied on this slab but in addition, this slab received corrosion inhibitor surface treatment (CI-S) on it. After the concrete patch had cured for 7 days, a coat of the corrosion inhibiting surface treatment (CI-S) was applied over the entire concrete surface.

Slab S14: After repairing the patch with standard patch mixture concrete (Table 4.5), and hardening, **Sacrificial Sheet Anode on Top Surface** was installed. This system, like slab S08 was designed as a galvanic cathodic protection system, but with external sheets as opposed to an embedded puck. The anode was made up of 0.25mm thick zinc foil, which was coated with an ionically conductive pressure sensitive adhesive with an embossed polypropylene release liner. The foil was laid out on the surface of the specimen in three strips and a connection was made to the reinforcement by means of an external switch. The strips were made electrically continuous by soldering a connection between them. Finally, the zinc sheets were covered with an epoxy surface coating, to protect the top surface of the zinc from the ponding, and for aesthetic purposes. The slab was then ponded with NaCl solution.

Slab S15: After repairing the patch with standard patch mixture concrete (Table 4.5), and hardening, similar treatment of slab 14 i.e. **Sacrificial Sheet Anode on Bottom Surface** was installed. Due to its position on bottom, no epoxy coating was needed. The slab was also ponded with NaCl solution.

4.4.1.4 Corrosion Activity Monitoring

This is the major part of this experimental program, which was started after the construction period and performed periodically, as required, and continued until end of the program but temporarily suspended during the repair stage. The corrosion activity monitoring included half-cell potential measurements, corrosion rate measurements, crack pattern monitoring, macrocell current measurements, computer monitoring of embedded sensors, and manual humidity readings are stated below.

4.4.1.4.1 Half-Cell Potential (HCP) Measurement

The objective of using this test method was to estimate electrical half-cell potential of the uncoated reinforcing steel bars of test specimens for the purpose of determining their corrosion activity. This method does not provide the actual rate of corrosion but only the probability of corrosion of the investigated region, which requires further examination in case of higher value. ASTM C 876-91 was followed to perform this test.

A half-cell potential measurement instrument was used for this test. The instrument consists of a voltmeter and a reference half-cell. The reference half-cell was a copper-copper sulphate cell but other combinations could be used (Bungey and Millard, 1996). It consisted of a rigid tube or container, composed of a dielectric material that is non-reactive with copper or copper sulphate, a porous wooden or plastic plug that remains wet by capillary action, and a copper rod that is immersed within the tube in a saturated solution of copper sulphate. A sectional view of a copper-copper sulphate half-cell is shown in Figure 4.4. The solution was prepared with reagent grade copper sulphate crystals dissolved in distilled or deionized water and it was considered saturated when an excess of crystals (undissolved) appeared at the bottom of the solution.

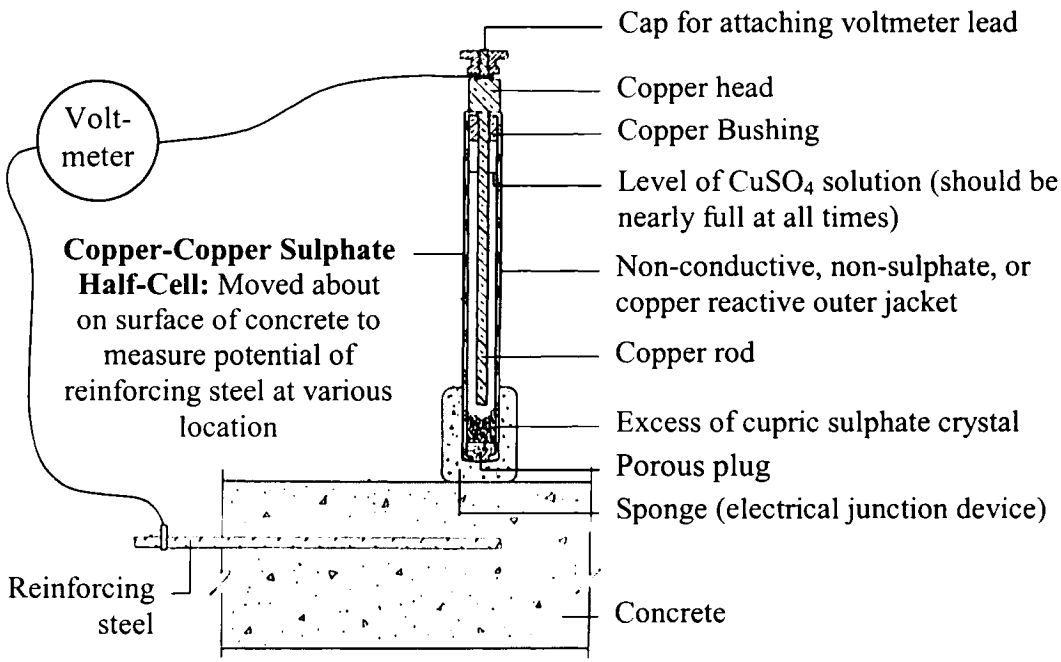

Figure 4.4: Sectional View of a Copper-Copper Sulphate Half-Cell and its Circuitry (ASTM C 876-91)

After "de-ponding" of salt water before each drying cycle, half-cell readings were taken on a weekly basis, at 49 nodal points designated as A1 ... G7, are shown in Figure 4.5.

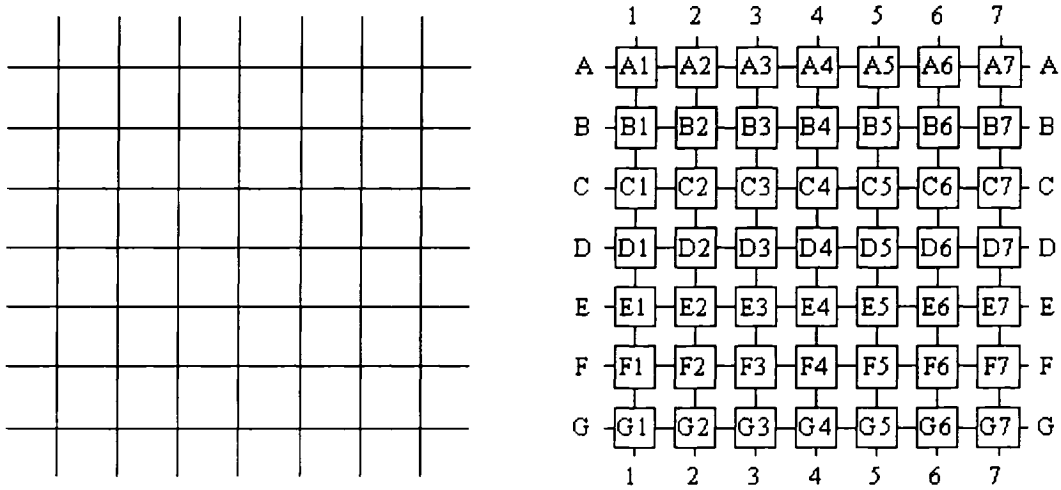

Typical Reinforcement Orientation

Nodal Points for Half-Cell Measurements

Figure 4.5: Typical Reinforcement Orientation and Nodal Positions

The positive terminal of the voltmeter was connected to the uncoated exposed part of the reinforcement and the negative terminal was connected to the electrode. Then, the electrode was placed at each nodal point to take the voltmeter reading when the reading was stable. Contact surface between the electrode and the concrete was kept wet during measurements. The results were then used to produce contour map of the half-cell potentials to study the probability of active corrosion in the different regions of the slab specimen according to Table 4.7.

Table 4.7: Interpretation of Half-Cell Potential vs. Probability of Corrosion Guideline
(Bungey and Millard, 1996)

Half-Cell Potential (mV)	Probability of Corrosion (%)
<-350	90
-200 to -350	50
>-200	10

4.4.1.4.2 Corrosion Rate Measurement

Linear Polarization Resistance (LPR) measurement is a perturbative electrochemical technique to determine the corrosion rate by measuring the response of corrosion interface to a small perturbation (Bungey and Millard, 1996).

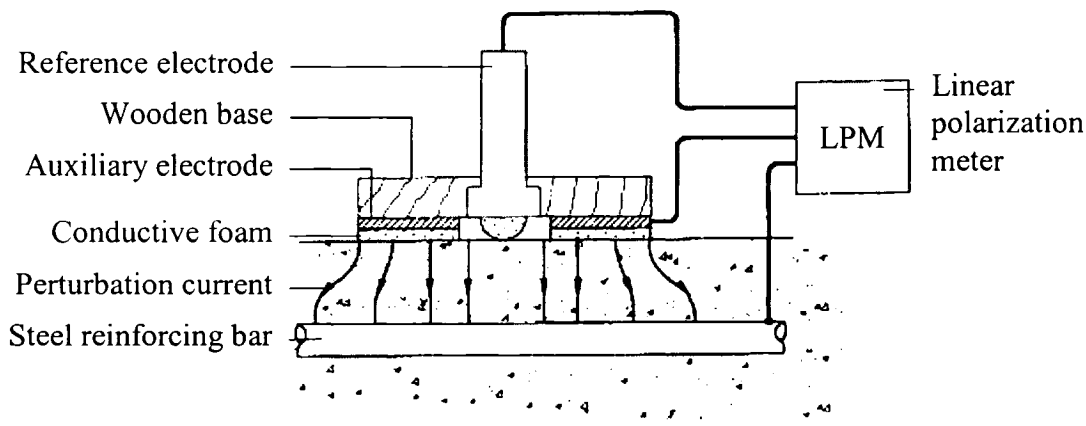

Figure 4.6: Linear Polarization Resistance Set-Up
(Bungey and Millard, 1996)

The LPR measurement was carried out by applying a small electrochemical perturbation to the steel reinforcement via an auxiliary electrode placed on the concrete surface (Figure 4.6). The perturbance was often a small DC potential charge, ΔE, to the half-cell potential of the steel in the range ± 20 mV. After a suitable equilibration time, typically 30 seconds to 2 minutes, the polarization resistance, R_p was obtained from a measurement of the resulting current, ΔI, where:

$$R_p = \frac{\Delta E}{\Delta I} \quad \ldots \quad \ldots \quad \ldots \quad (4.1)$$

Again, R_p is inversely proportional to the corrosion current, I_{corr} flowing between anodic and cathodic regions on the surface of the steel bar. Hence,

$$I_{corr} = \frac{B}{R_p} \quad \ldots \quad \ldots \quad \ldots \quad (4.2)$$

where, for steel in concrete the value of B normally is in between 25mV (active) and 50mV (passive). Then, the corrosion current density, i_{corr} is evaluated from:

$$i_{corr} = \frac{I_{corr}}{A} \quad \ldots \quad \ldots \quad \ldots \quad (4.3)$$

where A is the surface area of the steel bar that is perturbed by the test. Typical values of I_{corr} and the resulting rate of corrosion penetration are shown in Table 4.8.

Table 4.8: Typical Corrosion Rates for Steel in Concrete
(Bungey and Millard, 1996)

Corrosion Intensity	Corrosion Current Density, i_{corr} ($\mu A/cm^2$)	Corrosion Rate, *CR* (μm/year)
High	10-100	100-1000
Medium	1-10	10-100
Low	0.1-1	1-10
Passive	<0.1	<1

It was planned to conduct the corrosion rate measurements on a monthly basis using the linear polarization resistance method (LPR), however, a problem was detected with the

results when the first set of reading was completed. After much investigation, it was concluded that the LPR could no longer be used, and the Tafel plot method was used instead to determine the corrosion rates.

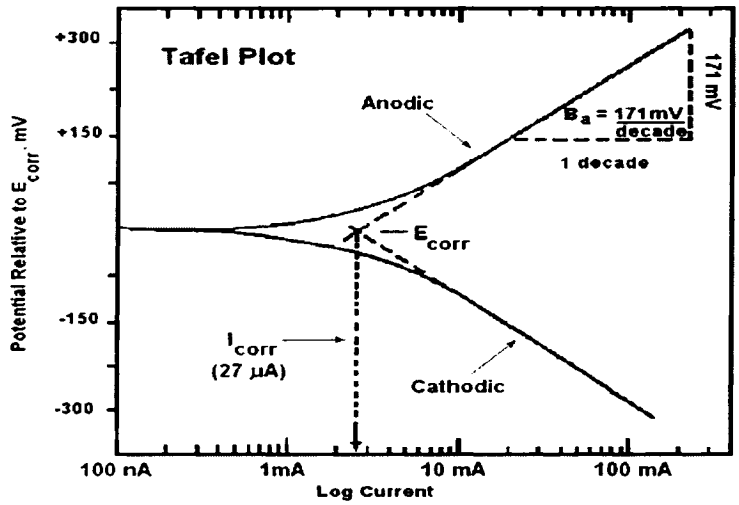

Figure 4.7: Typical Tafel Plot
(Ismail and Soleymani, 2002)

In the Tafel plot method, the applied potentials are scanned from E_{corr} to (E_{corr} ± 250) mV in cathodic and anodic direction, and plotted against the measured current on a log scale. It usually takes about 45 minutes to conduct the test. This plot provides a direct measure of the corrosion current, which can be used to calculate the corrosion rate. The slope of the linear portion of the Tafel Plot is called the Tafel constant, which is used in the polarization resistance measurements to calculate the corrosion current density, i_{corr}. A typical Tafel plot is shown in Figure: 4.7 and the theoretical derivation of Tafel equations are presented in Section 5.5.1 in Chapter Five.

The corrosion rate was measured at two locations for each slab, one in the upper region where the top steel surrounded the repair and another at the patch region. Due to the complication of arranging the testing equipment (potential scanner), it was not possible to

take monthly reading during the monitoring stage from June 2002 to August 2003. Only six sets of Tafel plots were produced from March 2003 to August 2003.

4.4.1.4.3 Crack Pattern Monitoring

Along the lines of the bar of top surface of each slab, crack widths were measured with appropriate crack width ruler; crack pattern were monitored, and sketched at a four moths interval through the monitoring stage.

4.4.1.4.4 Macro-Cell Current Measurement

Macrocell voltage drops were measured eight times during the monitoring stage between top and bottom mesh of each slab with a standard voltmeter. Same resistors were used for all slabs and then the macrocell currents were calculated using Ohm's law, $V = IR$.

4.4.1.4.5 Humidity, Resistivity and Temperature Monitoring

Different sensors were installed inside the patch and non-patch areas of each slab during the construction stage, and connected them with a data acquisition system and computer to measure humidity, resistivity and temperature. Special software was installed to take the reading at four-hour intervals. However, the system failed to produce any useable data due to over-saturation of the embedded sensors during the construction stage. However, it was important to know the variation of relative humidity between the coated and the uncoated slabs. Therefore, three holes were drilled and fitted with plastic tube and cap at upper, lower, and patch region of each slab. Humidity readings were then taken manually with a hygrometer at different points during the monitoring stage.

4.4.1.5 Coring of Sample for Chloride Content Test

Two samples were taken from each slab, one from the patch region and another from "non-patch" region of each slab. Standard 100 mm diameter core cutter was extended to the entire depth of the slab to get a 100 mm diameter by 200 mm high sample. Forty mm slice was taken at 25 mm from the top surface of the slab to represent the chloride content at the

center of top mesh bars. Thirty samples were taken form patch and "non-patch" region of each slab and kept in thirty different plastic bags to avoid mixing.

4.4.1.6 Demolition and Visual Examination

Slabs S06, S08, S10, and S13 were demolished to extract the bars for visual examination. A conventional hydraulic jackhammer was used to demolish the slabs. The bars were then cleaned properly from the concrete residue, labeled them, and placed them into the casting mould according to their original position, to get the visual image of corrosion. Subsequently, the rusting patterns were examined visually.

4.4.2 Phase-II

Phase-II of this project was implemented by the author. A detailed description of this phase follows:

4.4.2.1 Chloride Content Determination

According to ASTM C 1218-92: *Standard Test Method for Water-Soluble Chloride in Mortar and Concrete*, thirty samples were prepared and percent chloride content (by mass of concrete) was determined. A brief description is presented below.

4.4.2.1.1 Sample Preparation

According to Section 4.4.1.5, two 40 mm thick and 100 mm diameter slices were taken from two concrete cores of each slab..A total of thirty samples were collected to determine the chloride content by mass of concrete at the level of top mesh bars of each slab. Each sample was broken into small pieces (less than 25mm in maximum dimension) by an iron hammer, and crushed by electric rotating-puck grinding apparatus to convert it to powder. The ground sample was passed through 850 μm (No. 20) sieve and stored in a ziploc plastic bag. It took approximately 45 to 60 minuets to produce 30 to 40 gm of powder for each sample. The same procedure was followed to prepare all other samples. Care had been taken to avoid mixing of the different samples.

4.4.2.1.2 Test Procedure

A sample weighing 10 gm was obtained from the previously prepared sample, using a ±0.001 gm sensitive digital balance into a 250 ml beaker and dispersed with 75 ml of water. Without delay 25 ml of 1:1 nitric acid was added slowly and any lumps were broken, with a glass rod. Three drops of methyl orange indicator were added and stirred. The beaker was covered with a glass and allowed to stand for 1 to 2 min. Additional dilute nitric acid (1:1) was added in drops and stirred until a faint pink or red color persisted, and another 10 drops were added. The covered beaker was heated rapidly to boiling, and removed from the hotplate.

A 9 cm diameter coarse textured filter paper (No. 42) was placed on a Büchner funnel and wetted with small amount of water. The funnel was placed on a 500 ml filtration flask. The sample solution was filtered using the suction apparatus into the flask. The filtrate was transferred to the beaker and rinsed the flask once with water. Care was taken to keep the volume of the solution not more than 175 ml.

Two milliliters of 0.05N sodium chloride (NaCl) solution was pipetted into the sample solution. The beaker was placed on a magnetic stirrer and a TFE-fluorocarbon-coated magnetic stirring bar was used to stir the solution gently. A chloride ion electrode was immersed into the solution taking care that the stirring bar did not strike the electrode, and then connected to a potentiometer. A burette filled with 10 ml, 0.05N silver nitrate ($AgNO_3$) solution was clamped vertically above the sample solution.

Titration was started gradually with an increment of 0.2 ml $AgNO_3$ solution, and the corresponding milli-voltmeter readings were recorded when the minimum scale reading did not change within a period of two minutes. As the equivalence point was reached, the equal additions of $AgNO_3$ solution caused larger and larger changes in the milli-voltmeter readings. The titration was continued for another three readings past the approximate equivalence point. The burette reading and the corresponding potentiometer reading were

recorded on a data sheet to calculate percentage of the chloride content in the concrete. The calculation procedure is presented in Chapter Five, Section 5.3.1.

4.4.2.2 Demolition of Remaining Slabs

The next priority of this phase of the work was to demolish the remaining 11 slabs and to extract the rebars. It was essential to identify the rebars correctly in their current locations within the slabs, including their orientation so that they can be re-positioned within the wooden forms in their exact positions. For this purpose, vertical arrows were first be permanently marked on the ends of the bars. Bars were also relabelled to avoid the risk of loosing old labels during the crushing operation. A typical labelling convention of S01-1B ... S01-AT etc were maintained, where the designation, 'S01' represents the slab number varying from S01 to S15, '1' or 'A' represents bar number varying from 1 to 7 in numeric direction and A to G in alphabetic direction, and 'B' or 'T' represents bottom or top position of the bars. Typical orientation of the bars for each slab is presented in Figure 4.5. After marking and labelling, the slabs were demolished using a hydraulic jackhammer. Care was taken to avoid any local damage of the bars by the hammer. Seven bars of each layer were bundled into a group and placed in a designated place to identify them easily for the next set of tests.

4.4.2.3 Visual Records of Corrosion

At this stage the top and bottom bars of each slab were placed separately in a wooden frame according to their original position and orientation. The vertical arrows of all bars were set upward to have the same orientation as before demolition. Digital photography of upper face of top mesh was performed. Each bar was turned through 180° to obtain the photograph of the lower face of the same mesh. Same procedure was applied for the bottom bars, as well as all other slabs. The bars were again bundled and placed in the same location for further use.

4.4.2.4 Cleaning of Rebars

According to ASTM G 1-90, methods for cleaning corrosion product can be divided into three categories: mechanical, chemical, and electrolytic.

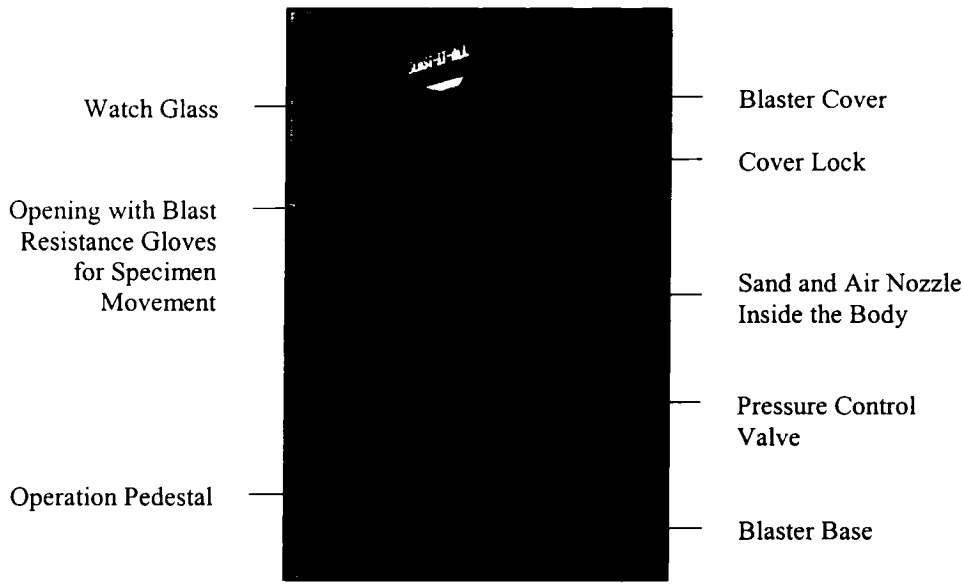

Figure 4.8: Sand Blaster

Chemical procedures involve immersion of the corroded specimen in a specific solution that is designed to remove the corrosion products with minimal dissolution of any base metal. Electrolytic cleaning such as cathodic treatment with carbon, platinum or stainless steel anode can also be utilized for removal of the corrosion products. Mechanical procedures includes scraping, scrubbing, brushing, ultrasonic cleaning, mechanical shocking, impact blasting (for example, sand blasting, water-jet blasting, etc). However, vigorous mechanical cleaning can result in the removal of some base metal, therefore, care should be exercised, and an appropriate mechanical force should be maintained to avoid base metal loss.

In this project, sand blasting was used to clean the bars. Initially mechanical wire brush was used but it was found that small concrete particles and corrosion products inside the pits

were not cleaned properly. Therefore, it was decided to use the sand blaster (Figure 4.8). It showed good results in the remove of the concrete residue and rust from the bars properly. Care had been taken to hit the bar with sand jet uniformly to avoid the base metal loss. An 80-psi constant pressure of the jet was maintained throughout the cleaning procedure. After cleaning, the bars were bundled again for the next procedure.

4.4.2.5 Calculation of Average Mass Loss

The length and mass of each bar were measured separately with a measuring tape and a digital weighing machine (Figure 4.9) with precision of 0.1cm and 0.1gm respectively. Then, the mass per unit length of each bar was calculated to obtain the percentage of the mass loss, and finally to obtain the average percent mass loss of the patch and the non-patch region of each slab and compare them with the results from the control specimens (S01 and S10).

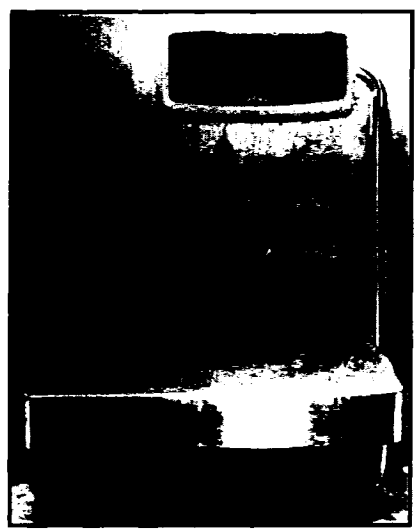

Figure 4.9: Digital Weighing Machine

4.4.2.5.1 Mass Loss of Patch Steel and Non-Patch Steel

According to the slab geometry (Figure 4.1 and 4.2) and bar orientation (Figure 4.5), six bars (3, 4, 5, and C, D, E) of top mesh were located in the patch area. Therefore, it was important to separate the patch steel from the "non-patch" steel rebars. For this purpose, the

bars designated as 3, 4, 5, and as C, D, E of the top mesh of each slab, were separated from their respective bundles, the middle length of 333 mm was marked by a marker, three parts of each bar were labeled to avoid mixing after cutting it using an electric saw. The same procedure was followed to calculate the percentage mass loss of the middle six bars of each slab and to compare these results for the different strategies of repair as well as effect of patch and non-patch environment upon corrosion.

4.4.2.6 Monitoring Grounding Effect on Half-Cell Readings

During this stage, slabs S02 and S05 were investigated before their demolition. Wooden blocks were placed under the slabs and on the metal frames to isolate them from the frames as well as from the ground. A styrofoam sheet measuring 60 mm high and 25 mm thick was glued with silicon for sealing along the outer edge of each slab and the core holes. The top surface of the slabs was then flooded with water and left to saturate for 7 days. After drying, half-cell readings were taken at each nodal point of the two slabs. The tests were repeated after removal of the wooden blocks. Comparing the two sets of data for each position, it was determined that the grounding of the metal frames did not have any adverse effect on the half-cell readings.

4.4.2.7 Monitoring Age Effect of $CuSO_4$ Solution on Half-Cell Readings

During this stage, slabs S02 and S05 were also investigated before their demolition. New copper sulphate ($CuSO_4$) solution was filled into the sulphate ion electrode and half-cell readings were taken at each nodal point of the two slabs. After 15 days, similar readings were taken keeping the slabs in their previous positions. Comparing the two sets of data for same electrolyte solution but at different intervals, helped to determine whether the age of the electrolyte solution adversely influence the half-cell readings, or not.

Chapter 5
Results and Discussion

5.1 Introduction

This chapter presents analysis of different data obtained from different laboratory investigations, along with appropriate tables and graphs to represent different outputs, and the results and discussion of the observations. Different non-destructive and destructive tests were performed to monitor corrosion activity of the specimens. Non-destructive tests include the half-cell potential measurements, corrosion penetration rates (CPR) measurement by the Tafel test, crack pattern monitoring, macrocell current measurements, internal humidity and temperature monitoring, and visual imaging of the corrosion of the steel reinforcement. Destructive tests include chloride content determination and mass loss calculation. Samples are taken from the "patch" and the "non-patch" regions of each slab using a concrete core cutter for chloride content tests and the slabs were then demolished using a hydraulic jack hammer for recovering the steel rebars for the mass loss test. The various investigations and observations are presented in the following sections.

5.2 Half-Cell Potential (HCP) Measurement

The description and procedure of this experiment are presented in Chapter Four. As mentioned earlier, the half-cell readings were taken on the "non-patch" region of each slab before the patch repair to check for initiation of corrosion, and on the "patch" and the "non-patch" region after repair to check the propagation of corrosion. Only the readings taken after the repair are analysed and presented. These readings were taken on a weekly basis on 49 nodes at top and 25 nodes at bottom of each slab (Figure 4.5) after removal of the salt solution. Twenty-four nodal readings on bottom surface along the slab periphery could not be taken because of the supporting frame obstruction. Weekly potentials of each node are converted into monthly average potentials of each node for each slab according to Equation

5.1. The monthly average potentials are then used to draw potential contour maps of all fifteen slabs for the top and the bottom layers of steel bars. These maps are presented by Leyne (2004). The average half-cell potential readings of the "patch", the "non-patch", and the bottom surface vs. time diagrams are presented in this report.

5.2.1 Calculation Procedure

The monthly average potential of ij^{th} node in mV is:

$$V_{ij}^{M} = \frac{1}{n}\sum V_{ij}^{W} \quad \ldots \quad \ldots \quad \ldots \quad (5.1)$$

where V_{ij}^{W} = Weekly potential of the ij^{th} node in mV

n = Number of weeks in corresponding month

i = Horizontal nodal position (varies from 1 to 7)

j = Vertical nodal position (varies from A to G)

The monthly average potentials are then classified into two groups for the "patch" and the "non-patch" regions of each slab, to examine the influence of repair on corrosion of reinforcing steel around the patch. The potential differences between the "patch" and the "non-patch" region are calculated according to the Equations 5.2 and 5.3.

The monthly average potential of 9 nodes for patch region in mV is:

$$V_{P}^{M} = \frac{1}{9}\sum V_{ij}^{M} \quad \ldots \quad \ldots \quad \ldots \quad (5.2)$$

where i varies from 3 to 5 and j varies from C to E within the patch region.

The monthly average potential of 40 nodes for "non-patch" region is:

$$V_{NP}^{M} = \frac{1}{40}\sum V_{ij}^{M} \quad \ldots \quad \ldots \quad \ldots \quad (5.3)$$

where i varies from 1 to 7 and j varies from A to G (except for the nodes previously considered for the "patch" region) within the "non-patch" region.

Therefore, the average potential difference between the "patch" and the "non-patch" region is:

$$\Delta V^M = V_P^M - V_{NP}^M \quad \ldots \quad \ldots \quad \ldots \quad (5.4)$$

The monthly average potential of 25 nodes for bottom surface is:

$$V_B^M = \frac{1}{25}\sum V_{ij}^M \quad \ldots \quad \ldots \quad \ldots \quad (5.5)$$

where i varies from 2 to 6 and j varies from B to F.

5.2.2 Interpretation of Results

The half-cell potential (HCP) vs. time diagrams have been drawn for each slab. Each diagram shows the variation of the half-cell potential difference (ΔV^M) on the right vertical scale, and monthly average half-cell potential of the "patch" (V_P^M), the "non-patch" (V_{NP}^M) and the bottom layer (V_B^M) on the left vertical scale, with the time beginning from the repair for the following thirteen months on the horizontal scale. The notation, "P ~ NP", "Top (P)", "Top (NP)", and "Bottom" of each diagram represent the monthly average potential difference between the "patch" and the "non-patch" region, monthly average potential of the "patch" and the "non-patch" region of the top mesh bars, and the bottom mesh bars, respectively.

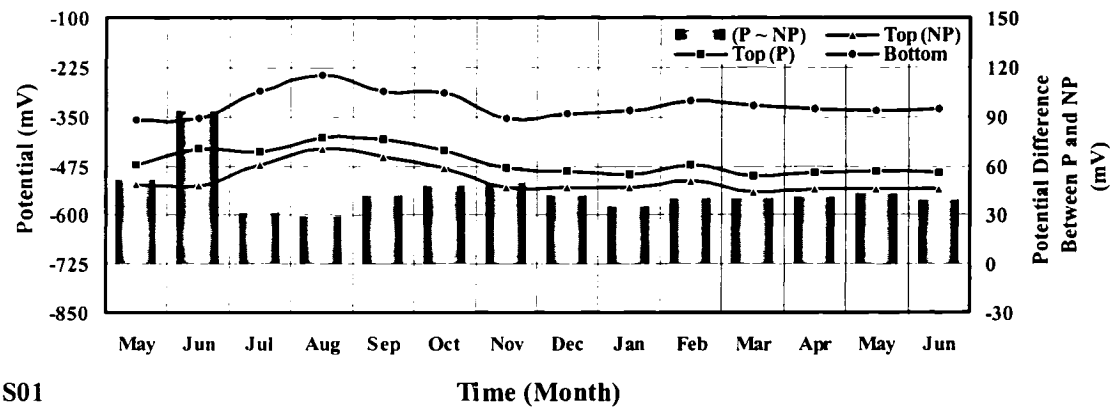

Figure 5.1: Typical Monthly Average HCP vs. Time Plot (Slab S01)

A typical monthly average half-cell potential vs. time diagram is shown in Figure 5.1. The HCP vs. time characteristics for all 15 specimens are shown in Figures A.1 to A.15 in Appendix A.

According to ASTM C876-91, the half-cell potentials show only the probability of active corrosion and not the rate of corrosion of the rebars. The potentials are interpreted according to the Table 5.1.

Table 5.1: Half-Cell Test Result Interpretation Guideline
(Bungey and Millard, 1996)

Half-Cell Potential (mV)	Probability of Corrosion (%)
< –350	90
–200 to –350	50
> –200	10

5.2.3 Observations and Discussion

The control specimen "A", Slab S01 is chosen for typical description. It was ponded with 15% NaCl solution with no protective barrier, and repaired with standard patch mix concrete. At the beginning of repair, the half-cell potentials of the "patch" (uncontaminated concrete) and the "non-patch" (chloride-contaminated concrete) were –471 and –523mV, respectively, which indicated more than 90% probability of corrosion. The potential difference between the "patch" and the "non-patch" region was 53mV. During the third month after repair, these potentials increased (algebraically) to –432 and –403mV, and the potential difference reduced to 29mV. But 3-4 months after repair, these values decreased again. However, these potentials always remained less than –350mV, i.e., probability of corrosion remained at more than 90%. The potential difference between the "patch" and the "non-patch" region remained almost constant with time, which accelerated corrosion around the patch region. Beaudette (2001) also made similar observation shown in Figure 5.2. Therefore, it can be concluded that conventional patch-repair partially improves the damage externally, but it accelerates the corrosion internally.

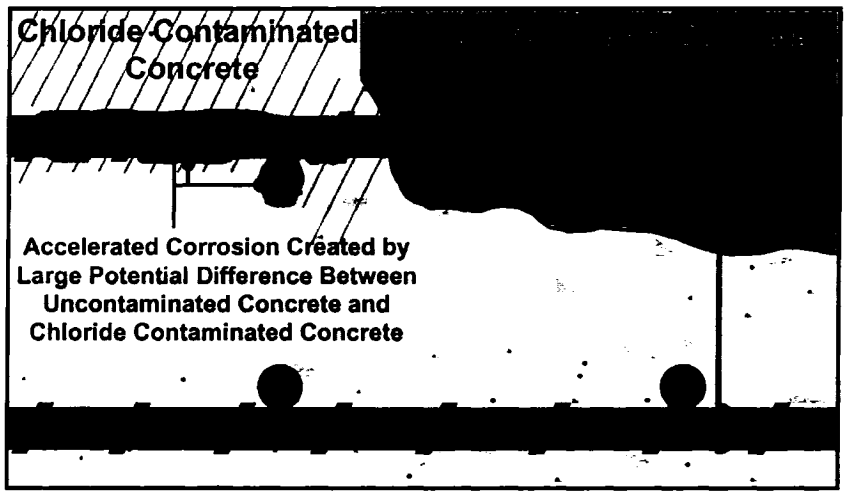

Figure 5.2: Accelerated Corrosion adjacent to the Patch Repair
(Beaudette, 2001)

Initially, the monthly average potential of the bottom slab was –360mV, it increased (algebraically) to –245mV and then decreased to –330mV, therefore, the probability of corrosion was almost 50%. But after demolition of the slab, no signs of corrosion were found on the bottom layers of steel bars, which is in conflict with the interpretation of this test results (Table 5.1). Therefore, more research needed to improve the reliability of this non-destructive test.

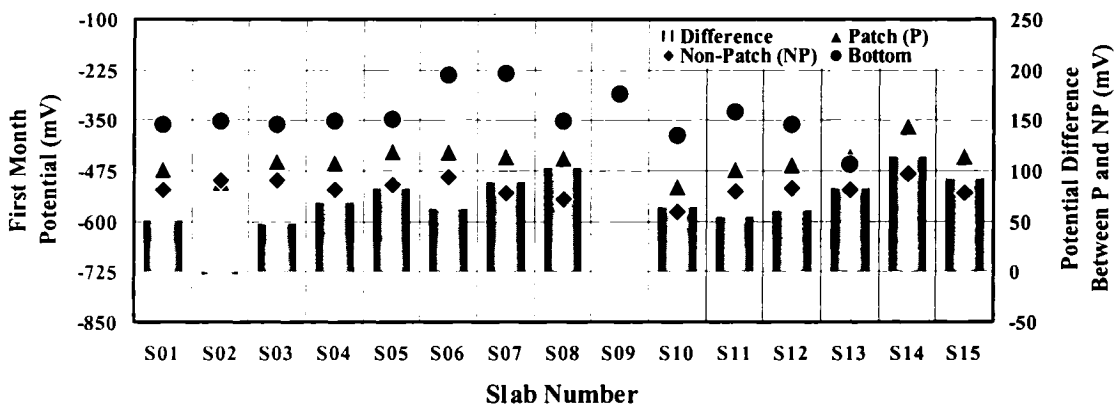

Figure 5.3: HCP Reading during First Month of Repair

Similar trends were observed in all other slabs. The half-cell potentials at the "patch", the "non-patch" and the bottom, and the potential difference between the "patch" and the "non-patch" during 1st, 4th and 13th month of repair of all slabs are shown in Figures 5.3, 5.4, and 5.5, respectively. The bar chart represents the potential difference. In these diagrams, the half-cell readings of the top surface of slab S09 are missing, because of its top surface was treated with a membrane and no openings were available at the nodal points to take the readings.

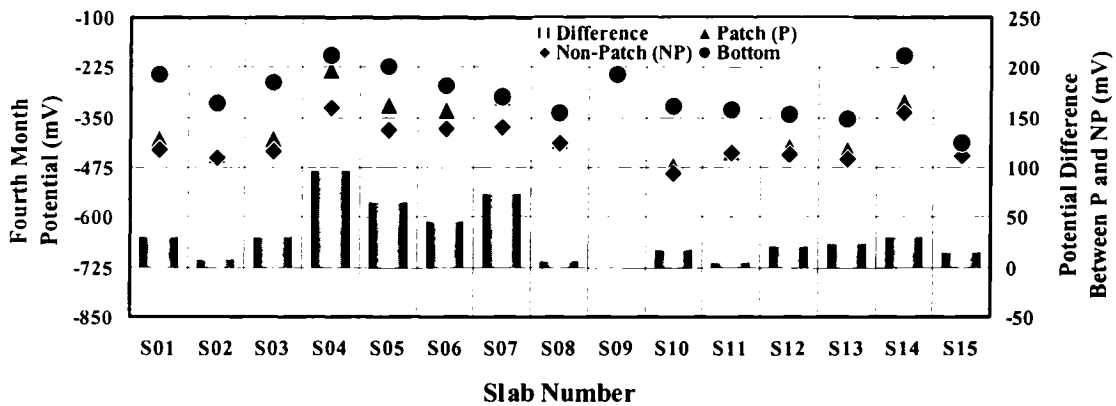

Figure 5.4: HCP Reading during Forth Month of Repair

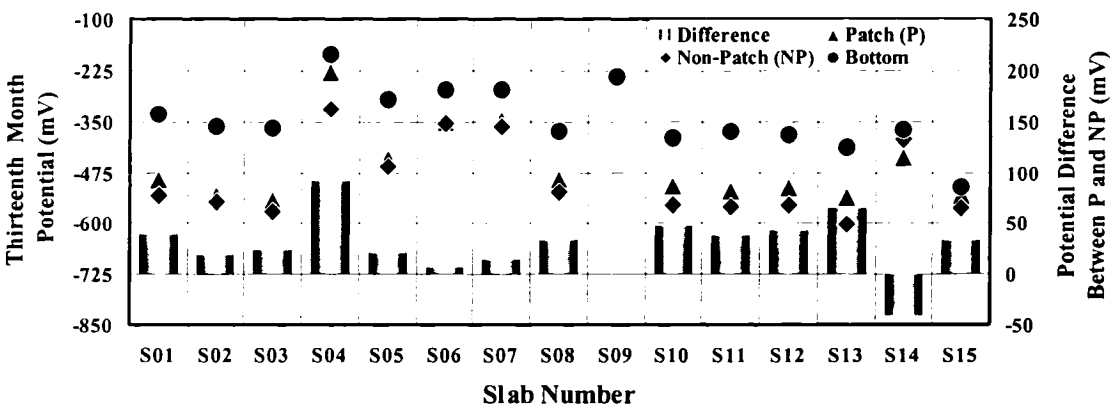

Figure 5.5: HCP Reading during Thirteenth Month of Repair

Based on the above results, the following comments can be made:

1. All specimens were of the same dimensions, however, they all had different W/C ratios in the "patch" concrete (0.45) and the "non-patch" concrete (0.52) regions, different strategies of repair, and two different exposure conditions. There could be some small variations in the concrete due to its inhomogeneous nature during casting. The common trend observed in the potential-time profile (Appendix A, Figure A.1 to A.15) of all repair strategies was that the potential increased during the 4^{th} and 5^{th} months after repair and then decreased again.

2. Two control specimens, Slabs S01 and S10, designated as Control-A and Control-B are identical excepting for the exposure conditions, being exposed to NaCl and KCl solutions, respectively. Both have more than 90% probability of corrosion, however, average half-cell potentials of Control-A specimen (Slab S01) were observed higher than in Control-B specimen (Slab S10), demonstrating a higher level of corrosion with KCl exposure than with NaCl exposure (Appendix A, Figure A.1 and A.10).

3. Slabs S02 and S03 had the steel rebar at the "patch" coated with epoxy and zinc, respectively; during 13^{th} month of repair, they showed lower potential (Figure 5.5) than Control-A specimen (Slab S01), almost similar potential-time profiles (Appendix A, Figure A.2 and A.3), and they demonstrated consistently higher than 90% probability of corrosion. However, a relatively smaller potential difference was observed between the "patch" and the "non-patch" regions of zinc-coated reinforcement than with the epoxy-coated reinforcement. This reflects a smaller probability of developing a ring anode around the "patch" with zinc-coated reinforcement than with the "patch" with epoxy-coated reinforcement.

4. The concrete top surfaces of Slabs S04, S05, and S06 were treated with penetrating sealer, impermeable epoxy surface coating, and breathable traffic-bearing

membrane, respectively. The Slab S04 displayed different characteristics compared with the others. Four months after repair, its potential remained higher (algebraically) at –350mV, reflecting 50% probability of corrosion, however, the potential difference between the "patch" and the "non-patch" regions (75 to 80 mV) was higher than that for the other slabs, therefore, corrosion activity accelerated around the patch, which is not acceptable. There is 90% probability of corrosion in Slabs S05 and S06, however, Slab S06 (breathable traffic-bearing membrane) showed a good trend towards an increase (algebraic) of the potential and decrease of the potential difference between the "patch" and the "non-patch" regions (ring anode). Due to the impermeable nature of the coating for Slab S05, the chloride ingress into the concrete decreased initially, however, after some time, moisture may have gotten trapped underneath the coating, which increased the corrosion activity. The potential vs. time profiles of these slabs are shown in Appendix A, Figure A.4, A.5, and A.6.

5. The Slab S07 was similar to the Slab S06, i.e., the concrete top surface was treated with breathable traffic-bearing membrane, however, additionally, the "patch" steel was treated with a zinc primer; it also demonstrated a 90% probability of corrosion. It was expected that the second barrier (zinc primer) would improve its performance and reduce the corrosion activity, however, it did not have any significant impact. The potential vs. time profile of this slab is shown in Appendix A, Figure A.7.

6. To repair the Slab S08, a small cylindrical sacrificial anode was embedded at the corner of its patch region. It showed the same 90% probability of corrosion, but it also showed a higher rate of reduction of potential difference between the "patch" and the "non-patch" regions within the first three to five months. After losing the performance of the anode, this difference increased again with time (Appendix A, Figure A.8).

7. The Slab S09 was also treated with breathable traffic-bearing membrane, like Slabs S06 and S07, but no tubes were attached at the top surface of each grid point before treatment to obtain the half-cell readings. Therefore, no potential readings are available for the top mesh of this specimen.

8. The Slabs S11, S12, and S13 were treated with different corrosion inhibitors: Corrosion inhibitor surface coating (CI-S) for top surface treatment, corrosion inhibitor grout (CI-G) for patch steel treatment, and corrosion inhibitor admixture (CI-A) for the concrete mixture. CI-G and CI-A were applied for all slabs, but CI-S was applied only on the concrete top surface of Slab S13. The Slab S11 was exposed to the KCl solution and other two were treated with the NaCl solution. All slabs showed almost similar potential vs. time profile (Appendix A, Figure A.11, A.12, and A.13), but the potential difference between the "patch" and the "non-patch" steel of Slab S11 was comparatively lower than that of other two. The Slab S11, compared with the Control-B specimen (Slab S10), and Slabs S12 and S13, compared with the Control-A specimen (Slab S01), showed no additional benefit of using corrosion inhibitor to stop or reduce the corrosion activity. All slabs indicated 90% probability of corrosion.

9. Sacrificial zinc anode sheet was attached at the top surface of Slab S14 and at the bottom of Slab S15. The half-cell readings were taken at two different conditions for Slab S14, after the top zinc sheet was connected to the reinforcing steel; there was no connection of the zinc sheet with the reinforcement. Appendix A, Figure A.14.1 and A.14.2 show the potential vs. time profile, which are very different in nature, compared with the response of the others. During the 1st and 2nd month after repair, both "connected" and "unconnected" positions showed the same behaviour; after 2nd month, the potential of the "connected" slab decreased then increased (concave), and for the "unconnected" slab, it increased and then decreased (convex) with time until about 9 months after repair. Nine to thirteen months after repair, both conditions again showed the same behaviour (convex). The potential

difference between the "patch" and the "non-patch" region dropped during 4th to 5th month after repair, and it gradually increased with time, but changed its polarization. An opposite polarization indicates the acceleration of corrosion activity inside the patch rather than around the patch, which differs from the response of the other specimens. For the "connected" condition, the half-cell readings do not reflect the corrosion activity of the reinforcing steel but the zinc sheet. The zinc sheet corrodes first before the rebars; therefore, the potential in the "connected" condition decreased, while the potential with the "unconnected" condition increased. After consumption of the zinc sheet by the salt solution, the potential of the steel rebars decreased again, which indicated an increase in the corrosion activity in the steel rebars. No logical reasons were found for the increase in the potential after nine months of repair. The Slab S15 showed behaviour similar to that of Control-A specimen (Slab S01), which did not represent any benefit of using zinc sheet at bottom (Appendix A, Figure A.15).

5.3 Chloride Content Determination

Chloride-induced corrosion of steel in concrete represents the most significant threat to reinforced concrete infrastructure. Therefore, it is very important to know the chloride content at a depth of concrete cover for investigating corrosion activity.

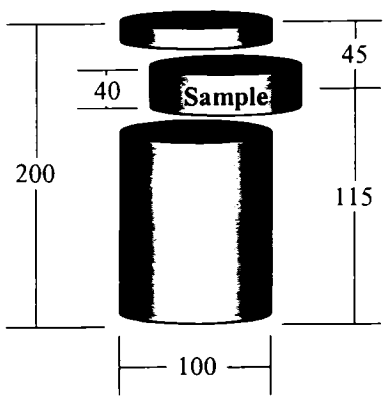

Figure 5.6: Depth of Sampling of Concrete Slice for Chloride Content Test

According to ASTM C 1218-92, detailed test description and procedure are presented in Chapter Four. As mentioned earlier, thirty concrete cores were collected from two different locations of fifteen slabs. One core was taken from the "patch" and other from the "non-patch" region of each slab. Care was taken to avoid cutting the steel reinforcement. The slice was cut as shown in Figure 5.6 to determine the chloride content of the concrete at the centre of the top mesh. Each slice was powdered by a rotating-puck grinding apparatus to prepare the sample for the chloride test. During the test titration readings were recorded for calculation. Percent chloride content was determined using Equations 5.6 and 5.7.

5.3.1 Calculation Procedure

The percentage chloride content by mass of concrete was calculated to the nearest 0.001% as follows:

$$\%\ \text{Cl by mass of concrete} = 3.5453 \times N \frac{V}{W} \quad \ldots \quad \ldots \quad \ldots \quad (5.6)$$

where V = Volume of 0.05N $AgNO_3$ solution used for titration of the sample at equivalence point in ml

N = Exact normality of 0.05N $AgNO_3$ solution, and

W = Mass of the concrete powder in gm

The equivalence point is the maximum potential difference, ΔmV, with respect to the volume of 0.05N $AgNO_3$ solution required for complete titration. Each result represents the percentage of the chloride content by mass of concrete at a depth of 45mm (25 + 40 ÷ 2 = 45) from top of the concrete surface.

The percentage of chloride content by mass of cement was calculated as follows:

$$\%\ \text{Cl by mass of cement} = \%\ \text{Cl by mass of concrete} \times \frac{100}{P} \quad \ldots \quad (5.7)$$

where P = Percentage of cement by mass in concrete, which is known from the concrete mixture design (Table 4.1 and 4.5).

5.3.2 Interpretation of Results

The percentage of chlorides in the concrete (by mass of cement or concrete) is indicative of the risk of corrosion for the reinforcing steel. This chloride may be present in three states: free chlorides ions in the pore solution, chlorides strongly bound, and chlorides loosely bound at the hcp pore walls. The free chlorides are the most significant contributors to the corrosion risk. They may be introduced from external sources (marine environment and de-icing salts), or carbonation may release the bound chlorides from internal sources. The nature of chloride is significant but while free chlorides are most relevant, it is the total (free and bound) chlorides level that is determined in the tests. Tests for the chloride level are generally based on acid-soluble chloride techniques that yield a value for total chlorides, but the water-soluble chloride levels better describe the presence of free chlorides (Richardson, 2002). In this project, water-soluble chloride test (ASTM C 1218-92) was used. The results expressed as single point values of percentage chloride by mass of cement must be compared with some reference point, which is generally the threshold level – the critical chloride content, at which depassivation of the reinforcement occurs and corrosion commences. This is irrespective of any visible damage on the concrete surface (Lindvall, 2001). The threshold level at which passivity is lost and corrosion commences is not clearly defined and significant variation exists in the literature on the critical chloride level. Everett and Treadaway (1980) suggested the following descriptions of corrosion risk, which were adopted by Building Research Establishment Digest 264 (1982) and the Concrete Society Technical Report No. 26 (1984):

Table 5.2.1: Chloride Content Interpretation Guideline-1
(Everett and Treadaway, 1980)

% Chloride by Mass of Cement	Risk of Corrosion
< 0.4	Low
0.4 to 1.0	Medium
> 1.0	High

Browne (1980) used a similar set of criteria for corrosion risk:

Table 5.2.2: Chloride Content Interpretation Guideline-2
(Browne, 1980)

% Chloride by Mass of Cement	Risk of Corrosion
< 0.4	Negligible
0.4 to 1.0	Possible
1.0 to 2.0	Probable
> 2.0	Certain

A review of the literature reveals a general agreement that 0.4 percent chloride by mass of cement represents an acceptable benchmark for design purposes (Richardson, 2002).

Different studies show a wide range of threshold values from a minimum of 0.06 percent to a maximum 2.5 percent by mass of cement. The Canadian Standard Association (CSA) uses very conservative guideline on the chloride ion content. According to CSA A23.1-15.1.6.1, the water-soluble chloride ion content by mass of the cementing material in the concrete before exposure shall not exceed the following values for the indicated applications:

(a) For prestressed concrete: 0.06%
(b) For reinforced concrete exposed to a moist environment or chlorides, or both: 0.15%
(c) For reinforced concrete exposed to neither a moist environment nor chlorides: 1.0%

The percentage of chloride content by mass of concrete and cement in the "patch" and the "non-patch" regions of all fifteen slabs are presented in Table 5.3, and graphically in Figure 5.7 and 5.8.

Table 5.3: Percent Chloride Content of Patch and Non-Patch Region of Different Slabs

Slab No.	Designation	% Cl Content (By Mass of Concrete)		% Cl Content (By Mass of Cement)		
		At Non-Patch (NP)	At Patch (P)	At Non-Patch (NP)	At Patch (P)	% Difference Between P and NP
S01	Control A	0.502	0.140	2.679	1.052	61
S02	Epoxy Primer	0.645	0.145	3.440	1.089	68
S03	Zinc Primer	0.441	0.150	2.352	1.128	52
(S04)	Penetrating Sealer	0.219	0.051	1.167	0.381	67
(S05)	Epoxy Coating	0.350	0.062	1.868	0.463	75
(S06)	Membrane	0.214	0.067	1.143	0.500	56
(S07)	Membrane and Zinc Primer	0.327	0.067	1.743	0.502	71
S08	Embedded Anode	0.484	0.074	2.581	0.556	78
(S09)	Membrane	0.171	0.066	0.911	0.491	46
S10	Control B	0.470	0.181	2.508	1.359	46
S11	Inhibitor	0.384	0.081	2.050	0.604	71
S12	Inhibitor	0.507	0.118	2.703	0.886	67
(S13)	Inhibitor + Surface Coating	0.587	0.027	3.129	0.200	94
(S14)	Zinc Sheet Top	0.274	0.056	1.462	0.419	71
S15	Zinc Sheet Bottom	0.446	0.136	2.380	1.023	57

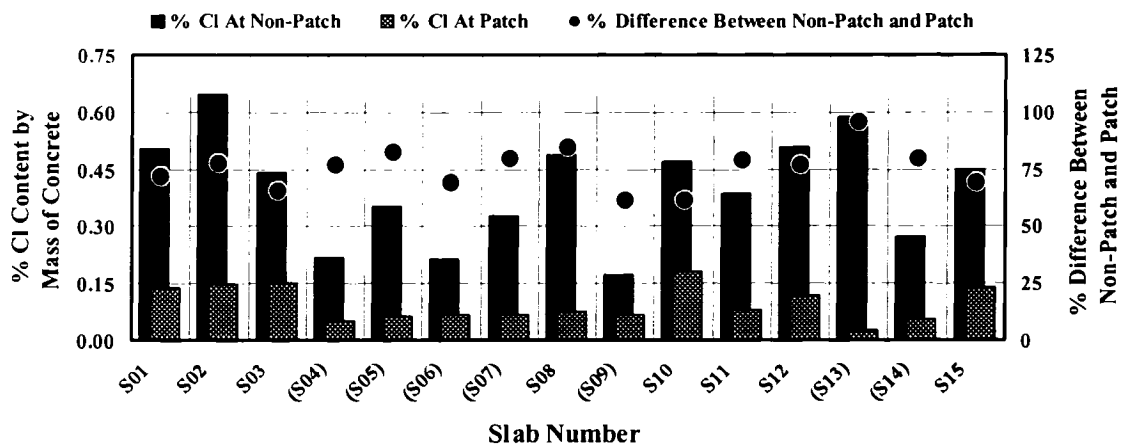

Figure 5.7: Percent Chloride Content (by Mass of Concrete) of Different Slabs

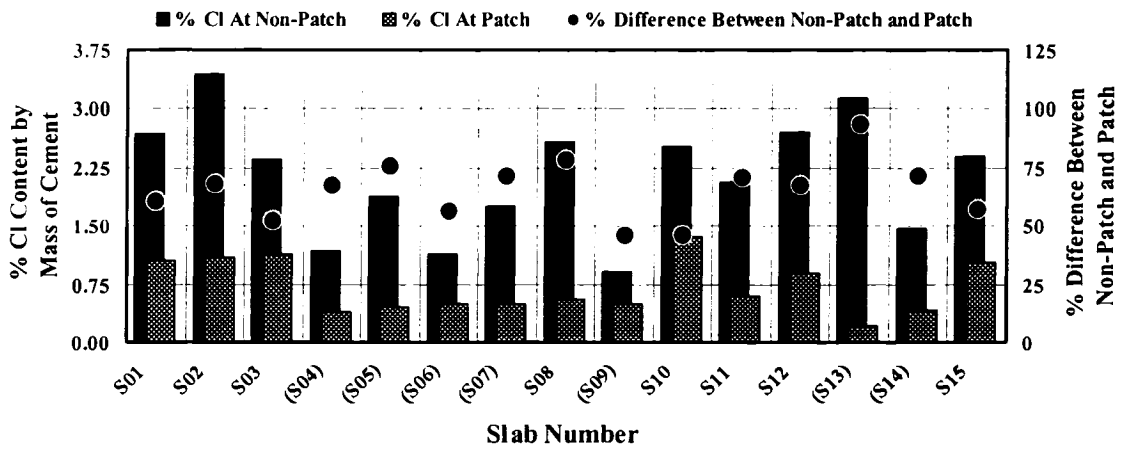

Figure 5.8: Percent Chloride Content (by Mass of Cement) of Different Slabs

As mentioned earlier, all slabs were treated with different strategies of repair. Slabs S10 and S11 exposed to 15% KCl solution, and all others were subjected to 15% NaCl solution. The top surface of the Slabs S04, S05, S06, S07, S09, S13, and S14 were treated with different protective barriers (penetrating sealer, impermeable epoxy surface coating, breathable traffic-bearing membrane, or an inhibitor) to reduce the chloride ingress into the concrete. In Table 5.3, and Figures 5.7 and 5.8, these slabs are distinguished from others by enclosing their nomenclature in parenthesis. Others were treated differently (patch steel treatment with epoxy or zinc, embedded sacrificial anode, corrosion inhibitor, or sacrificial zinc anode sheet) to reduce the corrosion activity except for Control-A specimen (Slabs S01) and Control-B specimen (Slab S10). Figures 5.7 and 5.8 represent the percent chloride content by mass of concrete and cement, respectively, at the "patch" and the "non-patch" regions.

5.2.3 Observations and Discussion

The results in Table 5.3, and Figures 5.7 and 5.8 lead to the following observations:

1. The "patch" region of each slab had more than 50% lower chloride penetrability than that of the "non-patch" region. This is obvious because of the lower W/C ratio used in the "patch" region (0.45) compared with the "non-patch" region (0.52).

Therefore, the former has a lower concrete permeability than the later; hence, the W/C ratio is a major governing factor to reduce the permeability of the concrete and the related chloride ingress.

2. The Control-A specimen (Slabs S01) and Control-B specimen (Slab S10) had the same material composition, but different exposure conditions. Slab S01 was exposed to 15% NaCl solution and Slab S10 to 15% KCl solution. Both had the different W/C ratio in "patch" (0.45) and "non-patch" (0.52) regions. Comparison of the patches of Slabs S01 and S10 shows that KCl solution had 22% higher penetrability than the NaCl solution. On the other hand, a decrease of W/C ratio from the "non-patch" (0.52) to the "patch" (0.45), the percentage of chlorides in the "patch" region of Slab S01 decreased by 61% compared with the "non-patch" region, while the percentage of chlorides in the "patch" region of Slab S10 decreased by 46% compared with the "non-patch" region of the same slab. Therefore, NaCl performs better as a de-icing salt compared with KCl, when no additional treatments are used. These are also reflected in the half-cell potential readings, with higher potential (algebraically) readings for Slab S01 than for Slab S10.

Table 5.4: Comparison Between % Chloride Content (by Mass of Cement) of Treated and Untreated Surface of Different Slabs

	Concrete Top Surface Treatment Status		**% Difference Between Treated and Untreated**
	Treated	**Untreated**	
Slab Number:	**4, 5, 6, 7, 9, 13 and 14**	**1, 2, 3, 8, 10, 11, 12 and 15**	
Average % Cl (Non-Patch):	1.632	2.587	**37**
Average % Cl (Patch):	0.422	0.962	**56**
% Difference of Patch and Non-Patch:	**74**	**63**	-

3. The top surface of Slabs S04, S05, S06, S07, S09, S13, and S14 were treated with different protective barriers such as penetrating sealer, impermeable epoxy surface coating, breathable traffic-bearing membrane, or an inhibitor. Table 5.4 shows the comparison between the percentage of chlorides (by mass of cement) for treated and untreated surfaces. The average percentage of chlorides in the top surface of the untreated concrete is 37% higher than that of treated concrete in the "non-patch" region (higher W/C ratio), and 56% higher at the "patch" region (lower W/C ratio). Again, the average percentage of chloride content of the "non-patch" concrete is 74% higher than that of the "patch" concrete for the top surface in a treated condition, and 56% higher for the top surface in a untreated condition. Therefore, any treatment of the concrete top surface has a greater impact on reducing the chloride ingress in the "patch" concrete with a lower W/C ratio.

Table 5.5: % Difference of Chloride Content with respect to Control-A Specimen (S01) for the Different Slabs (Top Surface Treated)

	Concrete Top Surface Treatment					
Slab Number:	**Sealer S04**	**Epoxy S05**	**Membrane S06**	**Membrane S07**	**Membrane S09**	**Epoxy S14**
Patch:	64	56	52	52	53	60
Non-Patch:	56	30	57	35	66	45

4. Three categories of concrete surface treatment were used: (a) the penetrating sealer, (b) the impermeable epoxy surface coating, and (c) the breathable traffic-bearing membrane. Table 5.5 shows that there is no significant difference between sealer, epoxy and membrane for reduction of chloride ingress into the concrete. The overall percentage of chloride content for the top surface treated concrete at the "patch" region is 50-65% and at the "non-patch" region is 30-65% lower than that of the Control-A specimen (Slab S01).

5. The top surfaces of Slabs S06, S07, and S09 were treated with the same breathable traffic-bearing membrane. Theoretically, their performance should be same. Table

5.5 shows that the difference between the percentage of chloride content of these slabs and the Control-A specimen (Slab S01) at the "patch" region were almost the same (52%, 52%, and 53%, respectively), but at the "non-patch" region, some dissimilarities were observed (57%, 35%, and 66%, respectively).

6. Three categories of corrosion inhibitor were used in this experiment: (a) corrosion inhibiting surface treatment (CI-S) on the exposed concrete surface, (b) corrosion inhibiting grout (CI-G) on the exposed steel surface, and (c) corrosion inhibiting concrete admixture (CI-A) for improving concrete mixture properties. The Slab S13 received three categories of inhibitor treatment (Table 4.6). Table 5.3, and Figures 5.7 and 5.8 show that the percentage of chloride content in the "patch" of Slab S13 had the lowest value. There was a large difference (94%) observed between the percentage of chloride content of the "patch" and the "non-patch" concrete of this slab. CI-S was applied on the "patch" and the "non-patch" concrete top surface of this slab, and CI-A was added in the concrete mixture to repair its "patch". Comparison between the "non-patch" concrete of Control-A specimen (Slab S01) and Slab S13 showed that the CI-S did not reduce the chloride ingress into the concrete, even though it increased the percentage of chloride content by 14% in the "non-patch" concrete of Slab S13 comparing with Control-A specimen (Slab S10), which is not desirable. However, combination of inhibitor surface treatment (CI-S) and inhibitor concrete admixture (CI-A) showed very good results. It reduced the percentage of chlorides in the "patch" region of Slab S13 by 81% of the "patch" concrete of Control-A specimen (Slab S01).

7. Both Slabs S11 and S12 received similar repair treatments, but had different exposure conditions. The corrosion activity in Slab S11 was accelerated with KCl solution while Slab S12 with NaCl solution. Corrosion inhibitor grout (CI-G) was applied for the "patch" steel treatment and corrosion inhibitor concrete admixture (CI-A) was added in the "patch" concrete of both slabs. Table 5.3, and Figures 5.7 and 5.8 show that the percentage of chlorides of Slab S12 (accelerated by NaCl)

was 24% higher at the "non-patch" region and 32% higher at the "patch" region than for Slab S11 (accelerated by KCl). This trend is the reverse of the comparison between Control-A (accelerated by NaCl) and Control-B (accelerated by KCl) specimens, discussed previously. The corrosion inhibitor may have slowed the acceleration of corrosion due to the KCl solution, and compared with that due to the NaCl solution.

Table 5.6: % Difference of Chloride Content with respect to Control-A Specimen (S01) of Different Slabs (Top Surface Untreated)

Slab Number:	Untreated Concrete Top Surface				
	S02	S03	S08	S12	S15
Patch:	-4	-7	47	16	3
Non-Patch:	-28	12	4	-1	11

8. Theoretically, all untreated slabs, where corrosion activity was accelerated using NaCl solution, should have the same percentage of chloride content as Control-A specimen (Slab S01), but Table 5.6 shows some variation. The negative sign indicates the slabs had higher chloride contents than the Control-A specimen (Slab S01). The percentage of chloride content at the "patch" of Slab S08 reduced by 47% as compared with Control-A specimen (Slab S01). It indicates that the embedded anode causes a reduction in the chloride ingress into the concrete.

9. The corrosion activity in Slabs S01 and S12 was accelerated using NaCl solution, and in Slabs S10 and S11 using KCl solution. No protective barrier was used in Slab S01 and S10, which were considered as Control-A and Control-B specimens, respectively. Corrosion inhibitor grout (CI-G) was applied for the "patch" steel treatment and corrosion inhibitor concrete admixture (CI-A) was added in the "patch" concrete of both Slabs S11 and S12. Analysis showed that, in NaCl environment, the percentage of chloride content of Slab S12 at the "patch" region was 16% higher and at the "non-patch" region it was the same as that in the

Control-A specimen (Slab S01). In KCl environment, the percentage of chloride content for Slab S11 at the "patch" region was 56% higher and at the "non-patch" region it was 18% higher than that of Control-B specimen (Slab S10). It proves that corrosion inhibitor works better in the KCl environment than in the NaCl environment.

5.4 Mass Loss Determination

Assessment of the remaining capacity of corrosion-damaged reinforced concrete members requires accurate measurement of the remaining cross-sectional area of the corroded reinforcing steel. Several traditional methods are available to quantify the average sectional area loss over the length. The most common method used to quantify the cross-sectional loss of corroded rebar is the mass loss determination method, which is used to measure the mass of the rebar before and after the accelerated corrosion exposure to determine the change in mass of the sample. The results provide an average mass, or cross-sectional area. However, average cross-sectional properties may not be sufficient to characterize the degree of corrosion damage, and the corresponding impact on the structural performance. If pitting corrosion occurs along the bar, which is very common in chloride-contaminated environment, the ductility loss due to concentrated yielding in the locally reduced area may result in a significant decrease in the member ductility. Furthermore, if the length of the rebar is large compared to the length of the pit, the average area obtained form the mass loss determination method will not identify these localized features. In the present research program, only average mass loss of each set of rebar was determined and compared with different strategies of repair.

5.4.1 Calculation Procedure

The rebar mass loss of rebar is the change in mass due to corrosion. It is the difference between the initial and the final mass of each bar before and after exposure, respectively. At the end of the project, when the slab concrete was demolished, almost no sign of corrosion was found on the bottom mesh bars of all slabs. Appendix B, Figure B.1 to B.30

shows the visual images of all bottom bars of fifteen slabs. Most of the photographs show no sign of corrosion except some minor corrosion in Slabs S08 (Figure B.16), S10 (Figure B.19), S11 (Figure B.22), and S13 (Figure B.26). Therefore, decision was made to select a datum line statistically from all bottom bars to calculate the percentage of mass loss per unit length of each bar according to Equation 5.8.

$$\% \text{ Mass loss} = \frac{W_u - W_c}{W_u} \times 100 \quad \ldots \quad \ldots \quad \ldots \quad (5.8)$$

where W_u = Mass of uncorroded bar per unit length (Statistically determined)

W_c = Mass of corroded bar per unit length (Measured after cleaning)

5.4.1.1 Selection of Datum Line

Table 5.7: Distribution Table of Mass per Unit Length of Bottom Bars

Class	Class Range (gm/cm)	Number of Bars within the Class	Expected Number of Bars
	22.00		0.00
1	22.10	0	0.06
2	22.20	6	0.56
3	22.30	5	3.34
4	22.40	9	12.86
5	**22.50**	**17**	32.01
6	**22.60**	**47**	51.41
7	**22.70**	**75**	53.34
8	**22.80**	**37**	35.75
9	**22.90**	**14**	15.47
10	23.00	0	5.20

Each of the 15 slabs had 28 of bars in 4 layers. Therefore, all 210 "uncorroded" bottom bars at the specimen bottom were considered to be the datum line statistically. The mass per unit length of each bar was calculated by dividing the measured mass in gm by the measured length in cm. The maximum and minimum mass per unit length of all bottom-bars was 22.89 and 22.13 gm/cm. All bars were grouped into ten classes according to the Table 5.7. The arithmetic mean and the standard deviation for the 210 bottom-bars were 22.61 gm/cm and 0.15 gm/cm, respectively.

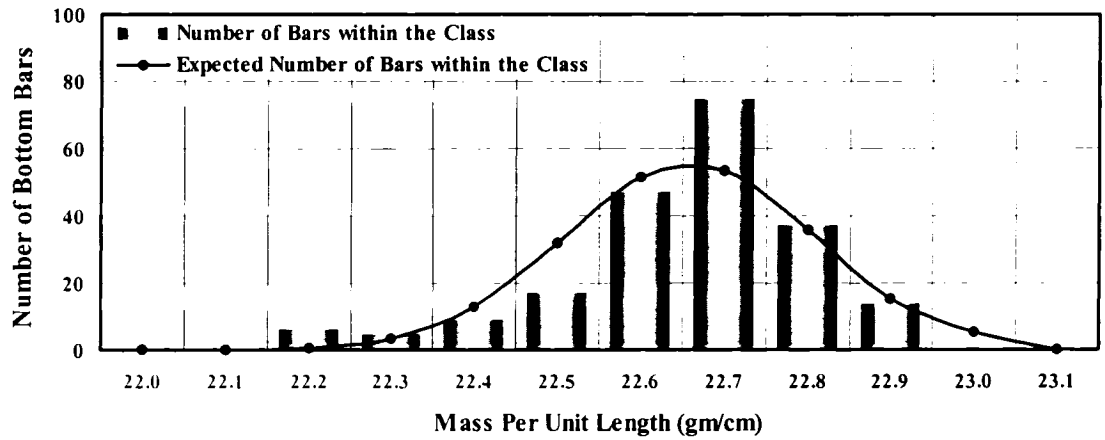

Figure 5.9: Distribution Chart of Mass per Unit Length of Bottom Bars

Table 5.7 and Figure 5.9 shows that 90% of bottom-bars remain within the class 5 and 9, and median of these five classes is 22.70 gm/cm. However, according to the Concrete Design Handbook, CAC (2001), Table 1.5, the standard mass per unit length of No. 20 bar is 23.55 gm/cm, which is 3.6% higher than that of this observed median value (22.70 gm/cm). Therefore, consideration of 22.70 gm/cm as a datum of mass per unit length of "uncorroded" bar, would be more rational to calculate the percentage of the mass loss of all other corroded bars, using Equation 5.8.

5.4.2 Interpretation of Results

Visual records of corrosion of all bottom and top bars of fifteen slabs are presented in Figure B.1 to B.30 (Appendix B) and Figure C.1 to C.30 (Appendix C), respectively. Four

photographs were taken for each slab, top mesh upper face, top mesh lower face, bottom mesh upper face, and bottom mesh lower face. Each photograph was taken according to the original position / orientation of the bars in the slab, therefore, each bar can be identified from each visual record according to Figure 4.5.

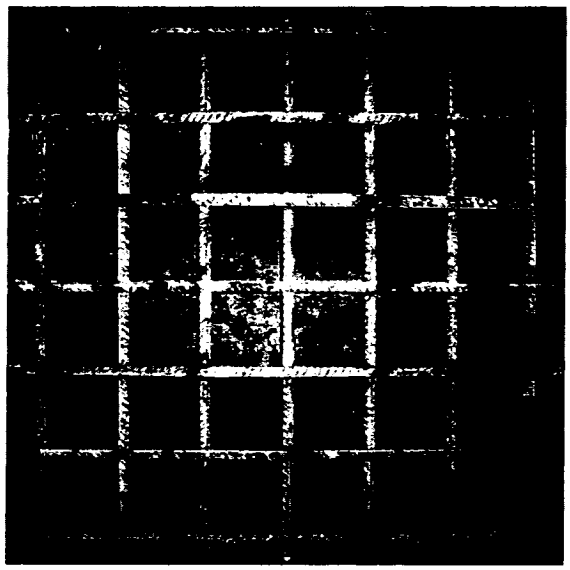

Figure 5.10.1: Visual Image of Corrosion of Slab S08 (Top Mesh Upper Face)

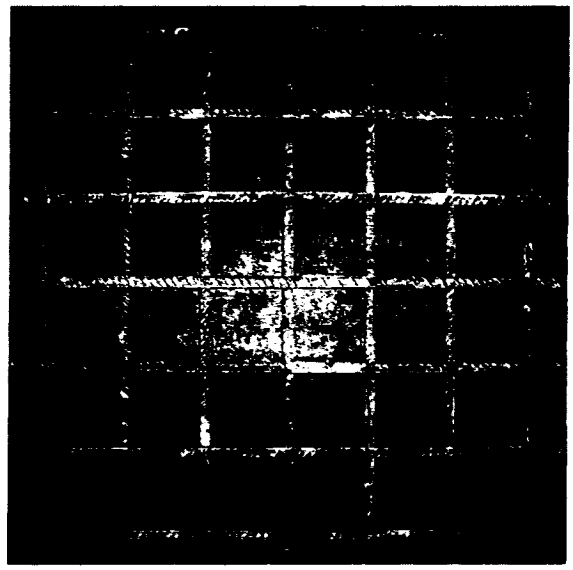

Figure 5.10.2: Visual Image of Corrosion of Slab S08 (Bottom Mesh Upper Face)

A sample visual record of Slab S08 for the top mesh, upper face and bottom mesh, lower face is presented Figures 5.10.1 and 5.10.2, respectively. According to Figure 4.5, each bar is designated as A to G from top to bottom (top-layer) and 1 to 7 from left to right (bottom-layer). After calculation, the percentage of mass loss for each bar of each layer is plotted and presented in Figures D.1 to D.15 (Appendix D). A sample percent mass loss diagram for top-mesh bars of Slab S01 is shown in Figure 5.11.

In Figure 5.11, the vertical left scale of each diagram represents the percentage of mass loss of each bar, bottom horizontal scale represents the position of seven "non-patch" bars, and top the horizontal scale represents the position of the "patch" steel bars.

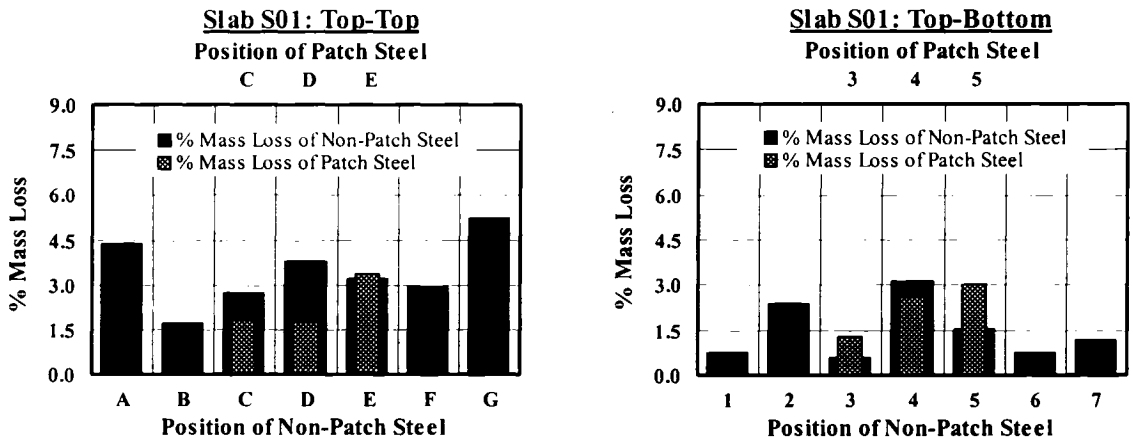

Figure 5.11: Percent Mass Loss of Top Mesh Bars of Slab S01

The average percentage of mass loss for each bar per unit length is then used to calculate the average percentage of mass loss of each layer of top mesh bars for each slab. The average percentage of mass loss of top mesh-top layer and top mesh bottom-layer bars are presented in Figure 5.12 to show the difference between them.

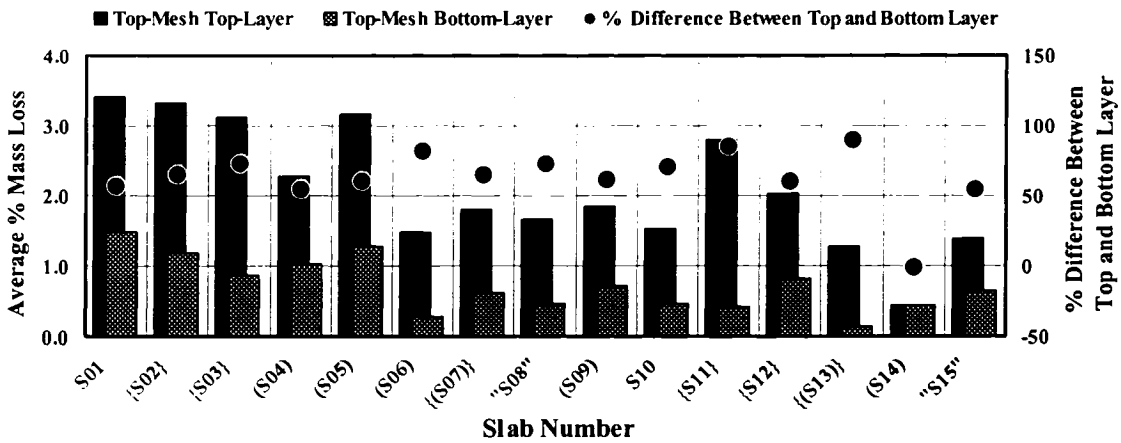

Figure 5.12: Average % Mass Loss of Each Layer of Top-Mesh Bars for Different Slabs

The average percentage of mass loss of the "patch" and the "non-patch" steel bars of the top mesh is then calculated to determine the change in the mass loss between them due to

the different strategies of patch-repair. Figure 5.13 presents the percentage of mass loss of the "non-patch" and the "patch" steel bars for different slabs.

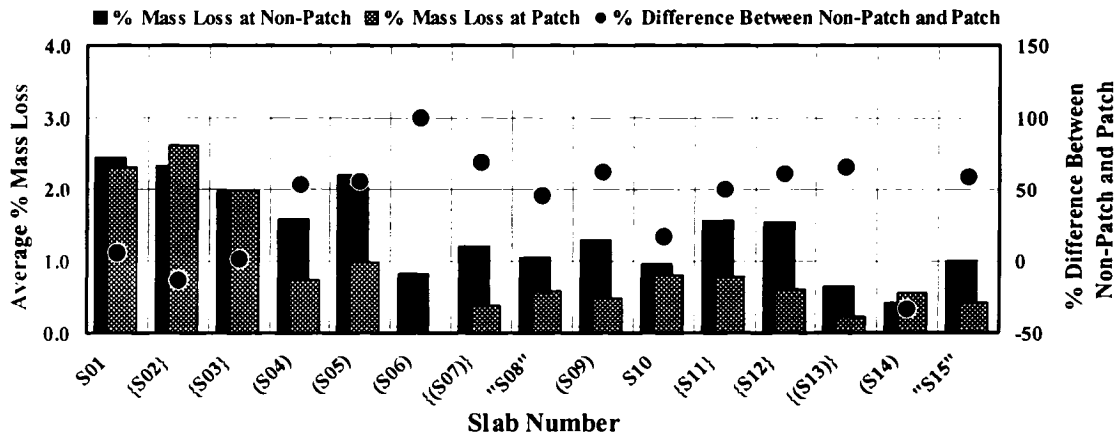

Figure 5.13: Average % Mass loss of Non-Patch and Patch Steel Bars for Different Slabs

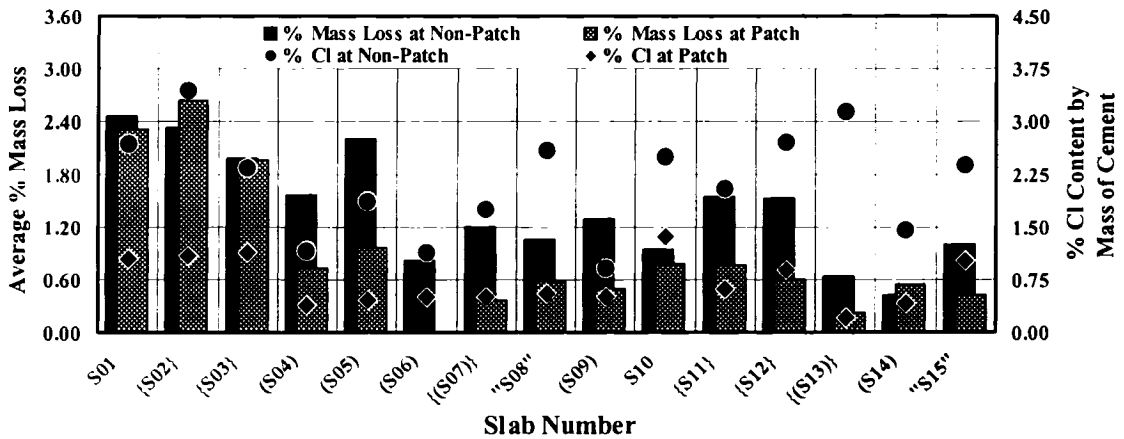

Figure 5.14: Comparison Between Average % Mass loss and % Chloride Content (by Mass of Cement) of Non-Patch and Patch Region of Different Slabs

Finally, the average percentage of mass loss of the "patch" and the "non-patch" steel bars of the top mesh and their corresponding percentage of chloride content (by mass of cement) are presented in Figure 5.14 to study the effect of chloride ions on the mass loss of

reinforcing bars. The vertical left scale represents the percentage of mass loss, and the vertical right scale represents the percentage of chloride content by mass of cement.

In these diagrams, slab nomenclatures enclosed with (...) parenthesis indicate the slab top surface treated with different coatings (sealer, epoxy, membrane or inhibitor), {...} parenthesis indicate the "patch" steel treated with different coating (epoxy, zinc or inhibitor), and "..." double quotation indicate the use of embedded anode, or anode sheet.

5.4.3 Observations and Discussion

The results in Table 5.7, Figure 5.9 to 5.14, and Appendix B to D lead to following observations:

1. No sign of corrosion was noticed on the bottom mesh of all slabs (Appendix B, Figures B.1 to B.30), because the chloride ions could not reach the bottom mesh, "non-availability" of carbon dioxide at that region, and the formation of macrocell between the top and bottom mesh.

Table 5.8: Comparison Between Different Test Results of Two Control Specimens

Slab Number	Non-Patch			Patch		
	HCP Reading (mV)	% Cl (By Mass of Cement)	% Mass Loss	HCP Reading (mV)	% Cl (By Mass of Cement)	% Mass Loss
Control-A (S01)	-533	2.68	2.45	-494	1.05	2.31
Control-B (S10)	-556	2.51	0.95	-509	1.36	0.79
% Difference	**-4**	**6**	**61**	**-3**	**-29**	**66**

2. Figure 5.12 shows that the percentage of mass loss of top layer steel of top mesh of all slabs is higher than that of bottom layer steel due to the higher chloride content at top layer than bottom layer. The maximum mass loss was noted in the Control-A

specimen (Slab S01). A comparison between the different test results of the two control specimens is shown in Table 5.8. The half-cell potential reading at the "patch" and the "non-patch" regions and the percentage of chloride content at the "patch" region of Control-B specimen (Slab S10) shows that KCl causes increased corrosion activity than NaCl, but the mass loss test shows that NaCl causes more corrosion reactive than KCl. The rebar mass loss observed in KCl contaminated environment is 60% smaller than that in NaCl.

3. Figure 5.14 shows that the percentage of mass loss of the "patch" steel bars of all slabs is smaller than that of the "non-patch" steel, except for Slab S02. The "patch" steel of Slab S02 was treated with an epoxy primer, therefore, theoretically it should have a smaller percentage of mass loss than its "non-patch" region, but it shows the opposite results. It may be due to the absence of the passive layer on the "patch" steel bars and some moisture might have been trapped underneath the coating. The reason for a lower mass loss observed in the "patch" steel bars due to a lower W/C (0.45 instead of 0.52) ratio in the "patch" concrete, and different protective measures applied on the patch steel bars.

4. The minimum rebar mass loss was noted in the "patch" region of Slab S13, which was treated in three ways, corrosion inhibitor admixture / superplasticizer was added in the "patch" concrete, corrosion inhibitor grout was coated on the "patch" steel, and corrosion inhibitor surface coating was applied on the slab top surface. It illustrates that corrosion inhibitor does not prevent corrosion completely, but it retards it. Similar observation was found in a Transports Quebec's research project undertaken by Daniel (1997).

5. The "patch" steel bars of Slabs S02 and S03 were coated with epoxy and zinc primer, respectively. Figure 5.13 shows that zinc primer had almost 25% more corrosion prevention capacity than the epoxy primer. The concrete top surface of Slab S04 and S05 were coated with sealer and epoxy, respectively, and Slabs S06

and S09 were provided with membranes. The maximum mass loss was found in Slab S05, which was coated with epoxy, therefore, the effectiveness of epoxy coating can be considered to be doubtful. Similar comment was made by Erdogdu et al. (2001). Performance of breathable traffic-bearing membrane was better than that of other two categories. Comparison between the "patch" steel treatment and the concrete top surface treatment shows that higher mass loss observed in the "patch" steel treated slabs than in the concrete top surface treated slabs. However, a combination of both treatments performs better than any individual treatment, which is reflected in the "patch" region of Slab S07. Therefore, in selecting a single barrier system, concrete top surface treatment with sealer or membrane is preferable in reducing the chloride ion ingress into the concrete.

6. A small puck-shaped sacrificial anode (64 mm diameter by 27 mm height) was embedded into a corner of the patch of Slab S08. However, a sacrificial anode sheet was attached on the concrete top surface of Slab S14 and bottom surface of Slab S15. In addition, the concrete top surface of Slab S14 was treated with epoxy coating. Figure 5.13 shows that there is no significant difference between different sacrificial anode systems. However, Slab S14 represents the minimum mass loss between these three specimens, due to the application of the additional epoxy coating on its top surface, which reduced the ingress of chlorides near the steel reinforcement. Epoxy coating was applied on the anode sheet to protect it from damage, as well as to provide additional defence against chloride ion ingress. However, for the benefit of the field performance, embedded anode is safer than the exposed anode sheet to avoid any external damage.

5.5 Corrosion Penetration Rate (CPR) Measurement

As mention earlier, corrosion is related to the flow of electrons. An element or compound that loses electrons is said to be oxidized (anode) and the one that gains electrons is said to be reduced (cathode). When metal oxides are formed, the metal atoms lose the electrons in the outer shell of the element. The metal atoms are oxidized and the oxygen is reduced.

This flow of electrons forms an electrochemical cell, where the positive electrode is the anode, while the other is the cathode. This cell may also occur with a so-called 'mixed electrode' in which the anode and cathode are on the same material. A 'mixed electrode' may occur in reinforced concrete if a number of following conditions apply:

(a) The passive film on the reinforcement must be destroyed locally

(b) The concrete must be moist enough to act as an electrolyte

(c) The cover must be permeable to oxygen.

Individually, the anodic and cathodic process would lead to an accumulation of positive and negative charges, respectively, on the reinforcement. This is not sustained because the hydroxyl ions diffuse towards the anode where they meet the counter-diffusion of ferrous ions. The resulting combination causes electrical neutralisation, if the anodic and cathodic processes are coupled together in the form of corrosion cell with no excess electrons. If there is no external source of electrons, the electrons produced by oxidation are fully consumed by reduction. Thus, the oxidation and reduction rates must be equal. Hence the anodic reaction rate must equal the cathodic reaction rate, which controls the rate of corrosion.

Thus, the rate of electron flow reflects the rate of corrosion. The rate of flow may be referred to as 'corrosion current density'. Essentially it is the number of electrons flowing per unit surface area of the rebar. A value at the upper end of the range of 'corrosion current density' would be 100 mA/m^2.

5.5.1 Calculation Procedure

A relationship exists between the measured current flow and the annual material loss through Faraday's Laws, which states that the mass of the substance liberated is proportional to the quantity of electric charge applied to it. Faraday's Second Law of Electrolysis concerns the mass of different substances liberated by the same quantity of electrical charge, i.e., the masses are proportional to the ratio of the atomic mass and the valance. Thus the mass loss may be calculated from:

$$m = \frac{MC}{zF} \quad \ldots \quad \ldots \quad \ldots \quad (5.9)$$

where m = Mass loss of corroded element

M = Atomic mass of the element

C = Electric charge

z = Valence of the element

F = Faraday constant (96,500 coulomb)

This ratio of atomic mass to valance is called the chemical equivalent. In the case of iron (Fe) and the ferrous ion (Fe^{2+}), the atomic mass is 55.85 amu (atomic mass unit) and the valence is two. Therefore, the chemical equivalent is 27.95 and oxidation of 27.95 gm of Fe occurs per Faraday of electrical charge. Coulomb is the electric charge conveyed in one second by a current of one ampere. For a corrosion current density of one milliampere per square meter (mA/m^2), equivalent to 0.001 coulomb/m^2/s, the Corrosion Rate (CR) in terms of mass loss is:

$$CR = \{(55.85)\,(0.001)\,(1)\} / \{(2)\,(96500)$$

$$= 2.89 \times 10^{-7}\ gm/m^2/s$$

Therefore, for i_{corr} (mA/m^2) of corrosion current density, the corrosion rate (CR) in terms of mass loss is:

$$CR = 2.89 \times 10^{-7}\ i_{corr}\ gm/m^2/s \quad \ldots \quad \ldots \quad (5.10)$$

where $$i_{corr} = \frac{I_{corr}}{A}\ mA/m^2 \quad \ldots \quad \ldots \quad (5.11)$$

I_{corr} is corrosion current measured in milli-amperes, and A is the surface area of corroded element measured in m^2. If the density of the mild steel is considered as 7.85 gm/cm^3 then the corrosion rate (CR) in terms of the volume loss becomes:

$$\{2.89 \times 10^{-7}\ i_{corr}\} / \{7.85\} = 3.68 \times 10^{-12}\ i_{corr}\ cm\text{-}m^2/m^2/s$$

which represents the corrosion penetration rate (CPR) in cm per second. Now, 1 year is

equal to 3.15×10^7 sec and 1 centimetre is equal to 10 millimetre, therefore, the corrosion penetration rate (CPR) becomes:

$$\text{CPR} = 1.16 \times 10^{-3}\, i_{corr} \text{ mm/year} \quad \ldots \quad \ldots \quad (5.12)$$

or,

$$\text{CPR} = 1.16\, i_{corr} \text{ μm/year} \quad \ldots \quad \ldots \quad (5.13)$$

where, i_{corr} is measured in mA/m^2 ($1mA/m^2 = 0.1\mu A/cm^2$).

This is the most useful equation to calculate the corrosion penetration rate in a non-destructive manner. Here, i_{corr} is the corrosion current density taken from the Tafel plot, which is the corresponding value of intersection of two extrapolated line of corrosion potential, E_{corr} due to two half-cell reaction of a corrosion cell. Six sets of readings were taken on both the "patch" and the "non-patch" regions of each slab, and compared with the actual rates of corrosion penetration, obtained from the destructive tests.

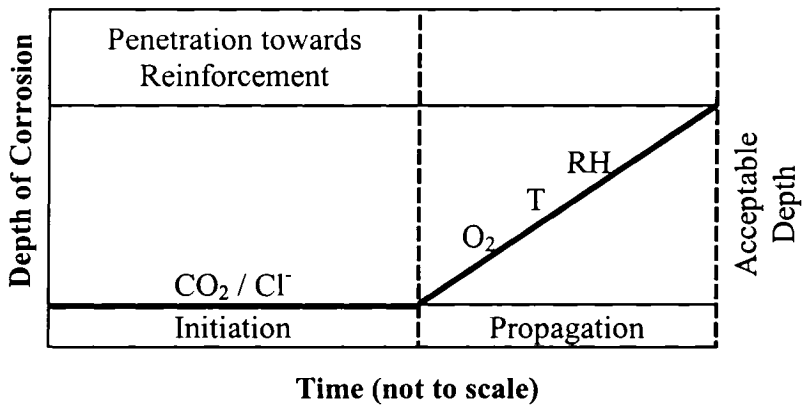

Figure 5.15: Model Showing Initiation and Propagation Time of Corrosion
(Tuutti, 1982)

To calculate the corrosion penetration rate, it is important to know the propagation period accurately. Tuutti (1982) proposed a model (Figure 5.15) to explain the corrosion of steel in concrete. In this model, the total time frame is divided into two parts, initiation time and propagation time. The time required for breaking the passive layer of the steel is generally called the initiation period. After the initiation period, corrosion commences and the depth

of corrosion increases with time. Time required to reach the acceptable depth of corrosion is called propagation period. Carbon dioxide (CO_2) and chloride ions (Cl^-) are the major driving force for breaking the passive layer, and oxygen (O_2), relative humidity (RH), electrolyte media and temperature (T) are responsible for keeping the environment favourable to commence, or accelerate corrosion. The mechanism of corrosion of embedded steel in concrete is described in Chapter Two.

Richardson (2002) noted that the carbonation depth often reaches a limit at very low values, or it may proceed at a rate that is slow enough to prevent depassivation of the steel reinforcement within the design life of the structure. However, corrosion of reinforcement due to chloride penetration is the most significant threat to the existing reinforced concrete infrastructure. Herein, only the effect of chloride penetration is considered to calculate the initiation time. But the critical level, at which the passivity is lost and corrosion commences is not clearly defined, and significant variations exist in the literature on the chloride level, which causes corrosion to initiate.

In this project, CSA recommended threshold value of 0.15% chloride ion content by mass of cement for reinforced concrete exposed to moist and chloride-contaminated environment (Section 5.3.2) was used to determine the initiation time of corrosion.

Service life prediction, that involves modelling the rate of chloride ingress, is complicated by the variety of complex mechanisms involved in both the uptake of chlorides from external sources and the processes that influence its penetration through the concrete cover. Nevertheless, it is recognised that the best parameter currently available is the apparent chloride diffusion coefficient based on Crank's solution to Fick's second law of diffusion. Despite its shortcoming, the solution by Crank allows prediction of future chloride profiles from which a design estimate can be made of the time taken for the critical chloride threshold to build up at the level of the reinforcement. It is recognised that the equation does not perfectly model the case of chloride ingress into the concrete but it can be usefully employed in an empirical manner. Nilsson et al. (2000) noted that this error function fits

well with the actual chloride penetration profile beyond a concrete cover thickness of 10 mm. An additional effect of absorption influences this function to fit well within the outer 10 mm of the concrete cover thickness. Therefore, an additional allowance of 10 mm can be added to the calculated cover thickness. For concrete cover thicknesses of more than 10 mm, this model can be used, and it is used here to calculate the initiation time of corrosion in fifteen test slabs.

Fick's second law of diffusion concerns the rate of change of concentration (C) with respect to time (t). It may be stated as follows for diffusion in a semi-infinite, homogenous medium, where the diffusion coefficient (D) is independent of the dependent and independent variables:

$$\frac{\partial C}{\partial t} = D\frac{\partial^2 C}{\partial x^2} \quad \ldots \quad \ldots \quad \ldots \quad (5.14)$$

with the boundary conditions of:

$$C_x = 0 \quad \text{at } t = 0 \text{ and } 0 < x < \infty$$

$$C_x = C_s \quad \text{at } x = 0 \text{ and } 0 < t < \infty$$

where C_x = Chloride concentration at depth x

and C_s = Surface chloride concentration

Crank's solution of Fick's second law of diffusion can be stated as follows:

$$\frac{C_x}{C_s} = \left[1 - erf\left\{\frac{x}{2(Dt)^{1/2}}\right\}\right] \quad \ldots \quad \ldots \quad \ldots \quad (5.15)$$

where erf = Error function

t = Time of exposure in seconds

x = Depth from the exposure surface in mm

and D = Apparent diffusion coefficient in mm^2/s.

In this experiment, the surface chloride concentration (C_s) was 15% by mass of water for all specimens. To get the surface chloride concentration 6.75% and 7.8% by mass of cement

for the "patch" and the "non-patch" regions, it was multiplied by individual water-cement ratio 0.45 (for the "patch" concrete) and 0.52 (for the "non-patch" concrete), respectively. Concrete samples for the chloride content test was collected at a depth of 45 mm from the exposed surface of the "patch" and the "non-patch" regions of each slab. Therefore, the depth from the exposed surface (x) is 45 mm, common for all specimens. The samples were collected after 28 months of casting of each slab. The time taken for hardening, curing and preparation for initial wetting/drying cycle was 6 months and to accelerate corrosion of the "non-patch" steel bars before patch repair (initial ponding time) was 5 months. Two months were taken to repair and harden all the patches. Therefore, two sets of time of exposure were found, one for the "patch" region (t_p) and the other for the "non-patch" region (t_n). The total time of exposure for the "patch" region (t_p) and the "non-patch" region (t_n) were 15 months and 20 months, respectively. The chloride concentration (C_x) at 45 mm depth for the "patch" and the "non-patch" region of each slab was taken from the chloride content test result (Table 5.3).

Using the above data and Equation 5.15, the apparent diffusion coefficients (D) of the "patch" and the "non-patch" concrete of each slab, whose concrete top surface were not treated with any kind of surface coating (S01, S02, S03, S08, S10, S11, S12, and S15), were calculated. Theoretically, the concrete cast with similar concrete mixture and procedure, should have similar diffusion coefficients at a particular time and depth. But dissimilarities may be observed due to the variations during construction and "non-homogeneous" nature of the concrete. In this experiment, three categories of concrete were used, the "non-patch" concrete with a water-cement ratio of 0.52, the "patch" concrete with a water-cement ratio of 0.45, and some "patch" concrete (Slabs S11, S12 and S13) additionally mixed with corrosion inhibitor admixture (CI-A). Therefore, diffusion coefficient for the "patch" concrete, the "non-patch" concrete, and the "patch" concrete mixed with CI-A were obtained by making the average of the diffusion coefficients of similar categories. These diffusion coefficients were then used to determine the surface chloride content underneath the coating of the Slab S04, S05, S06, S07, S09, S13 and S14. Using the equivalent surface chloride content and the average diffusion coefficient, the

corrosion initiation time for each slab was calculated to achieve the chloride threshold value of 0.15% by mass of cement (CSA A23.1-15.1.6.1) at a depth of 25 mm (clear concrete cover) from the concrete top surface. The corrosion propagation time of reinforcement in each slab was then calculated by subtracting the corrosion initiation time from the total exposure time.

The mass loss per unit length of each bar was calculated earlier. It is now converted into a volume loss per unit length by dividing it with the density of mild steel and then the total penetration depth is calculated by dividing the volume with the average surface area of the bar. Finally, the actual corrosion penetration rate of the reinforcement in each slab is obtained by dividing the total penetration with the individual corrosion propagation time. The results are not completely accurate due to the deficiency of the model, however, it still provides a guideline to check the results with the corrosion penetration rate obtained in the Tafel test.

5.5.2 Interpretation of Results

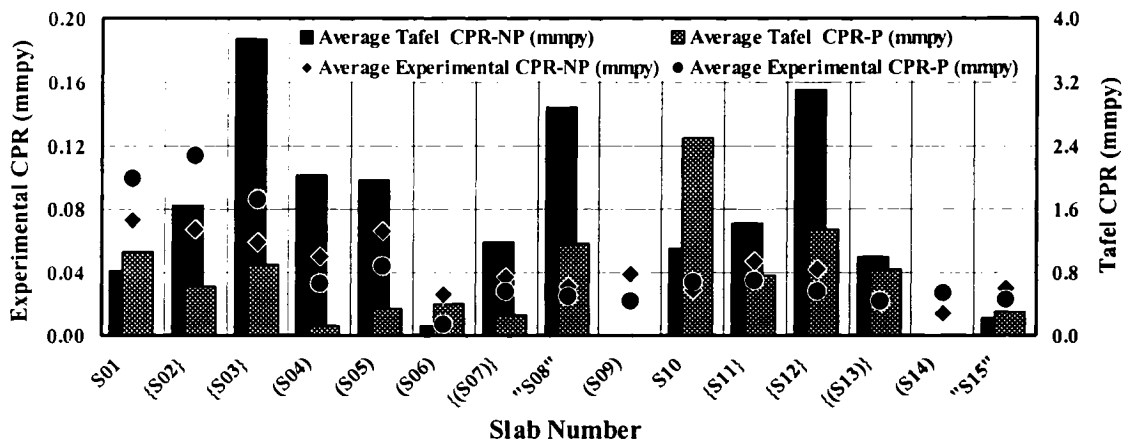

Figure 5.16: Average Corrosion Penetration Rate (Experimental vs. Tafel)

The average corrosion penetration rate (CPR), predicted by Tafel measurement, and the average experimental (actual) CPR, calculated from the mass loss data of the reinforcement at the "patch" (P) and the "non-patch" (NP) regions of each slab, are presented in Figure 5.16 and Table 5.10, along with the average experimental CPR calculated from the mass loss data in millimetre per year (mmpy). In the case of Slabs S09 and S14, meaningful Tafel plot could not be produced, therefore, no corrosion rates are available, which represent the missing bars in the figure. The ratio between the predicted (Tafel) CPR and the experimental CPR for the "patch" and the "non-patch" regions are also shown in Table 5.10.

Table 5.9: Corrosion Rates of Steel in Concrete
(Millard et al, 2001)

Corrosion Intensity	Corrosion Penetration Rate, CPR (μmpy)	Corrosion Penetration Rate, CPR (mmpy)
Very High	100 - 1000	0.1 - 1.0
High	10 - 100	0.01 - 0.1
Low to Moderate	1 - 10	0.001 - 0.01
Passive	< 1	< 0.001

Millard et al. (2001) suggested an interpretation guideline (Table 5.9), as an indication of the severity of corrosion, based on typical corrosion rates for the steel reinforcement embedded in concrete. The corrosion intensity varies from passive to very high rates and the ranges are shown in both micrometer per year (μmpy) and millimeter per year (mmpy).

Again, in Figure 5.16 and Table 5.10 slab, nomenclatures enclosed with (...) parenthesis indicate the slab top surface treated with different coatings (sealer, epoxy, membrane or inhibitor), {...} parenthesis indicate the "patch" steel treated with different coating (epoxy, zinc or inhibitor), and "..." double quotations indicate the use of an embedded anode, or anode sheet.

Table 5.10: Comparison Between Experimental Corrosion Penetration Rate (CPR) and Tafel Results

Slab Number	Average Experimental CPR (mmpy)		Average Tafel CPR (mmpy)		Ratio of Tafel and Experimental	
	Non-Patch	Patch	Non-Patch	Patch	Non-Patch	Patch
S01	0.073	0.099	0.830	1.067	11	11
{S02}	0.067	0.113	1.648	0.628	24	6
{S03}	0.059	0.086	3.731	0.906	63	11
(S04)	0.050	0.033	2.039	0.115	41	3
(S05)	0.066	0.044	1.970	0.338	30	8
(S06)	0.027	0.007	0.117	0.406	4	61
{(S07)}	0.037	0.028	1.190	0.252	32	9
"S08"	0.031	0.025	2.882	1.158	92	47
(S09)	0.039	0.022	-	-	-	-
S10	0.030	0.034	1.111	2.485	38	72
{S11}	0.048	0.035	1.425	0.771	30	22
{S12}	0.042	0.028	3.087	1.346	73	49
{(S13)}	0.021	0.022	0.999	0.836	48	37
(S14)	0.014	0.027	-	-	-	-
"S15"	0.030	0.023	0.223	0.299	7	13

5.5.3 Observations and Discussion

The results in Figure 5.16 and Table 5.10 leading to the following observations:

1. There is a large difference between the experimental CPR and predicted (Tafel) CPR, which are shown in Figure 5.16 and Table 5.10. The maximum difference observed at the "non-patch" region of Slab S08, where the predicted (Tafel) CPR is 92 times higher than actual (experimental) CPR, and it is not acceptable. Obviously, during calculation of actual CPR, propagation time was estimated roughly, but this rough estimation is not the only reason of this large difference.

2. Millard et al. (2003) performed a test to correlate between the experimental mass loss and the predicted mass loss. The linear polarization resistance (LPR) technique was used to predict the mass loss. They concluded, "The mean ratio of LPR mass loss to the measured (actual) mass loss for all specimens is 2.1:1, which corresponds to a mean overestimate of 110% for the total mass of steel lost". In this experiment predicted (Tafel) CPR at the "patch" region of Slab S04 and the "non-patch" region of Slab S06 is 3 and 4 times higher than that of experimental CPR, respectively. This over-estimation may be acceptable with a considerable reservation. The rest of the predicted (Tafel) CPR is abnormally higher than the experimental CPR, which is questionable and needs further research.

3. An underestimate of the predicted corrosion rate would result in an inappropriate decision for taking any protective measures against corrosion, and owner or the designer may get confused to start maintenance. In this experiment, all predicted (Tafel) CPR values (Table 5.10) overestimate of the mass loss of the bars, however, the amount of overestimation of the predicted CPR of most of the slabs is very large and needs further investigation.

4. Theoretically, CPR of the "patch" steel should be less than the "non-patch" steel. However, experimental CPR of the "patch" steel of Slab S01, S02, S03, S10 and S14, and the predicted (Tafel) CPR of the "patch" steel of Slab S01, S06, S10 and S15 are higher than that of the "non-patch" steel, which is not a desirable situation.

5. According to the interpretation guideline (Table 5.9) of corrosion intensity, experimental corrosion penetration rate of the "patch" and the "non-patch" steel of all slabs except for the "patch" steel of Slab S06 show "High" levels of corrosion and the "patch" steel of Slab S06 represents "Low to Moderate" levels of corrosion. The predicted (Tafel) corrosion penetration rate of the "patch" and the "non-patch" steel of all other slabs shows "Very High" levels of corrosion.

5.6 Effect of Grounding on Half-Cell Reading

Each specimen was kept on a metal frame to handle it easily during the period of accelerated corrosion. Therefore, each specimen was directly connected with the ground through the metal frame; it was decided to determine whether the grounding of the metal frames had any effect on the half-cell readings. Slabs S02 and S05 were selected to investigate before their demolition. Wooden blocks were placed between the slab and the metal frame to isolate them from the frame as well as from the ground.

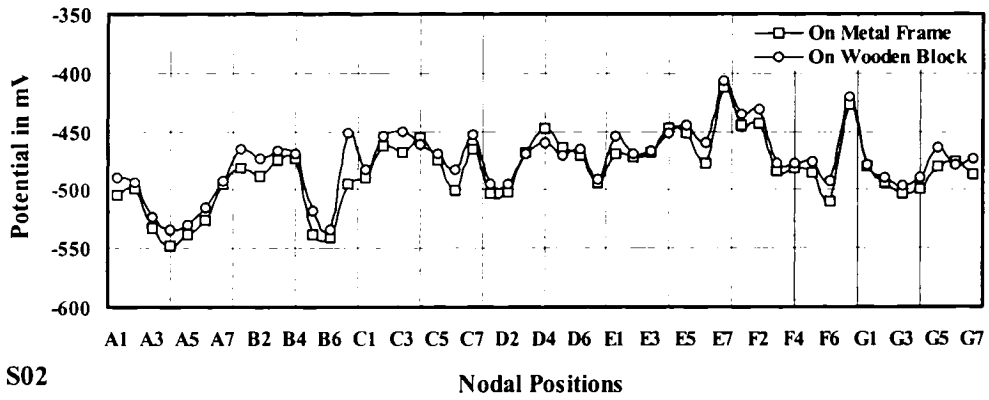

Figure 5.17: Effect of Grounding on Half-Cell Reading of Slab No. 2

The slab tops were kept moist before taking half-cell readings. Readings were taken on each grid point (as previously described) keeping the slab on wooden blocks and after removing the blocks. The two sets of half-cell reading for each slab are presented graphically in Figure 5.17 and 5.18.

Figure 5.17 and 5.18 show that there is no significant difference between the two conditions, keeping the slab on the wooden block and on the metal frame. The plot designated by "On Metal Frame" and "On Wooden Block" overlap closely. Therefore, grounding of the slab has not any significant effect on the half-cell readings.

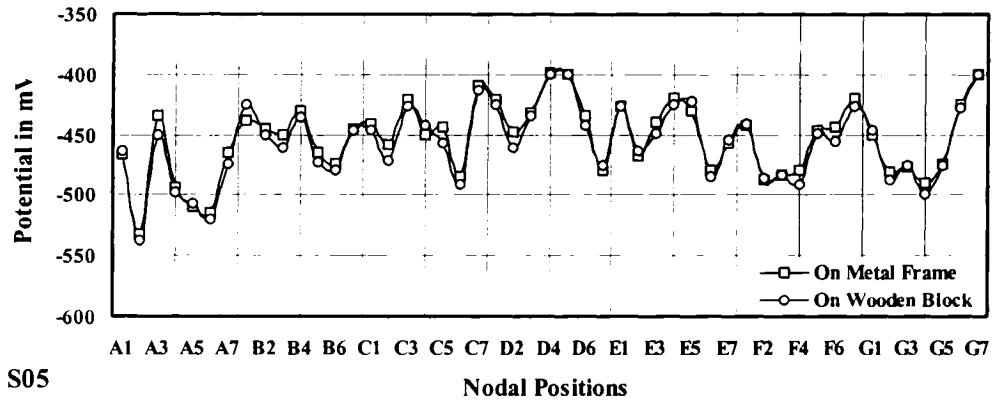

Figure 5.18: Effect of Grounding on Half-Cell Reading of Slab No. 5

5.7 Effect of Electrolyte Age on Half-Cell Reading

The Slabs S02 and S05 were also investigated to examine the effect of the age of electrolyte on the half-cell potential readings. New copper sulphate ($CuSO_4$) solution was filled into the sulphate ion electrode and half-cell readings were taken at each nodal point of each slab. After 15 days similar readings were taken keeping the slabs in their previous position. The corresponding readings are also available from the previous test using the same half-cell electrode filled with an old solution.

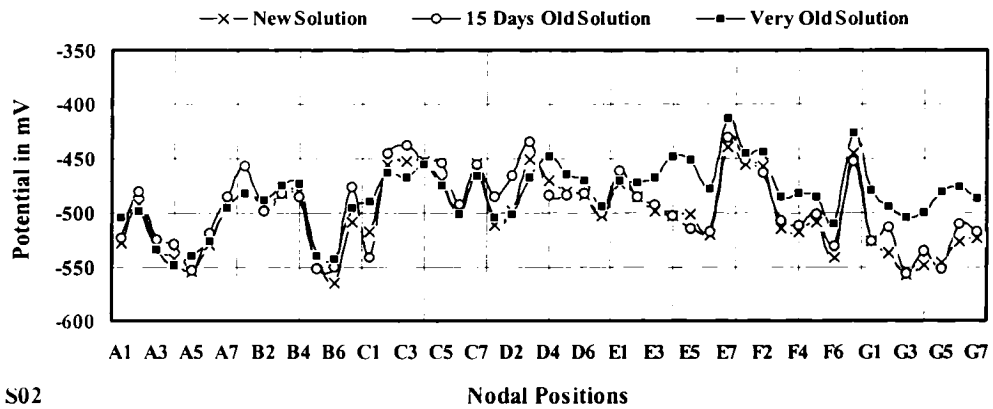

Figure 5.19: Effect of Electrolyte Age on Half-Cell Reading of Slab No. 2

The two sets of data are plotted in Figures 5.19 and 5.20; each set contains three different readings, the first set of readings was obtained using the electrode filled with an old solution, the second set with a new solution on the day of filling, and the third set with a fifteen days old solution.

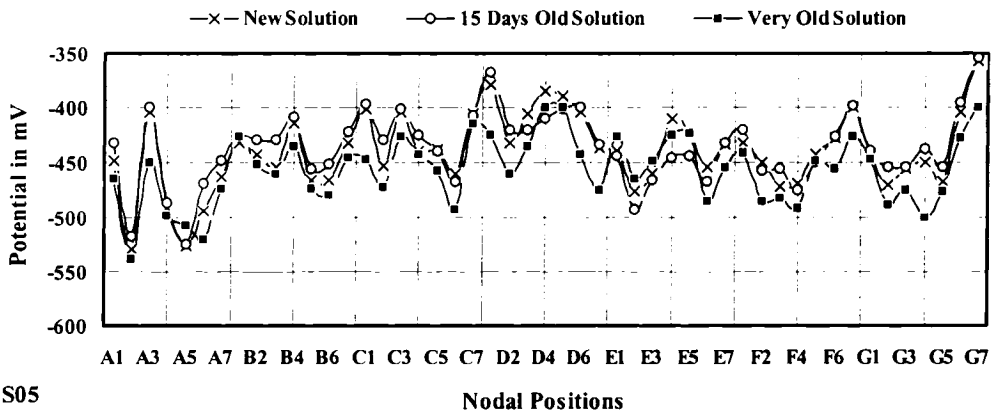

Figure 5.20: Effect of Electrolyte Age on Half-Cell Reading of Slab No. 5

Figures 5.19 and 5.20 show that there is no significant difference between the different readings excepting for the readings obtained using the electrode with the old solution, which have a tendency to deviate from the readings obtained using the electrode with the new solution. However, the readings obtained using a fresh solution and a 15-day old copper sulphate solution is quite close. Therefore, care must be taken to avoid the error during half-cell potential measurement using an electrode filled with solution older than two or three weeks and at most one month, as suggested by ASTM C 876-91.

Chapter 6

Conclusions and Recommendations

6.1 Introduction

Durability of reinforced concrete infrastructure is severely affected by the corrosion of the reinforcing steel. Electrochemical incompatibility between the "repaired-patch" concrete and the existing "old" concrete is one of the main reasons for further deterioration of repaired system. This research was undertaken to compare the performance of different repair strategies with respect to the conventional repair.

Fifteen 1000 x 1000 x 200 mm reinforced concrete slabs were cast to represent a section of the deteriorated reinforced concrete bridge deck of the demolished Dickson Bridge in Montreal. A 333 x 333 x 100 mm patch was left at the central part of each slab. The slab reinforcement was corroded in an accelerated manner, using a 15% salt solution, and 3-days wetting and 4-days drying cycle, for a period of five months. After initial ponding, the patches were repaired using eleven different techniques specified by different industrial partners. Then the slabs were corroded again using a similar acceleration procedure for the next fifteen months, and different electrochemical and other tests were performed to monitor the corrosion activity of each slab.

6.2 Conclusions

The results of this experiment are summarized and relevant conclusions are drawn as follows:

1. Observation of electrochemical incompatibility between the chloride-contaminated "non-patch" concrete and chloride free patch concrete of all the repair system leads to local corrosion around the patch, however, the extent of corrosion varies from one repair technique to another. This incompatibility is reflected as a maximum

potential difference at the beginning of the repair, however, it decreases suddenly and increases again with time.

2. Use of a sacrificial anode can reduce this potential difference by a remarkable amount two months after the repair, however, it loses its performance gradually (Slab S08, Figure A.8). The use of zinc sheet anode on the top of the slab shows almost similar behavior six months after repair (Slab S14, Figure A.14). Equal amount of rebar mass loss (0.6%) is observed in the patch region of each slab within one and half year of the propagation time. Epoxy coating was additionally applied on the zinc sheet top to protect it from external damage, which also acts as a secondary barrier to reduce the chloride ingress into the concrete i.e. reduce the rebar mass loss, but in the case of the sacrificial anode, no additional barrier was applied. A comparison of their individual performances showed that the sacrificial anode performed better; it is less costly and easy to install. Therefore, increasing the number of sacrificial anodes distributed uniformly throughout the patch region can possibly increase the service life of the repaired system.

3. No evidence of corrosion is observed at the bottom mesh of all slabs due to:
   (a) Formation of macrocell between top and bottom mesh of the reinforcement,
   (b) "Non-availability" of chloride ion ingress from the top surface, and
   (c) "Non-availability" of moisture and oxygen in that region.

4. Three categories of corrosion inhibitors were used in this experiment: (a) corrosion inhibitor admixture / superplasticizer (CI-A) for patch mix concrete, (b) corrosion inhibitor grout (CI-G) for patch steel coating, and (c) corrosion inhibitor surface coating (CI-S) for slab top application. Combination of these three inhibitors shows the best performance. CI-A and CI-G works together better in a KCl environment than in a NaCl environment. The CI-S is not effective to reduce chloride ingress into the concrete. Finally, it illustrates that a corrosion inhibitor does not prevent

corrosion completely, but it retards the process. Similar observation was noted in a research project of Ministére de Transports du Québec (Daniel, 1997).

5. The concrete top surface treatment such as penetrating sealer, impermeable epoxy surface coating, or breathable traffic-bearing membrane cannot stop the chloride ingress into the concrete completely, however, it can reduce this ingress by 50% of the "non-treated" surface. Epoxy surface coating can reduce the chloride ingress into the concrete, however, it cannot reduce the corrosion activity as well, because moisture inside the concrete is trapped underneath the coating, which can accelerate further corrosion. Therefore, effectiveness of epoxy coating is questionable. Similar conclusion was reached by Erdogdu, et al. (2001).

6. An underestimate of corrosion rate would result in significant damage prior to the monitoring, indicating a strong need for inspection. The results show that all predicted corrosion penetration rate (CPR) by Tafel test were an overestimate of the mass loss of the bars. This requires a more detailed examination, and the designers and managers need to be more vigilant.

7. Each specimen was kept on a metal frame during investigation, therefore, it was directly connected to the ground. Test shows that grounding of the slab does not have any significant effect on its half-cell readings.

8. The half-cell potential reading, using an electrode with a very old solution tend to deviate from the "actual" reading, therefore, it is recommended that a new solution be used each time to avoid erroneous results. The ASTM C 876-91 standard also recommends that the copper sulphate solution should be renewed either monthly or before each use, whichever is the longer period.

6.3 Recommendations

This research illustrates that for new construction, concrete must have a low diffusivity to avoid premature deterioration. For repair, the use of electrochemical protection systems such as cathodic protection, embedded anode, corrosion inhibitor, and chloride extraction should be considered to increase the service life of the repaired system. Surface coatings such as zinc, epoxy, sealer or a membrane can be used as an additional line of defence. In addition, the existing cracks must be treated, and the bridge deck drainage system and expansion joints must be designed properly to avoid ingress of chloride-contaminated water into the concrete. This research shows that the lack of electrochemical compatibility between the "repaired" concrete and the original "chloride-infested" concrete can result in failure of the repair due to further aggravated corrosion. These results can be helpful for the concrete repair industry, as well as for future research to mitigate corrosion.

Presently, the level of deterioration of reinforced concrete infrastructure is so high that rehabilitation costs are growing exponentially. Corrosion of steel in concrete due to chloride-contamination is the principal cause for this deterioration. Conventional patch-repair of concrete deck system cannot provide adequate service life, because the electrochemical incompatibility between chloride-contaminated "non-patch" concrete and chloride-free patch concrete promotes further corrosion. The nature and consequence of electrochemical activities in a repair system, as compared with new construction, are still not well understood. This results in an inability to accurately predict the performance of a protective repair system and the service life of a repaired structure. The first part of the investigation to understand these phenomena was undertaken by Leyne (2004) and Saifuzzaman (2004), however, much more research is needed in this area. The following objectives are recommended for the future research program:

1. To verify the existing electrochemical testing procedures to determine the deterioration conditions in the field, and to possibly develop a new and more reliable testing procedure.

2. The accuracy of the half-cell potential test, normally used to detect probable corrosion, has been questioned by several investigators, therefore, more research is needed to reexamine the interpretation guideline associated with the test.

3. To develop some interpretation guideline to correlate the laboratory test results, taken from different accelerated corrosion procedures (extent, cycle and duration of exposure condition) with the field data for a few selected deteriorated bridges.

4. To study experimentally the permeability of concrete and the associated diffusivity of the chloride ions for concretes made with different water / cementitious materials ratios. This data can be helpful for future research and also to consulting engineers in designing for durability against the various permeability-related phenomena.

5. To further examine the electrochemical incompatibility between chloride-contaminated concrete and chloride-free repair patch.

6. To study the mitigating effect of cathodic protection with patch repairs

7. To develop simple guidelines for design of durable concrete structures against deterioration due to corrosion of the reinforcing steel.

References

[01] Andrade, C., Alonso, C., Gonzalez, J. (1986), *Some Laboratory Experiments on the Inhibitor Effect of Sodium Nitrite on Reinforcement Corrosion*, Cement Concrete and Aggregate 8: 110-16.

[02] Amleh, L. (1996), *Influence of Corrosion of Reinforcing Bars on the Bond between Steel and Concrete*, M. Engineering Thesis, Department of Civil Engineering and Applied Mechanics, McGill University, Montreal, Canada.

[03] Amleh, L. (2000), *Bond Deterioration of Reinforcing Steel in Concrete due to Corrosion*, Ph.D. Thesis, Department of Civil Engineering and Applied Mechanics, McGill University, Montreal, Canada.

[04] ASTM C 114 (1992), *Standard Test Methods for Chemical Analysis of Hydraulic Cement*, Section 19 – Chloride (Reference Test Method), Volume: 04.01, pp. 104-113.

[05] ASTM C 1218 (1992), *Standard Test Method for Water-Soluble Chloride in Mortar and Concrete*, Volume: 04.02, pp. 626-628.

[06] ASTM C 876-91 (1992), *Standard Test Method for Half-Cell Potentials of Uncoated Reinforcing Steel in Concrete*, Volume: 03.02, pp. 433-438.

[07] ASTM G1-90 (Reapproved 1999), *Standard Practice for Preparing, Cleaning, and Evaluating Corrosion Test Specimens*, Volume: 03.02, pp. 15-21.

[08] Beaudette, R.M. (2001), *Investigation of Patch Accelerated Corrosion with Galvanized XP*, Interim Report, Crosier-Kilgour Research Slabs, January 31.

[09] Beaudoin, J.J., Gu, P., Mailvaganam, N.P. and Tumidajski, P.J. (1997), *Electrochemical Incompatibility of Patches in Reinforced Concrete*, Concrete International, V.19, No.8, pp. 68-72.

[10] Bentur, A., Berke, N.S., and Diamond, S. (1997), *Steel Corrosion in Concrete*, E and FN Spon, London.

[11] Browne, R. (1980), Concrete in the Oceans: Marine Durability of the Tongue Sand Tower, CIRIA Technical Report No. 5, Cement and Concrete Association, London.

[12] Browne, R. (1988), *Durability of Reinforced Concrete Structures*, Proceedings, Pacific Concrete Conference, New Zealand, 847 86.

[13] Bungey, J.H., and Millard, S.G. (1996), *Testing of Concrete in Structures*, Third Edition, Blackie Academic and Professional, Glasgow

[14] CEB-Comité Euro-International du Béton (1992), *Durable Concrete Structures-Design Guid*, Thomas Telford, London.

[15] Cleland, D.J., Long, A.E., and Yeoh, K.M. (1997), *Corrosion of Reinforcement in Concrete Repair*, Construction and Building Materials, V.11, No.4, pp. 233-238.

[16] CSA-A23.1-15.1.6, *Limits on Chloride Ion Content*, Concrete Materials and Methods of Concrete Construction / Methods of Test for Concrete, Canadian Standards Association, 2000.

[17] Daniel, V. (1997), *Performance of Corrosion Inhibitors*, Info DLC V.2, No.7, Research and Development Projects, Transports Quebec, Quebec, Canada.

[18] Dias, W.P.S. (2000), *Reduction of Concrete Sorptivity with Age through Carbonation*, Cement and Concrete Research, Vol. 30, pp. 1255-1261.

[19] El Maaddawy, T.A., and Soudki, K.A. (2003), *Effectiveness of impressed current technique to simulate corrosion of steel reinforcement in concrete*, Journal of Materials in Civil Engineering, V.15, No.1, pp.41-47.

[20] Elsener, B. (2002), *Macrocell Corrosion of Steel in Concrete - Implications for Corrosion Monitoring*, Cement and Concrete Composites, V.24, No.1, pp. 65-72.

[21] Emmons, P.H., and Vaysburd, A.M. (2000), *How to Make Today's Repairs Durable for Tomorrow - Corrosion Protection in Concrete Repair*, Construction and Building Materials, V.14, No.4, pp. 189-197.

[22] Emmons, P.H., and Vaysburd, A.M. (2003), *Corrosion Inhibitors and Other Protective Systems in Concrete Repair: Concepts or Misconcepts*, Cement & Concrete Composites, V.26, pp.255-263.

[23] Erdogdu, S., Bremner, T.W., and Kondratova, I.L. (2001), *Accelerated Testing of Plain and Epoxy-Coated Reinforcement in Simulated Seawater and Chloride Solution*, Cement and Concrete Research, V.31, No.6, pp. 861-867.

[24] Erdogdu, S., Bremner, T.W., and Kondratova, I.L. (2001), *Accelerated Testing of Plain and Epoxy-Coated Reinforcement in Simulated Seawater and Chloride Solution*, Cement and Concrete Research, V.31, No.6, pp. 861-867.

[25] Everett, L., and Treadaway, K. (1980), *Deterioration due to Corrosion in Reinforced Concrete*, Information Paper 12/80, Building Research Establishment.

[26] Farah, F. (1993), *Accelerated Corrosion Testing of Reinforcing Steel Embedded in Concrete*, M. Engineering Thesis, Department of Civil Engineering and Applied Mechanics, McGill University, Montreal, Canada.

[27] Fazio, R. (1996), *Flexural Behaviour of Corroded Reinforced Concrete Beam*, M. Engineering Thesis, Department of Civil Engineering and Applied Mechanics, McGill University, Montreal, Canada.

[28] Heckroodt, R.O. (2002), *Guide to the Deterioration and Failure of Building Materials*, Thomas Telford, London.

[29] Ismail, M., and Soleymani, H.R. (2002), Monitoring Corrosion Rate for Ordinary Portland Concrete and High-Performance Concrete Specimens Subjected to Chloride Attack, Canadian Journal of Civil Engineering, V.29, No.6, pp. 863-874.

[30] Law, D.W., and Cairns, J.J. (2003), Department of Civil and Offshore Engineering, Heriot-Watt University, Edinburgh, UK, *Evaluation of Corrosion Loss of Steel Reinforcing Bars in Concrete Using Linear Polarization Resistance Measurements*, BAM International Symposium (NDT-CE 2003), Non-Destructive Testing in Civil Engineering 2003.

[31] Leyne, E. (2004), *Corrosion in Reinforced Concrete Repair*, M. Engineering Thesis, Department of Civil Engineering and Applied Mechanics and Applied Mechanics, McGill University, Montreal, Canada.

[32] Li, C.Q. (2000), *Corrosion Initiation of Reinforcing Steel in Concrete under Natural Salt Spray and Service Loading - Results and Analysis*, ACI Materials Journal, V.97, No.6, pp. 690-697.

[33] Lindvall, A. (2001), *Environmental Actions and Response - Reinforced Concrete Structures Exposed in Road and Marine Environments*, Thesis for the Degree of Licentiate of Engineering, Department of Building Materials, Chalmers University of Technology, Göteborg, Sweden.

[34] Millard, S.G., Bungey, J.H., Cairns, J., and Law, D. (2001), *Environmental Influences on Linear Polarisation Corrosion Rate Measurement in Reinforced Concrete*, NDT and E International, V.34, No.6, pp. 409-417.

[35] Millard, S.G., and Bungey, J.H. (2003), Department of Civil Engineering and Applied Mechanics, Liverpool University, Liverpool, UK, *Evaluation of Corrosion Loss of Steel Reinforcing Bars in Concrete Using Linear Polarization Resistance Measurements*, BAM International Symposium (NDT-CE 2003), Non-Destructive Testing in Civil Engineering 2003.

[36] Mirza, M.S. (1997), Professor of Civil Engineering and Applied Mechanics, McGill University, Montreal, Canada, *Infrastructure Management – National Experience*, Technical Report.

[37] Mirza, M.S. (1998), *Canada's Deteriorating Infrastructure*, Manitoba Heavy News Annual, Infrastructure Policies, Financing and Sustainable Development, pp. 16-23.

[38] Malhotra, V.M., Zhang, M.H., and Leaman, G.H. (2000), *Long-Term Performance of Steel Reinforcing Bars in Portland Cement Concrete and Concrete Incorporating Moderate and High Volumes of ASTM Class F Fly Ash*, ACI Materials Journal, V.97, No.4, pp. 409-417.

[39] Möller, J.S. (1994), *Measurement of Carbonation in Cement Based Material*, Publication 93:11, Department of Building Materials, Chalmers University of Technology, Göteborg, Sweden.

[40] Nilsson, L.O., Andersen, A., Luping, T., and Utgennant, P. (2000), Chloride Ingress Data from Field Exposure in a Swedish Road Environment, Publication P-00: 5, Department of Building Materials, Chalmers University of Technology, Göteborg, Sweden.

[41] Parrott, L. (1994), *Design for Avoiding Damage due to Carbonation-Induced Corrosion*, in V. Malhotra (ed.) Proceedings, Third International Conference on Durability of Concrete, Nice, Special Publication SP-145, American Concrete Institute, pp. 283-98.

[42] Palumbo, N. (1991), *Accelerated Corrosion Testing of Steel Reinforcement in Concrete*, M. Engineering Thesis, Department of Civil Engineering and Applied Mechanics and Applied Mechanics, McGill University, Montreal, Canada.

[43] Pourbaix, M. (1966), *Atlas of Electrochemical Equilibrium in Aqueous Solutions*, Pergamon Press, New York.

[44] Raupach, M. (1996), *Chloride-Induced Macrocell Corrosion of Steel in Concrete - Theoretical Background and Practical Consequences*, Construction and Building Materials, V.10, No.5, pp. 329-338.

[45] Richardson, M.G. (2002), *Fundamentals of Durable Reinforced Concrete*, Spon Press, London and New York.

[46] Sandberg, P. (1998), *Chloride Initiated Reinforcement Corrosion in Marine Concrete*, Report TVBM-1015, Division of Building Materials, Lund Institute of Technology, Lund.

[47] Scully, J.C. (1990), *The Fundamentals of Corrosion*, 3rd Edition, Pergamon Press, New York.

[48] Tuutti, K. (1982), *Corrosion of Steel in Concrete*, No.4.82, CBI Research, Stockholm.

[49] Vector Corrosion Technology (2003), *Technical Report on the Concrete Restoration and Protection System*, Winnipeg, Canada.

Appendix A

Monthly Average Half Cell Potential Readings vs. Time Plots for Different Slabs

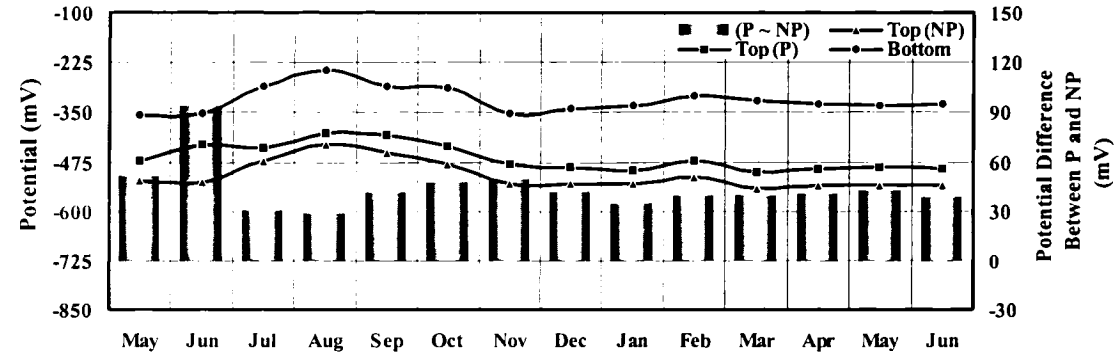

S01

Figure A.1: Monthly Average Half-Cell Potentials of Slab S01

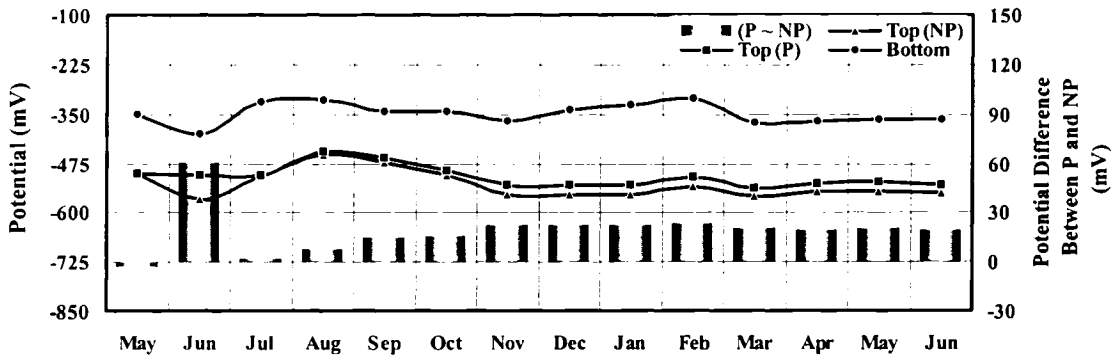

S02

Figure A.2: Monthly Average Half-Cell Potentials of Slab S02

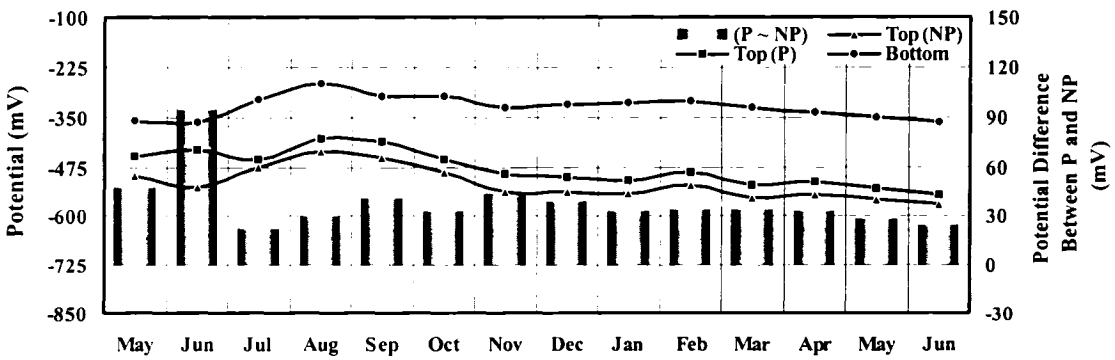

S03

Figure A.3: Monthly Average Half-Cell Potentials of Slab S03

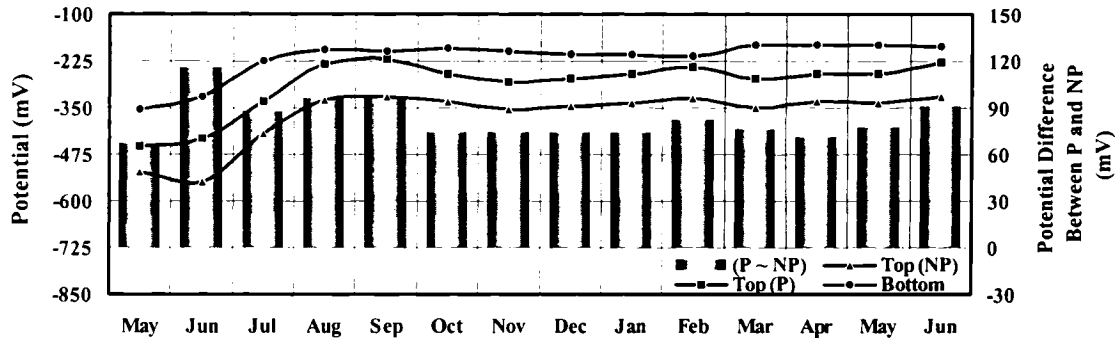

S04

Figure A.4: Monthly Average Half-Cell Potentials of Slab S04

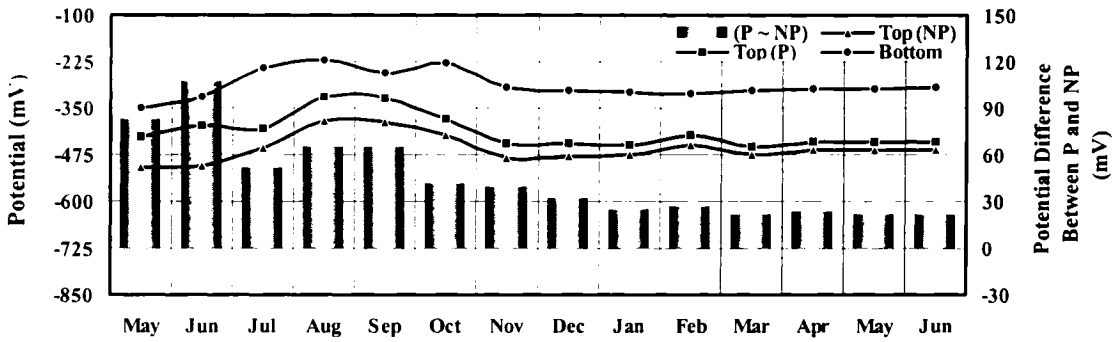

S05

Figure A.5: Monthly Average Half-Cell Potentials of Slab S05

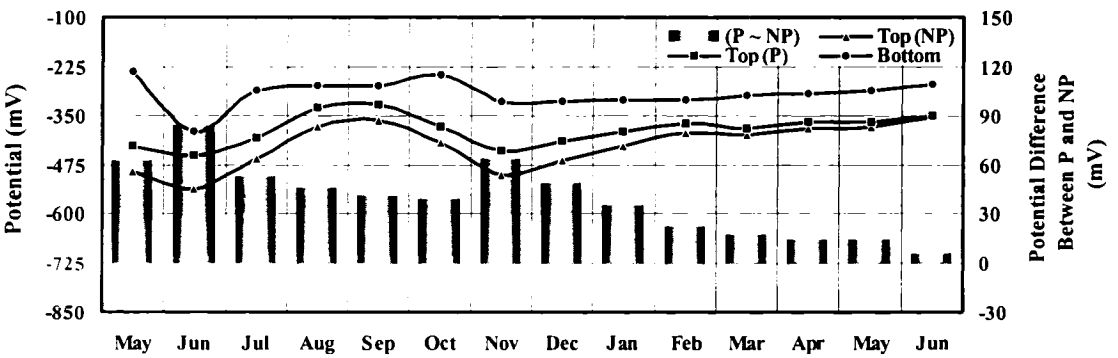

S06

Figure A.6: Monthly Average Half-Cell Potentials of Slab S06

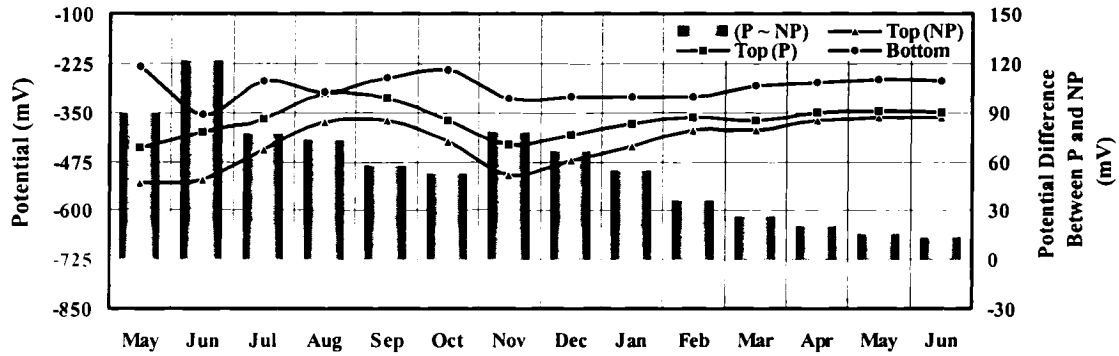

S07

Figure A.7: Monthly Average Half-Cell Potentials of Slab S07

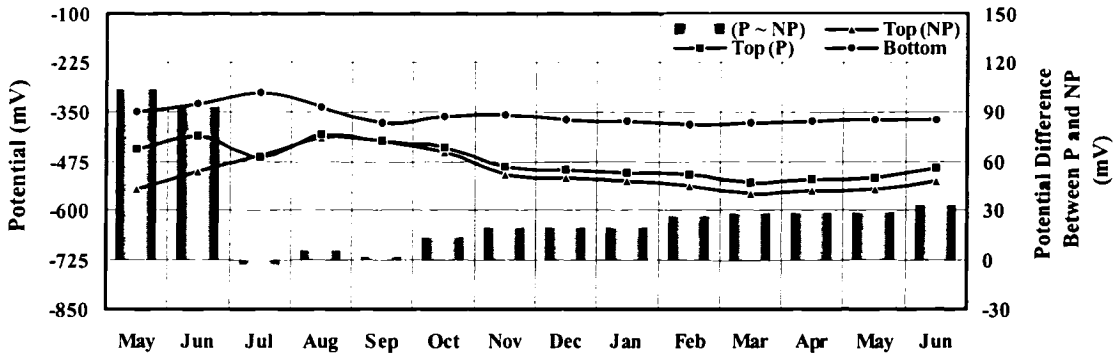

S08

Figure A.8: Monthly Average Half-Cell Potentials of Slab S08

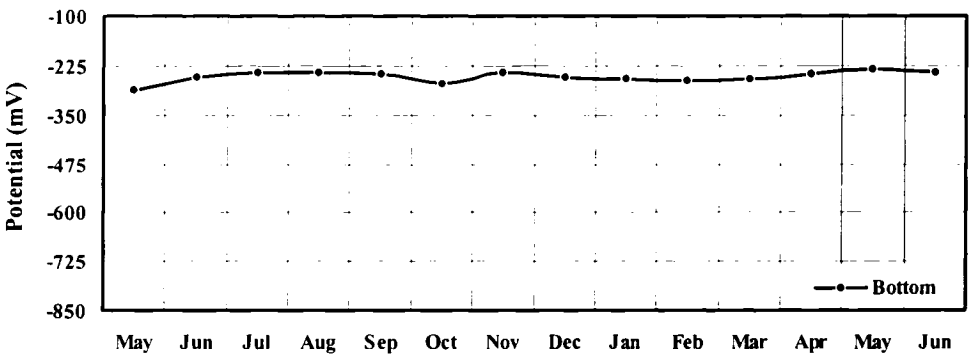

S09

Figure A.9: Monthly Average Half-Cell Potentials of Slab S09

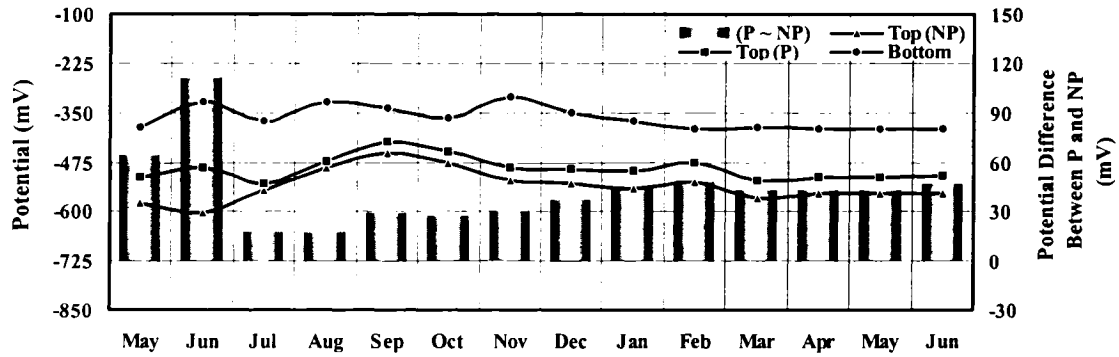

S10

Figure A.10: Monthly Average Half-Cell Potentials of Slab S10

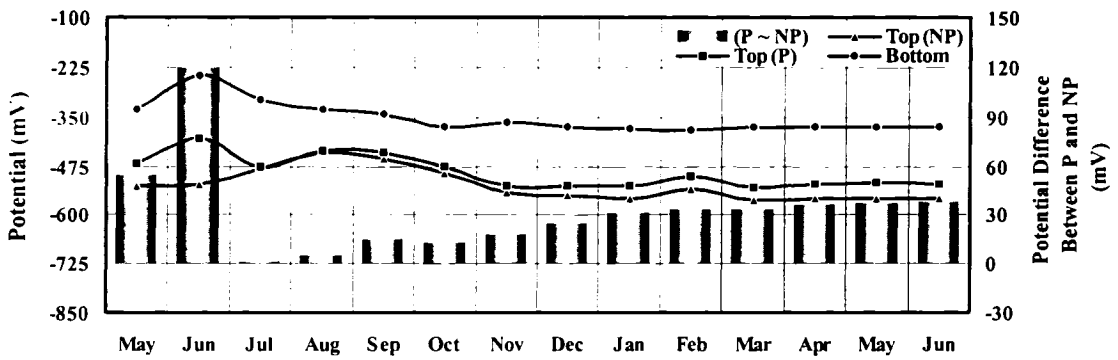

S11

Figure A.11: Monthly Average Half-Cell Potentials of Slab S11

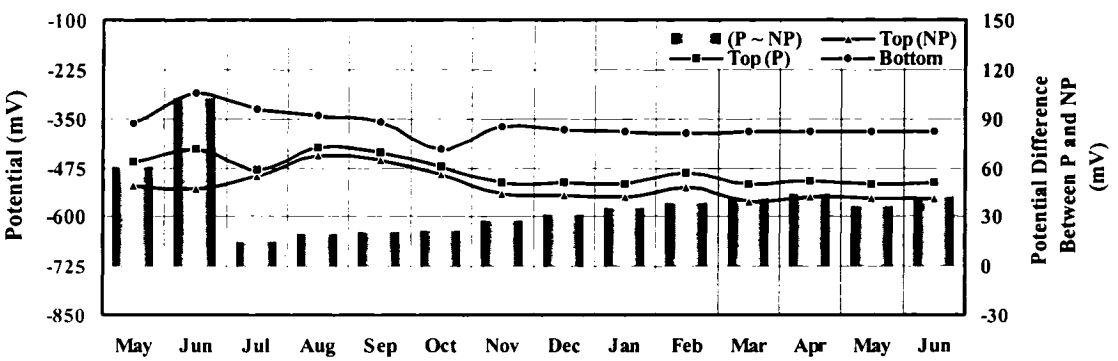

S12

Figure A.12: Monthly Average Half-Cell Potentials of Slab S12

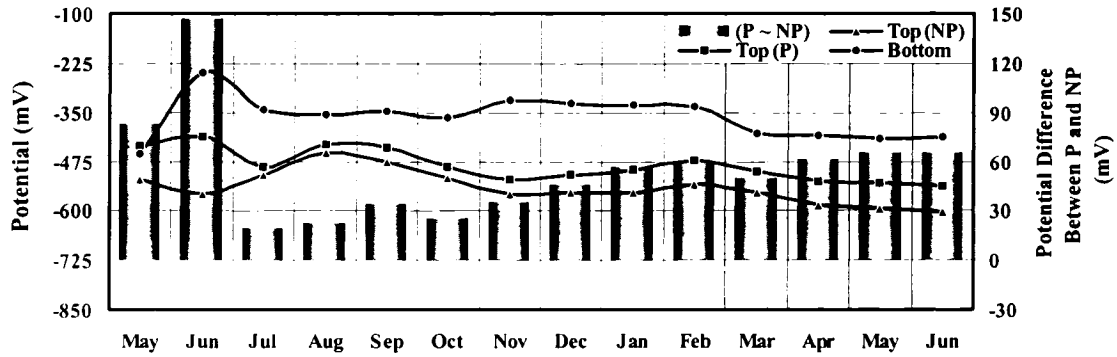

S13

Figure A.13: Monthly Average Half-Cell Potentials of Slab S13

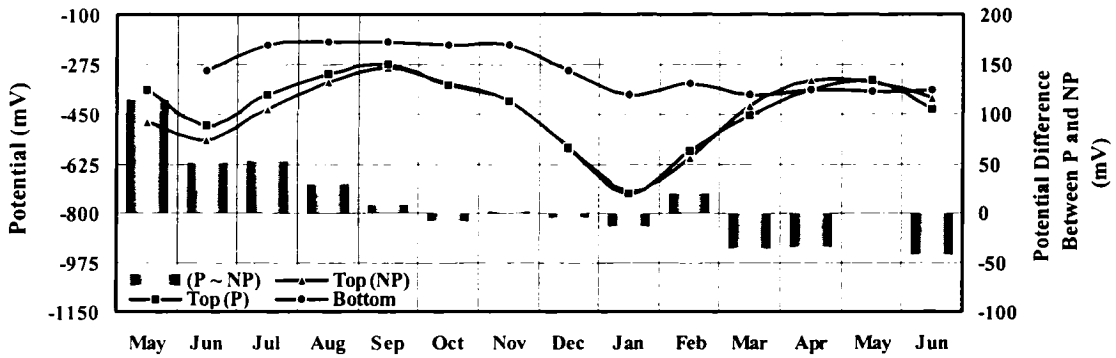

S14-UC

Figure A.14.1: Monthly Average Half-Cell Potentials of Slab S14 (Unconnected)

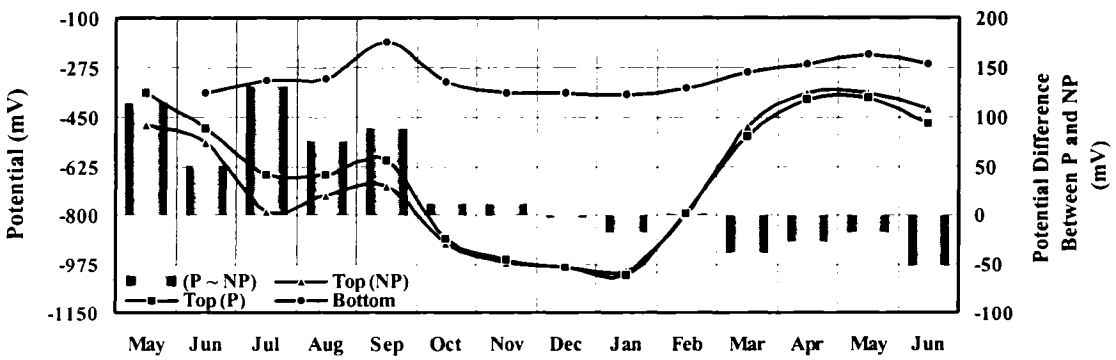

S14-C

Figure A.14.2: Monthly Average Half-Cell Potentials of Slab S14 (Connected)

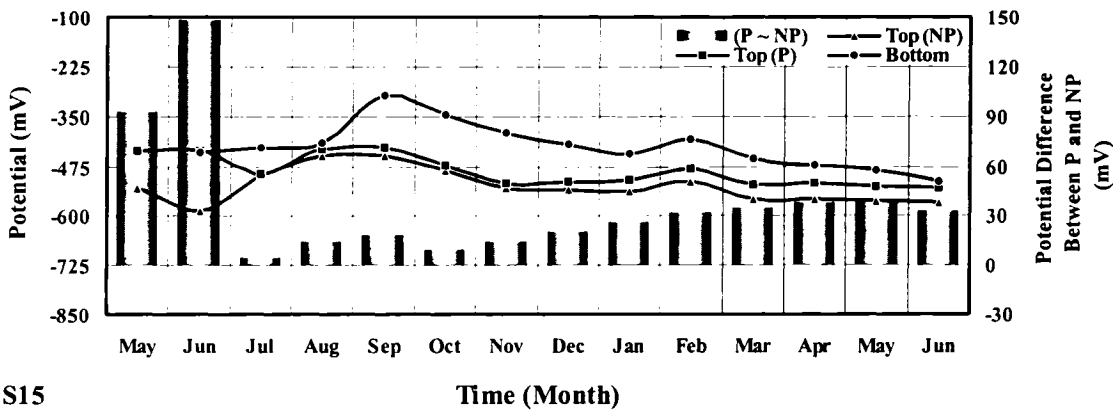

Figure A.15: Monthly Average Half-Cell Potentials of Slab S15

Appendix B

Visual Records of Corrosion of All Bottom Bars for Different Slabs

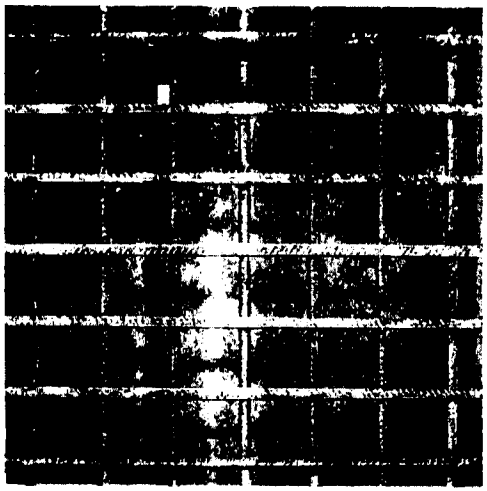

Fig. B.1: Slab S01 (Bottom Mesh Upper Face)

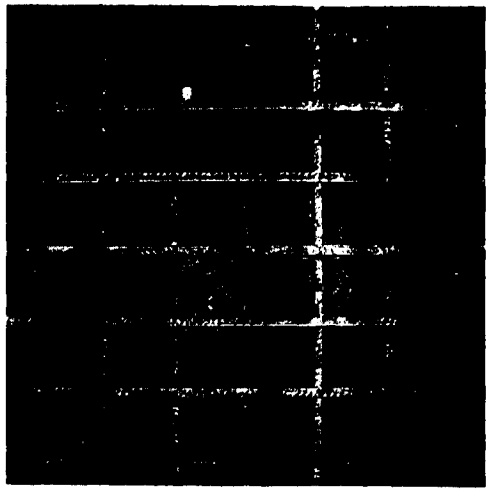

Fig. B.2: Slab S01 (Bottom Mesh Lower Face)

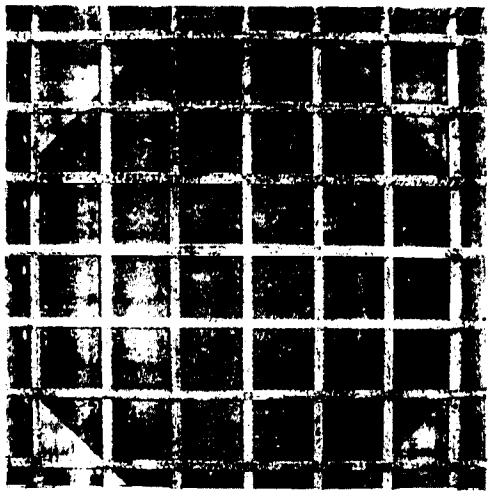

Fig. B.3: Slab S02 (Bottom Mesh Upper Face)

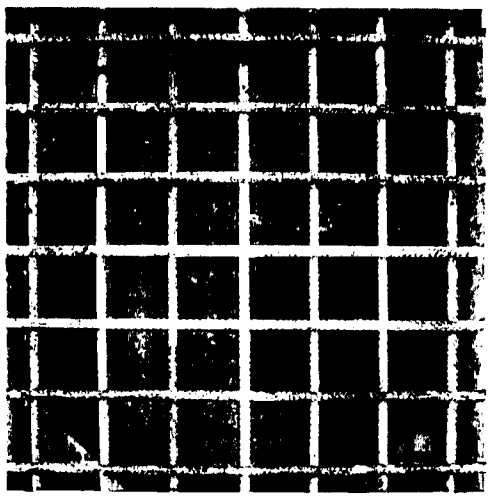

Fig. B.4: Slab S02 (Bottom Mesh Lower Face)

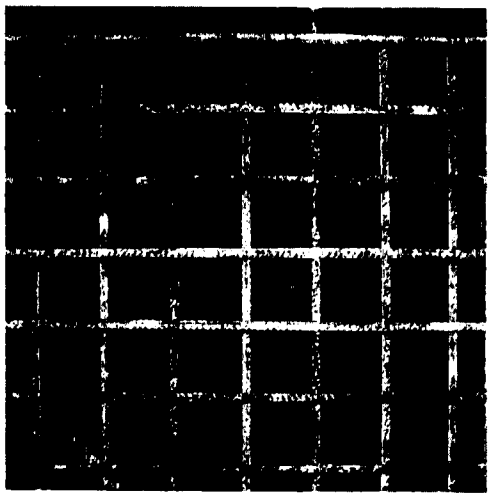

Fig. B.5: Slab S03 (Bottom Mesh Upper Face)

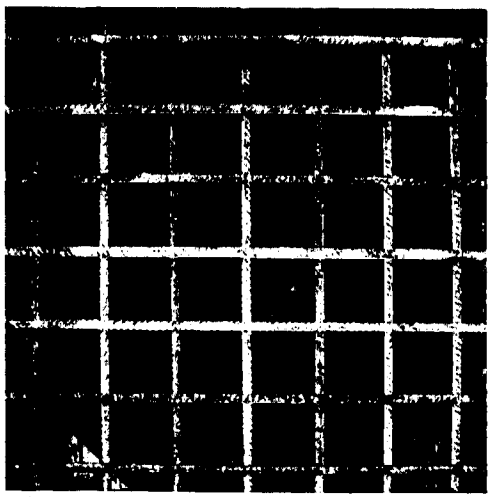

Fig. B.6: Slab S03 (Bottom Mesh Lower Face)

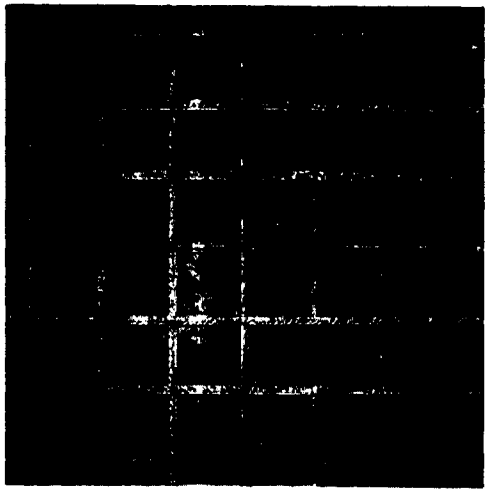

Fig. B.7: Slab S04 (Bottom Mesh Upper Face)

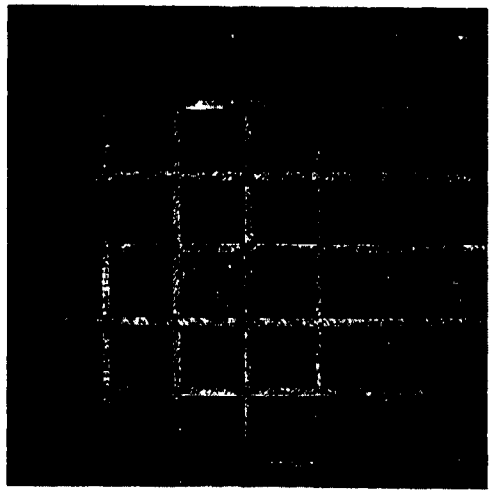

Fig. B.8: Slab S04 (Bottom Mesh Lower Face)

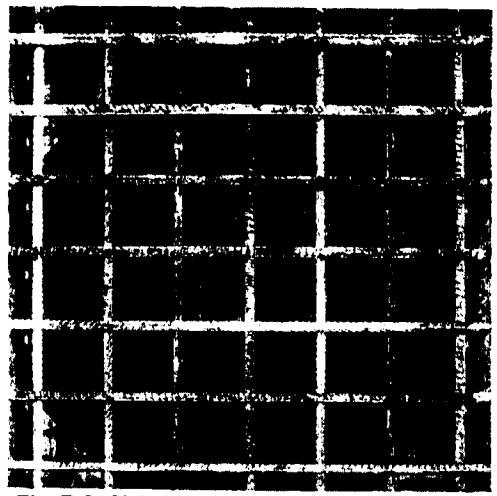

Fig. B.9: Slab S05 (Bottom Mesh Upper Face)

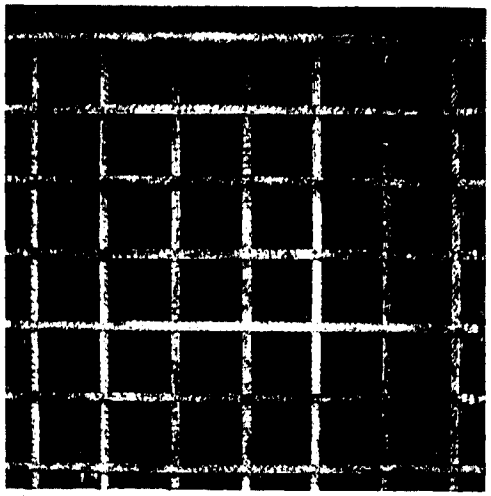

Fig. B.10: Slab S05 (Bottom Mesh Lower Face)

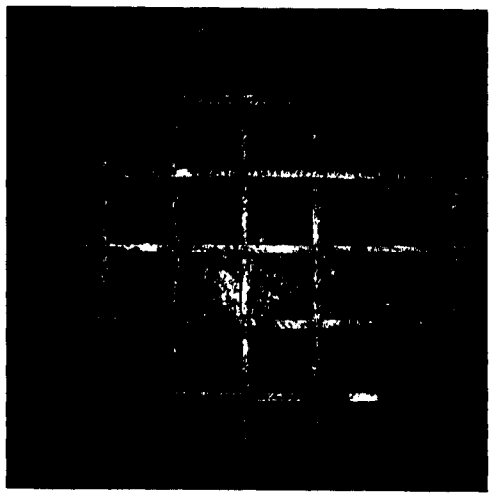

Fig. B.11: Slab S06 (Bottom Mesh Upper Face)

Fig. B.12: Slab S06 (Bottom Mesh Lower Face)

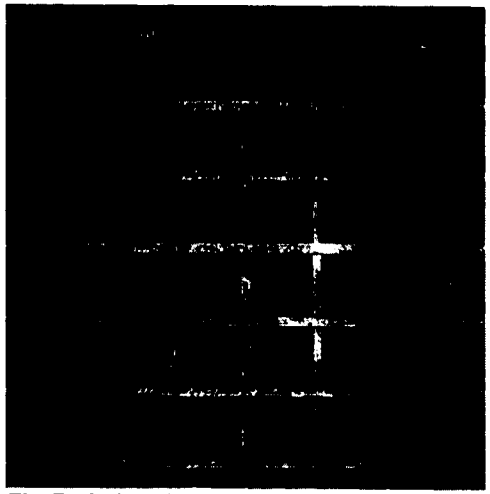

Fig. B.13: Slab S07 (Bottom Mesh Upper Face)

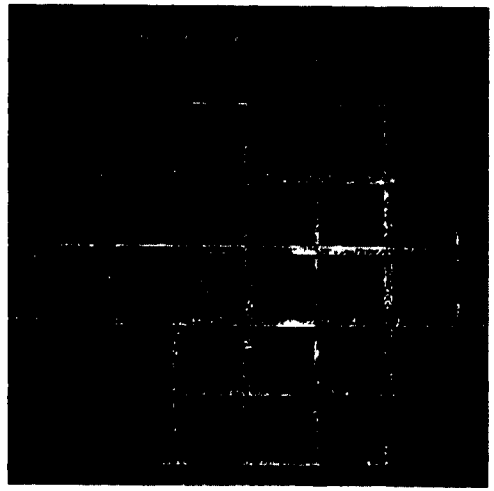

Fig. B.14: Slab S07 (Bottom Mesh Lower Face)

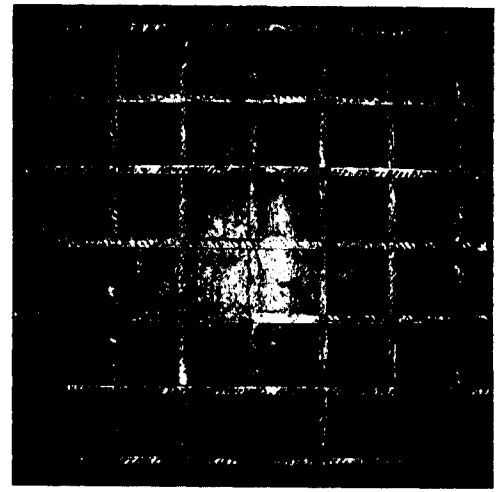

Fig. B.15: Slab S08 (Bottom Mesh Upper Face)

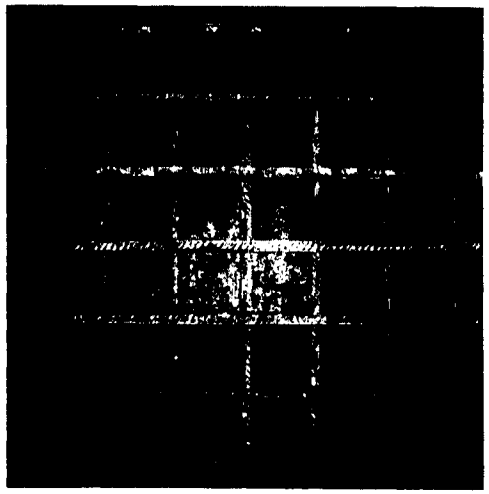

Fig. B.16: Slab S08 (Bottom Mesh Lower Face)

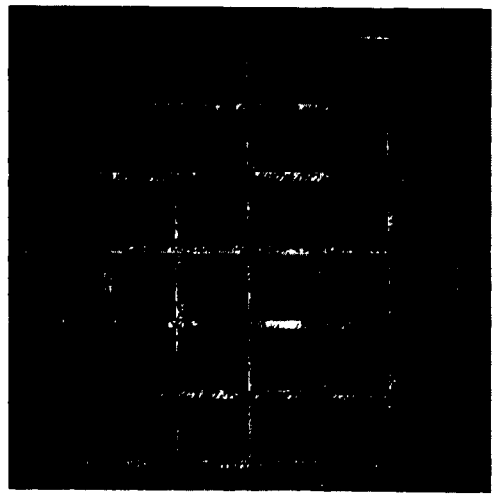

Fig. B.17: Slab S09 (Bottom Mesh Upper Face)

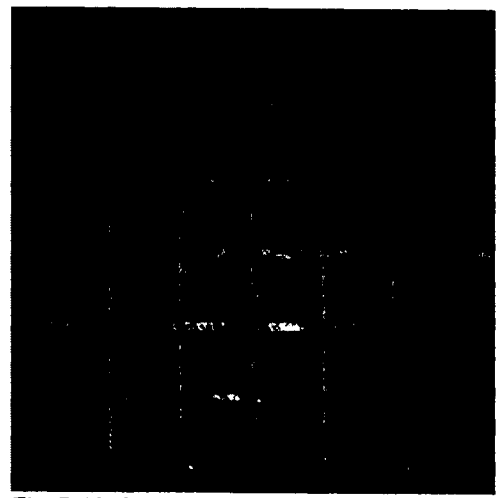

Fig. B.18: Slab S09 (Bottom Mesh Lower Face)

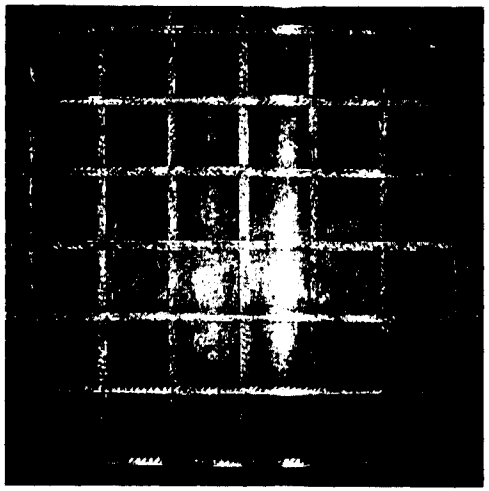

Fig. B.19: Slab S10 (Bottom Mesh Upper Face)

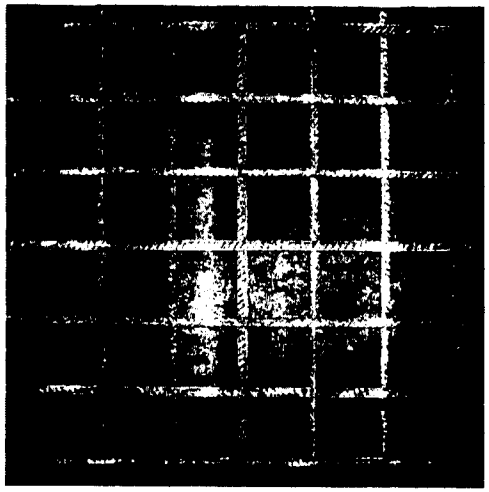

Fig. B.20: Slab S10 (Bottom Mesh Lower Face)

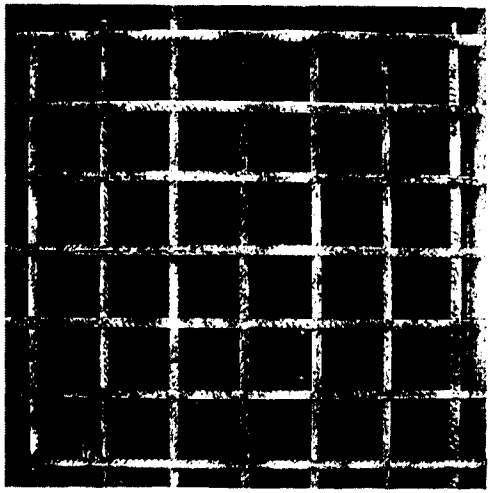

Fig. B.21: Slab S11 (Bottom Mesh Upper Face)

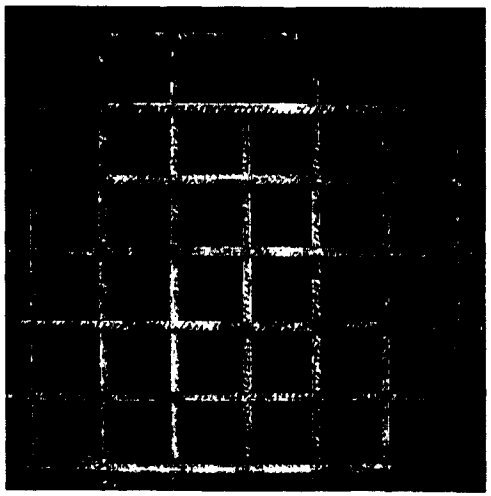

Fig. B.22: Slab S11 (Bottom Mesh Lower Face)

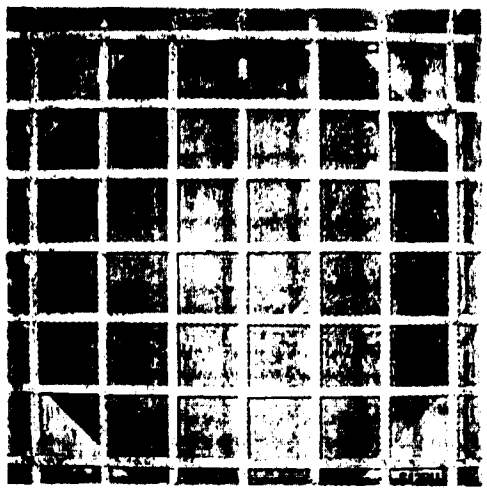

Fig. B.23: Slab S12 (Bottom Mesh Upper Face)

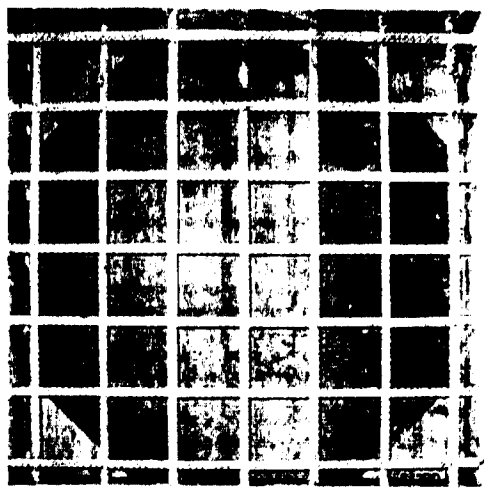

Fig. B.24: Slab S12 (Bottom Mesh Lower Face)

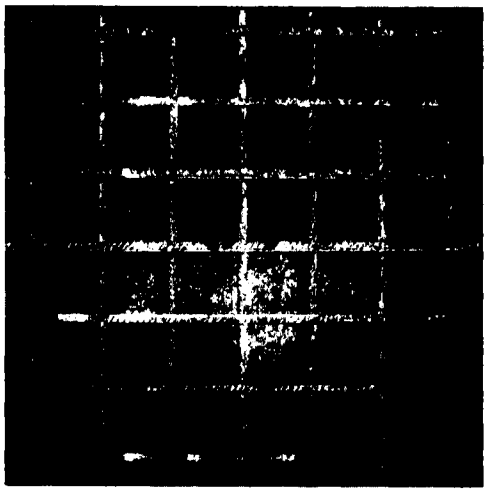

Fig. B.25: Slab S13 (Bottom Mesh Upper Face)

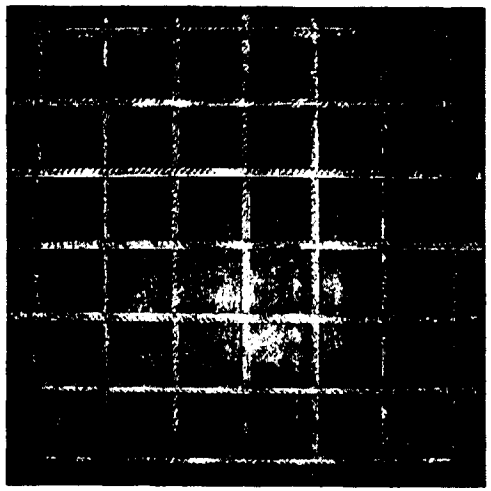

Fig. B.26: Slab S13 (Bottom Mesh Lower Face)

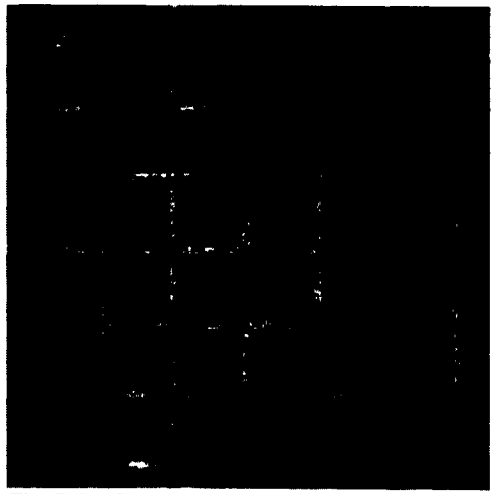

Fig. B.27: Slab S14 (Bottom Mesh Upper Face)

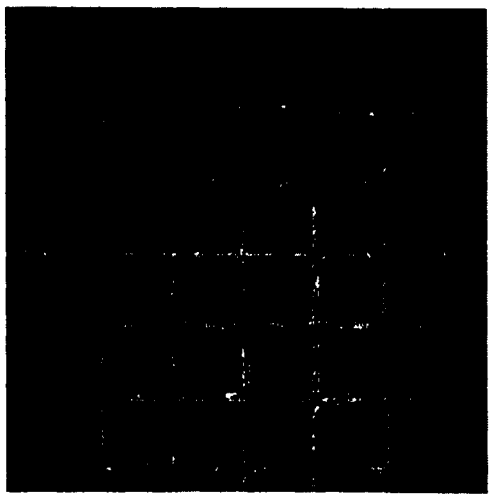

Fig. B.28: Slab S14 (Bottom Mesh Lower Face)

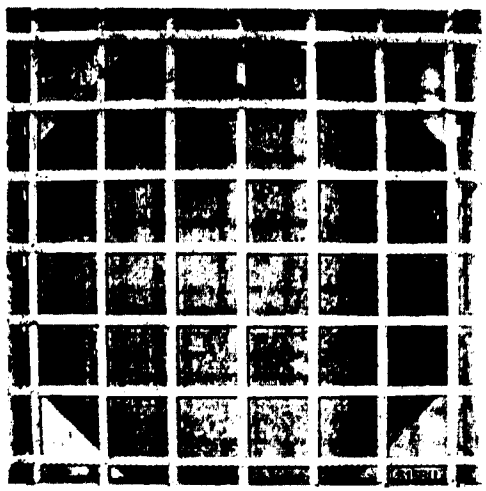

Fig. B.29: Slab S15 (Bottom Mesh Upper Face)

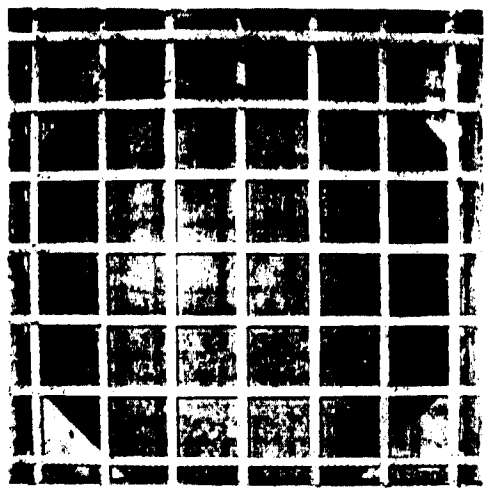

Fig. B.30: Slab S15 (Bottom Mesh Lower Face)

Appendix C

Visual Records of Corrosion of All Top Bars for Different Slabs

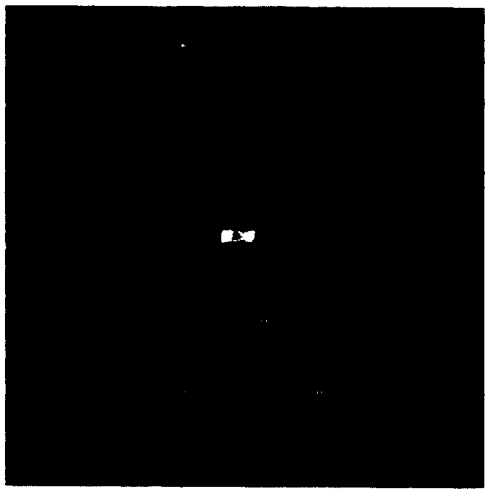

Fig. C.1: Slab S01 (Top Mesh Upper Face)

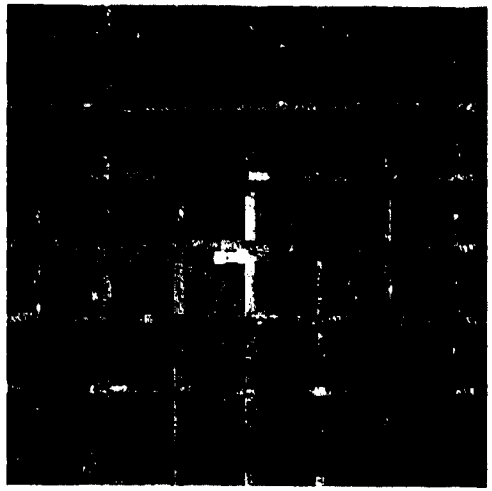

Fig. C.2: Slab S01 (Top Mesh Lower Face)

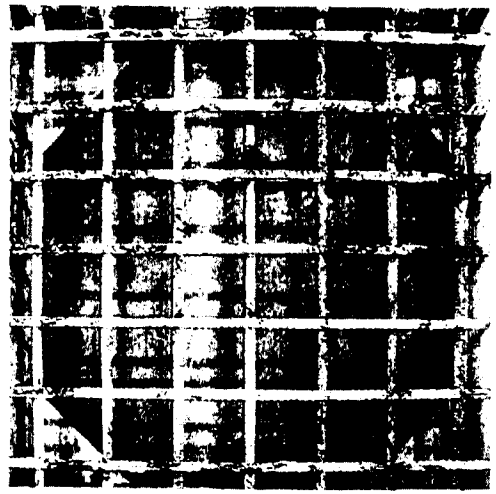

Fig. C.3: Slab S02 (Top Mesh Upper Face)

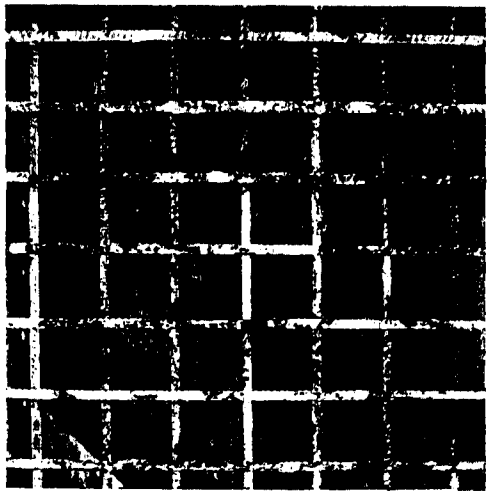

Fig. C.4: Slab S02 (Top Mesh Lower Face)

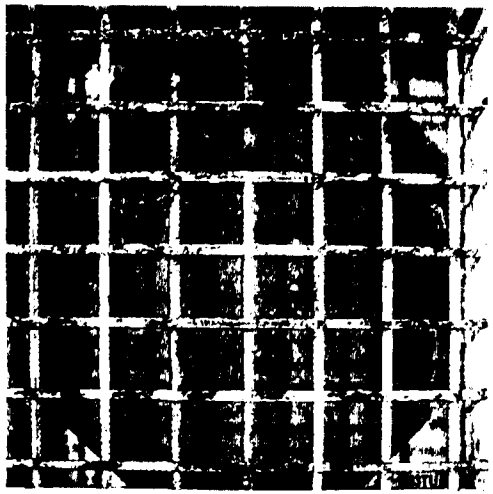

Fig. C.5: Slab S03 (Top Mesh Upper Face)

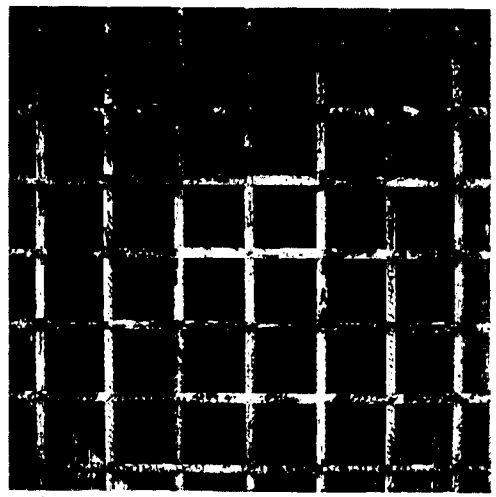

Fig. C.6: Slab S03 (Top Mesh Lower Face)

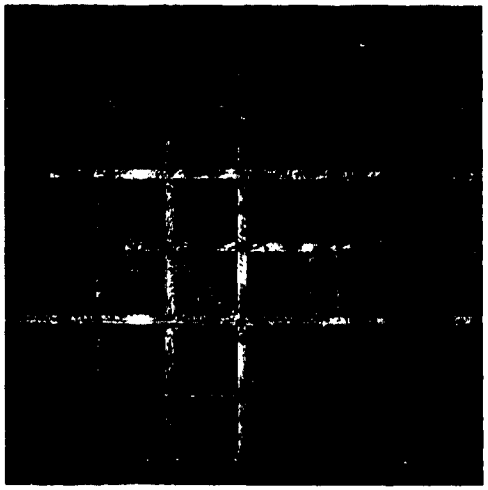

Fig. C.7: Slab S04 (Top Mesh Upper Face)

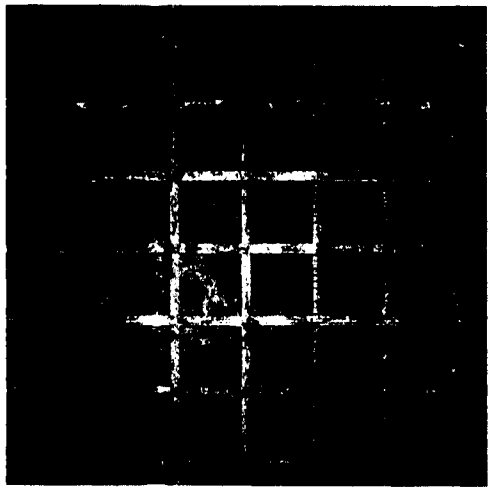

Fig. C.8: Slab S04 (Top Mesh Lower Face)

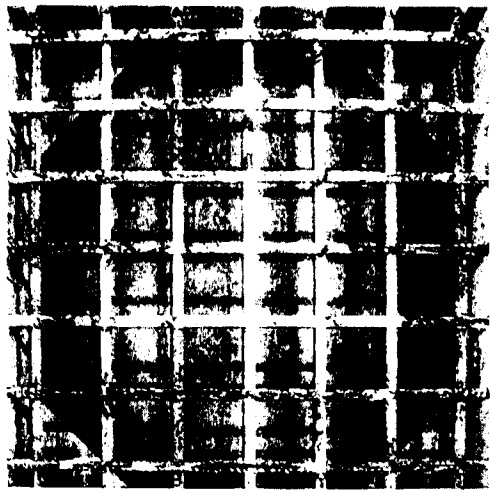

Fig. C.9: Slab S05 (Top Mesh Upper Face)

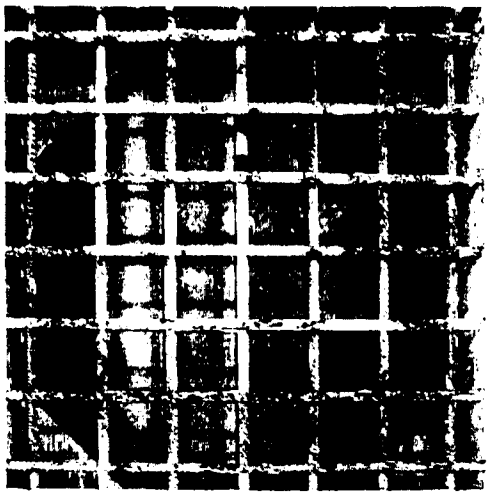

Fig. C.10: Slab S05 (Top Mesh Lower Face)

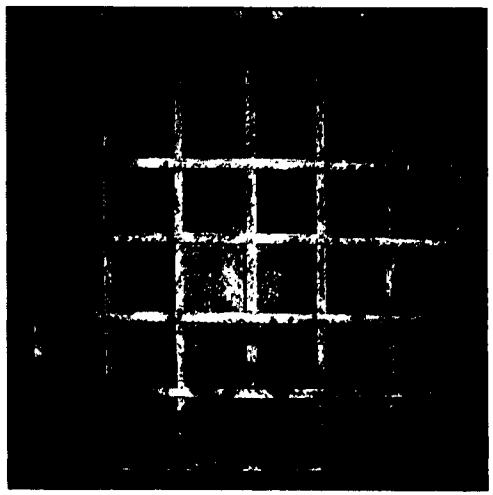

Fig. C.11: Slab S06 (Top Mesh Upper Face)

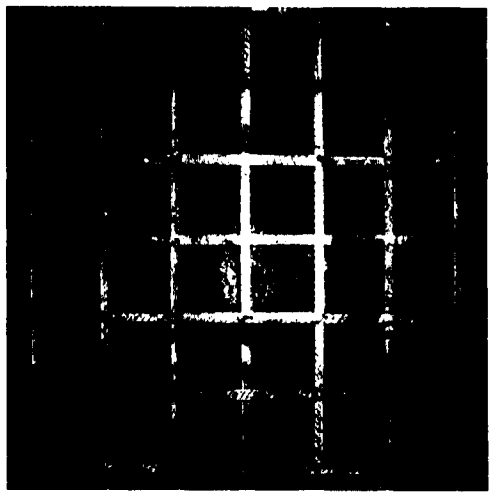

Fig. C.12: Slab S06 (Top Mesh Lower Face)

Fig. C.13: Slab S07 (Top Mesh Upper Face)

Fig. C.14: Slab S07 (Top Mesh Lower Face)

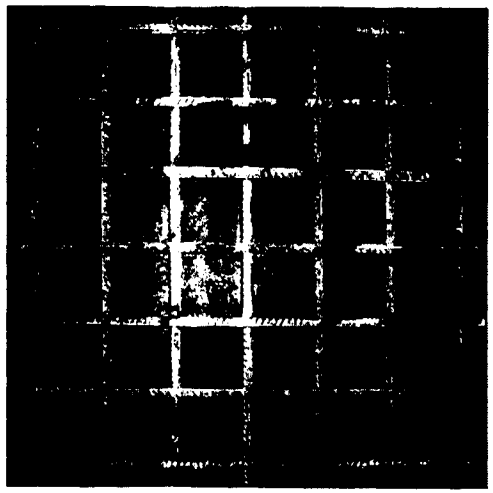

Fig. C.15: Slab S08 (Top Mesh Upper Face)

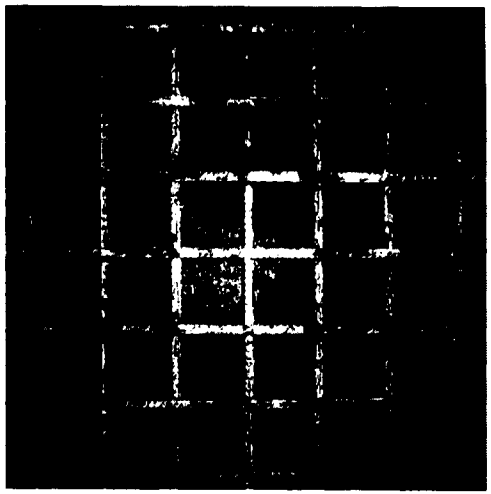

Fig. C.16: Slab S08 (Top Mesh Lower Face)

Fig. C.17: Slab S09 (Top Mesh Upper Face)

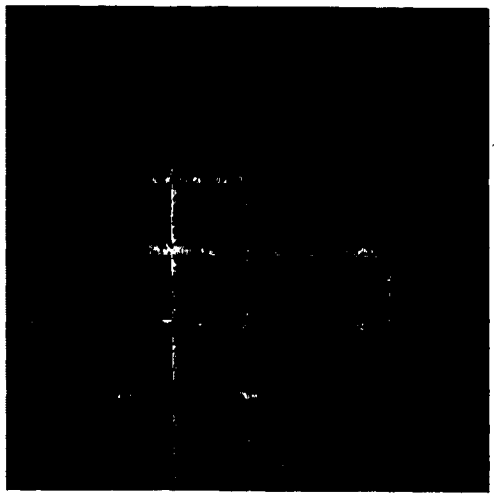

Fig. C.18: Slab S09 (Top Mesh Lower Face)

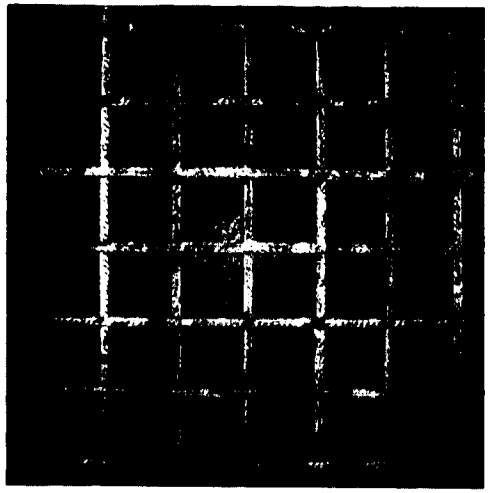

Fig. C.19: Slab S10 (Top Mesh Upper Face)

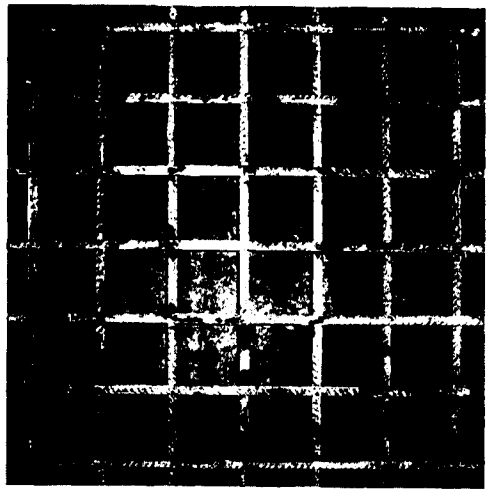

Fig. C.20: Slab S10 (Top Mesh Lower Face)

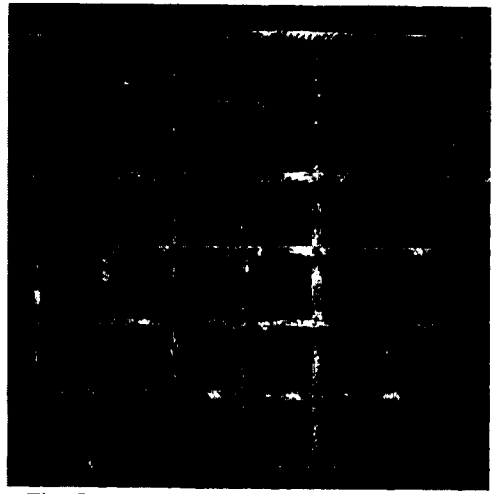

Fig. C.21: Slab S11 (Top Mesh Upper Face)

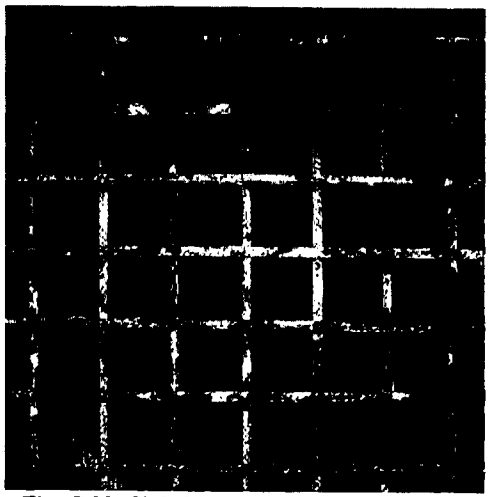

Fig. C.22: Slab S11 (Top Mesh Lower Face)

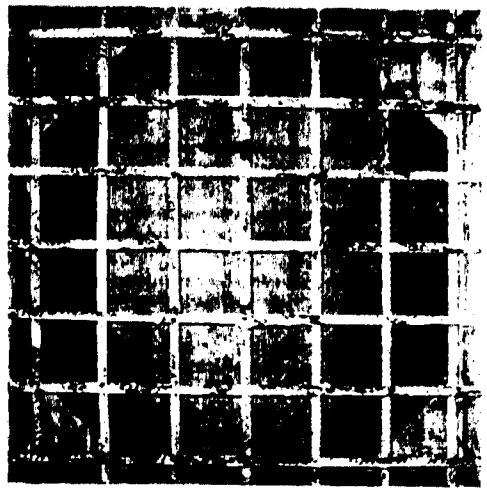

Fig. C.23: Slab S12 (Top Mesh Upper Face)

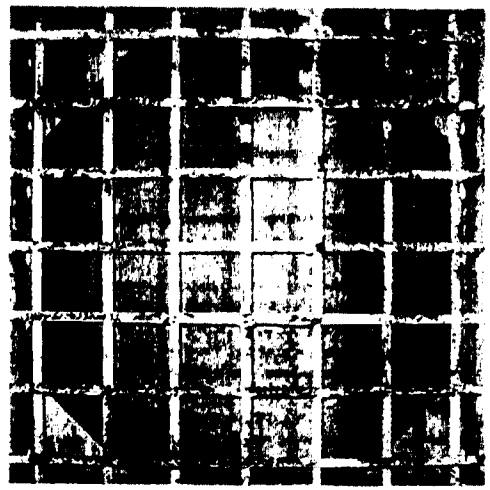

Fig. C.24: Slab S12 (Top Mesh Lower Face)

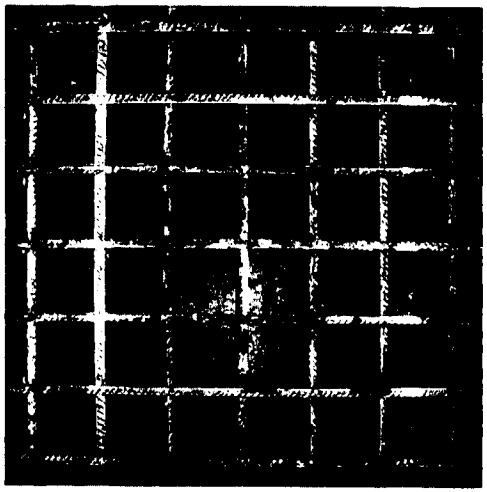

Fig. C.25: Slab S13 (Top Mesh Upper Face)

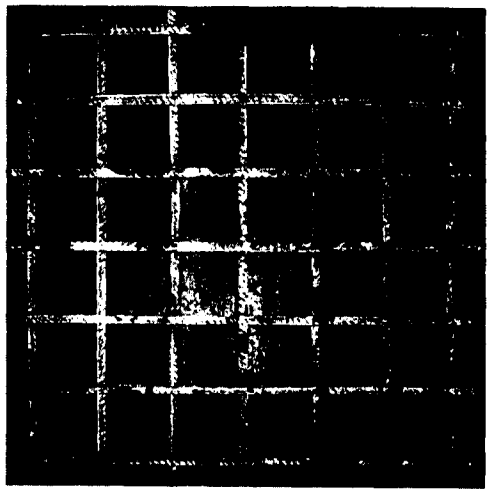

Fig. C.26: Slab S13 (Top Mesh Lower Face)

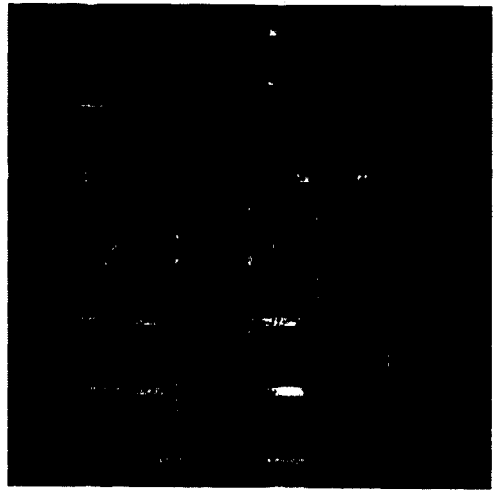

Fig. C.27: Slab S14 (Top Mesh Upper Face)

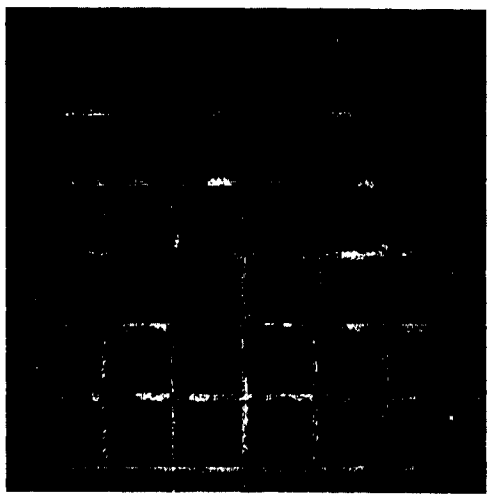

Fig. C.28: Slab S14 (Top Mesh Lower Face)

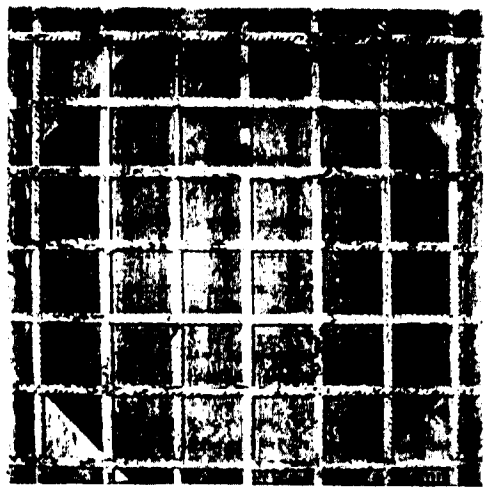

Fig. C.29: Slab S15 (Top Mesh Upper Face)

Fig. C.30: Slab S15 (Top Mesh Lower Face)

Appendix D

Mass-Loss Charts of Top Mesh Bars for Different Slabs

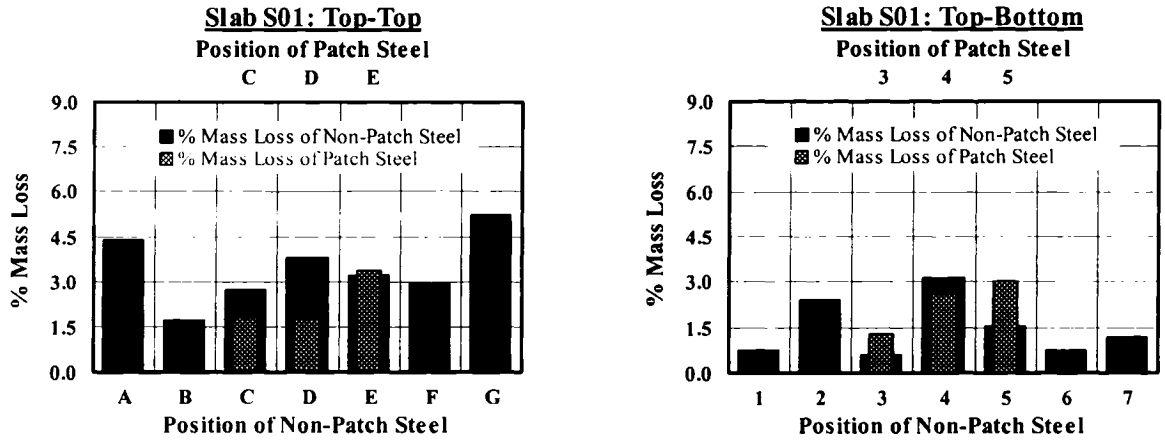

Figure D.1: Percent Mass-Loss of Top Mesh Bars of Slab S01

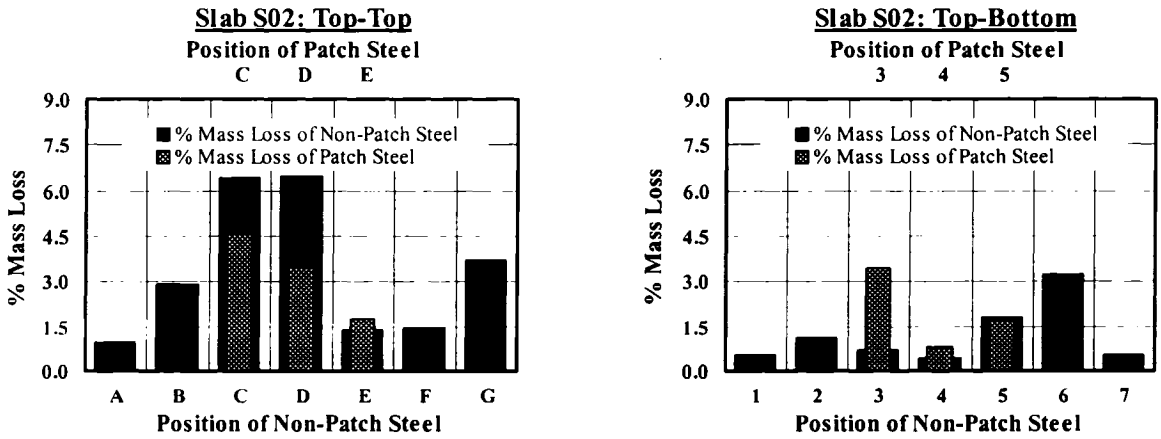

Figure D.2: Percent Mass-Loss of Top Mesh Bars of Slab S02

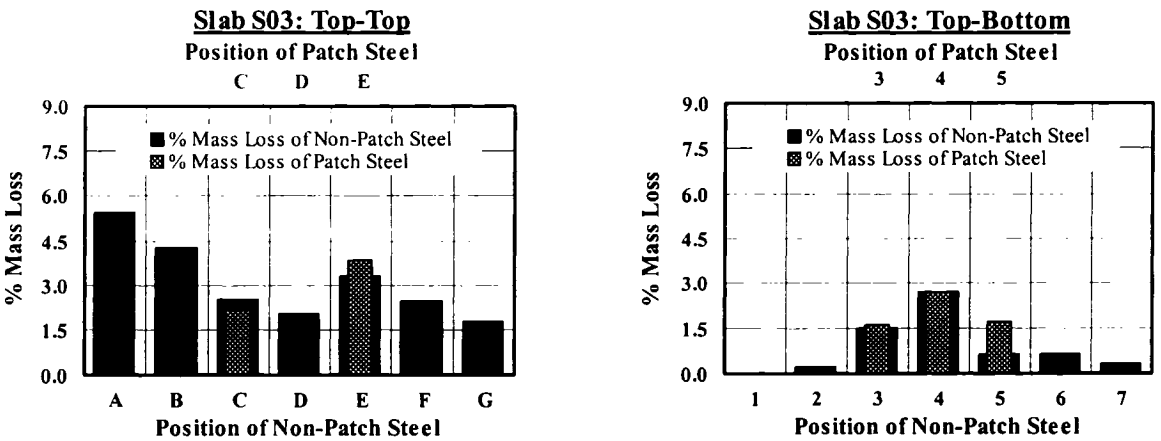

Figure D.3: Percent Mass-Loss of Top Mesh Bars of Slab S03

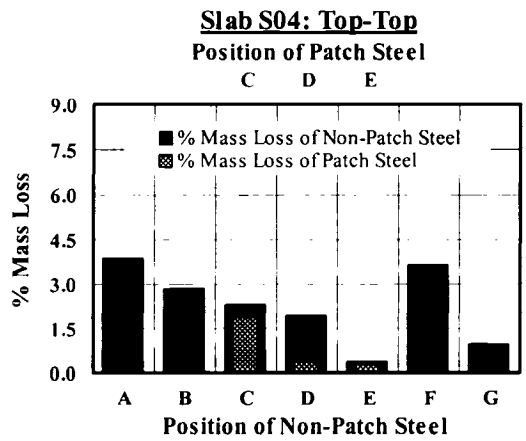

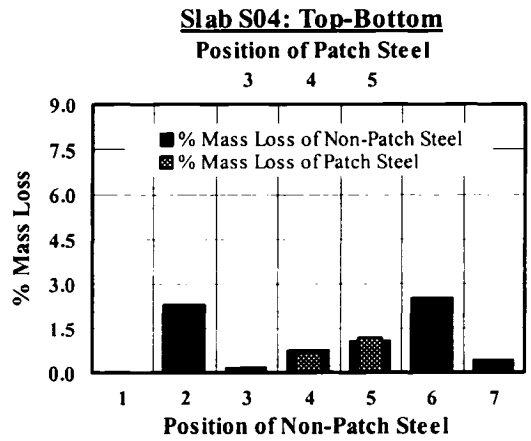

Figure D.4: Percent Mass-Loss of Top Mesh Bars of Slab S04

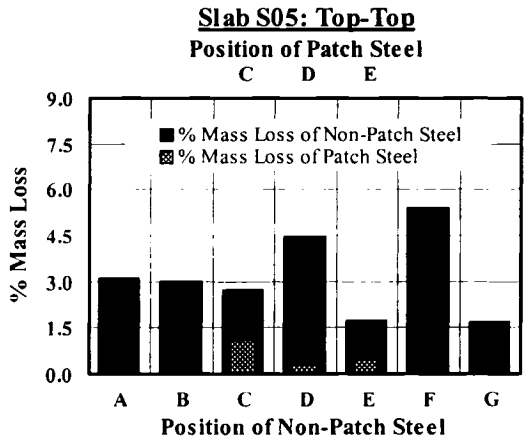

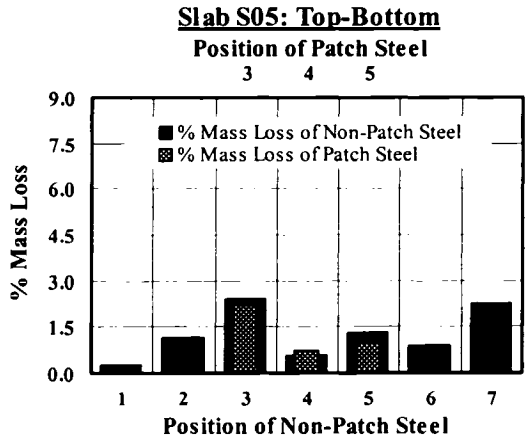

Figure D.5: Percent Mass-Loss of Top Mesh Bars of Slab S05

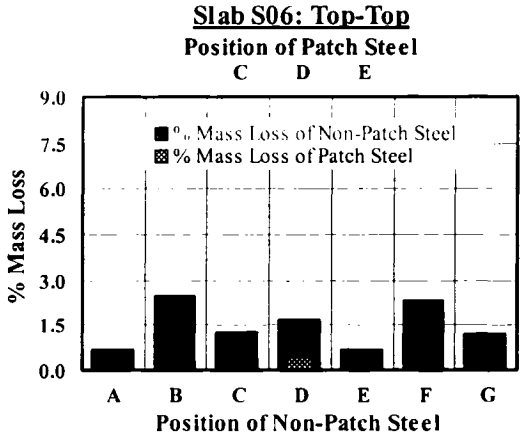

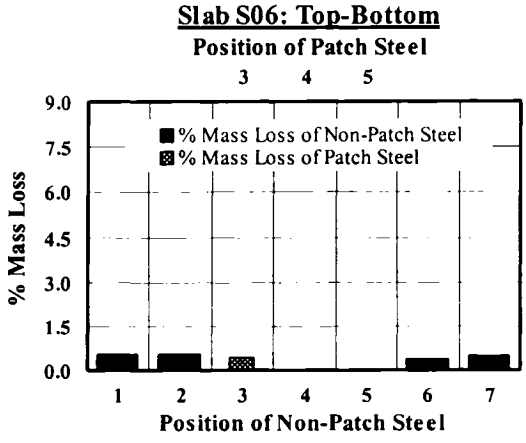

Figure D.6: Percent Mass-Loss of Top Mesh Bars of Slab S06

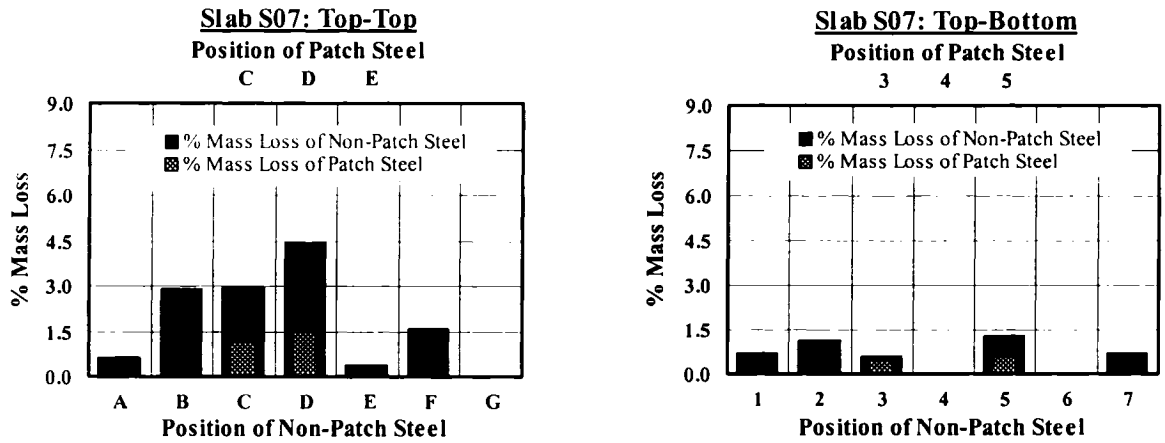

Figure D.7: Percent Mass-Loss of Top Mesh Bars of Slab S07

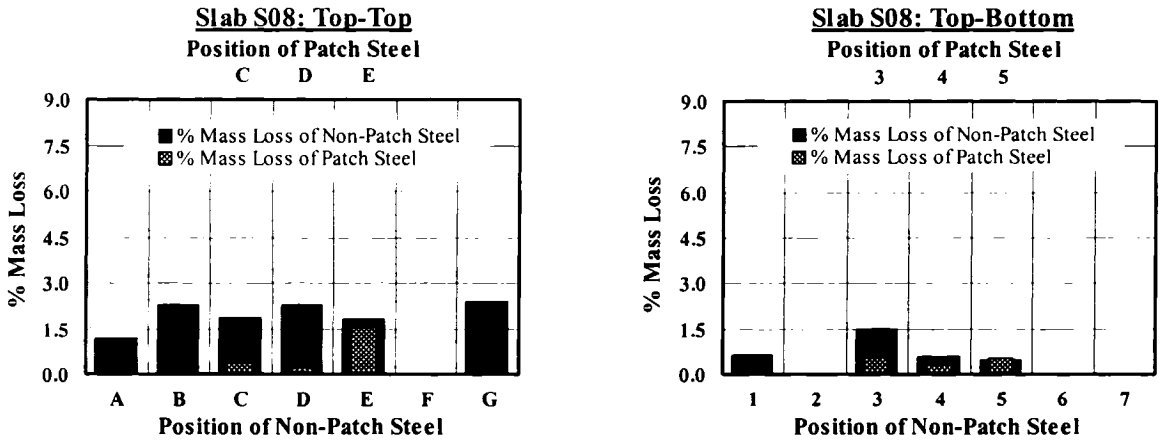

Figure D.8: Percent Mass-Loss of Top Mesh Bars of Slab S08

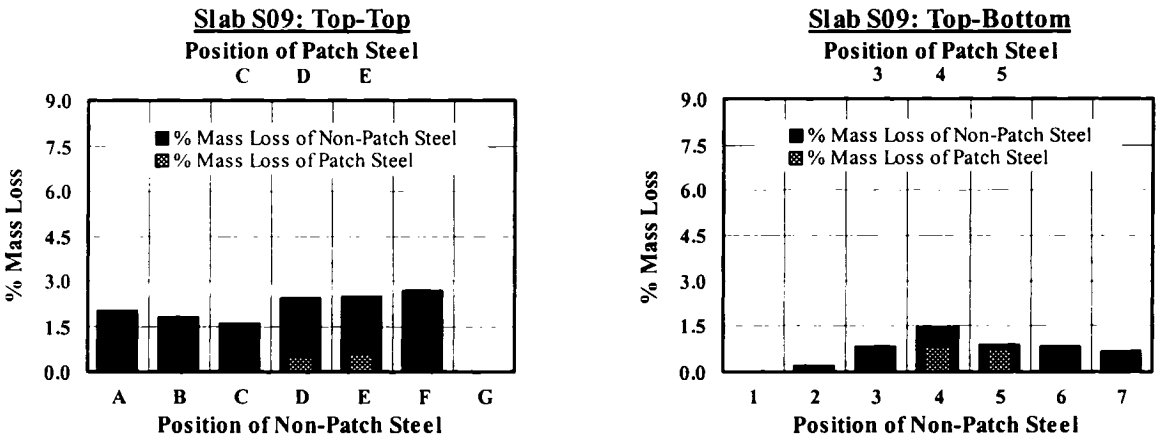

Figure D.9: Percent Mass-Loss of Top Mesh Bars of Slab S09

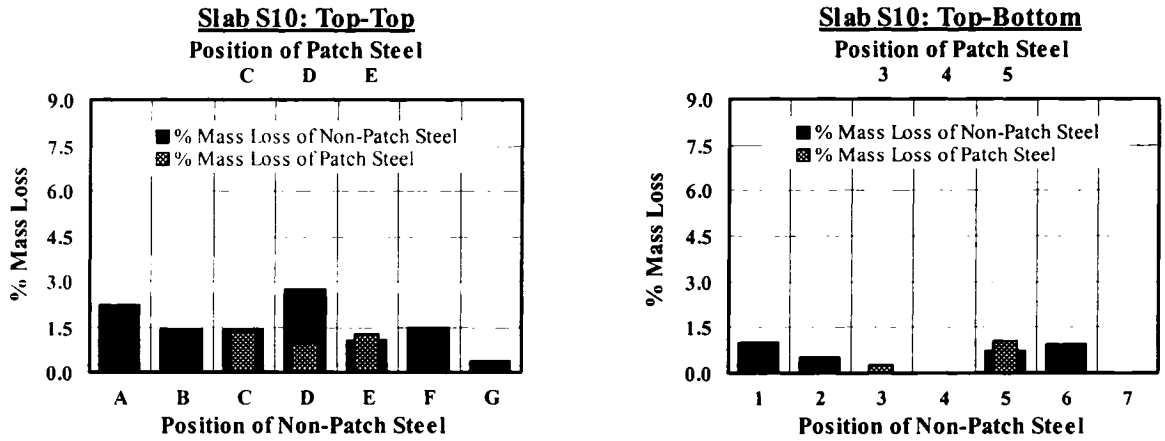

Figure D.10: Percent Mass-Loss of Top Mesh Bars of Slab S10

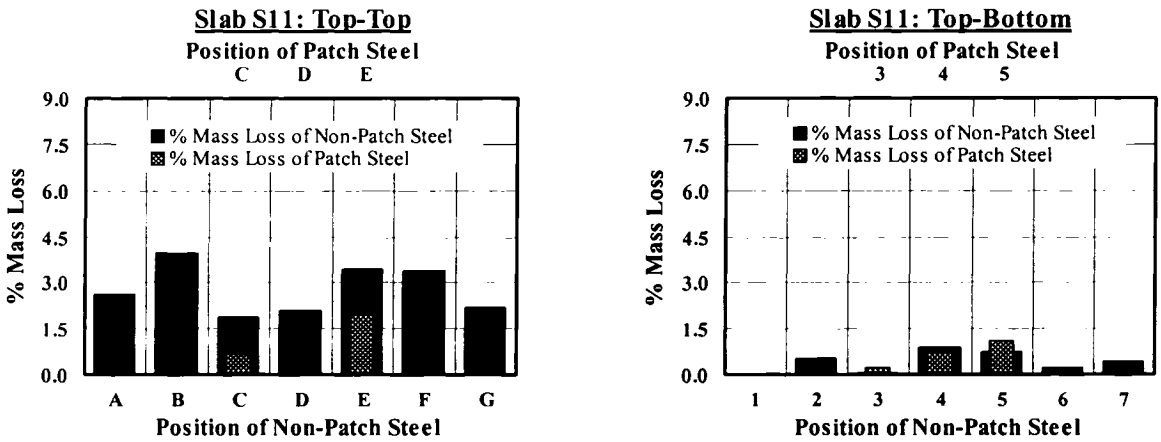

Figure D.11: Percent Mass-Loss of Top Mesh Bars of Slab S11

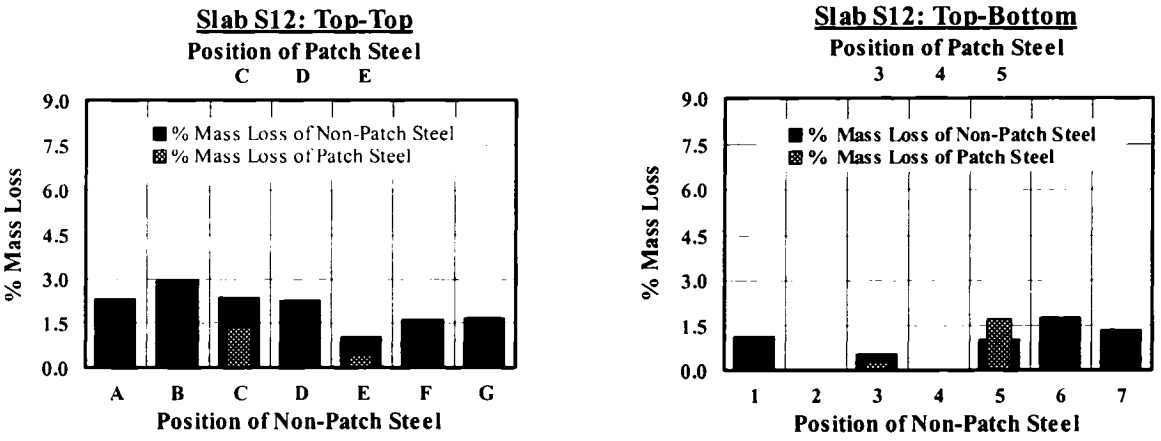

Figure D.12: Percent Mass-Loss of Top Mesh Bars of Slab S12

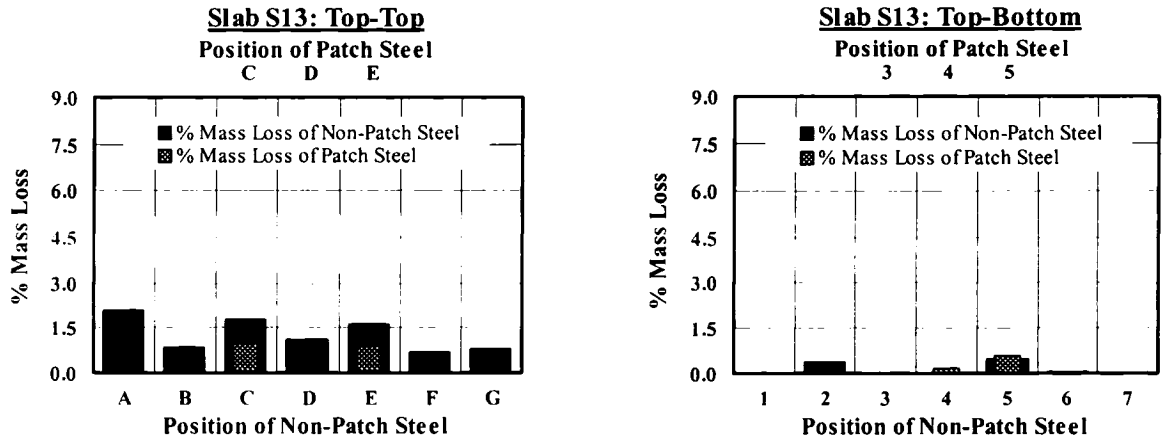

Figure D.13: Percent Mass-Loss of Top Mesh Bars of Slab S13

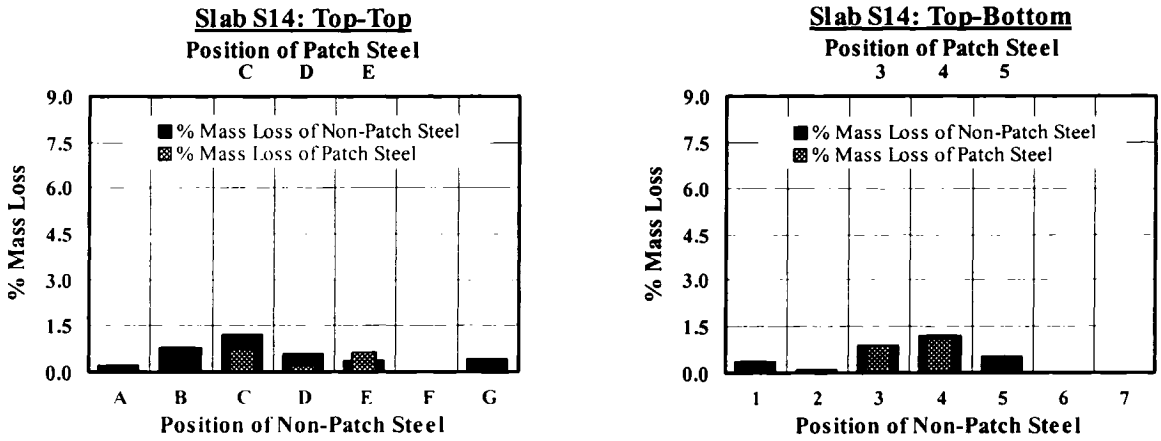

Figure D.14: Percent Mass-Loss of Top Mesh Bars of Slab S14

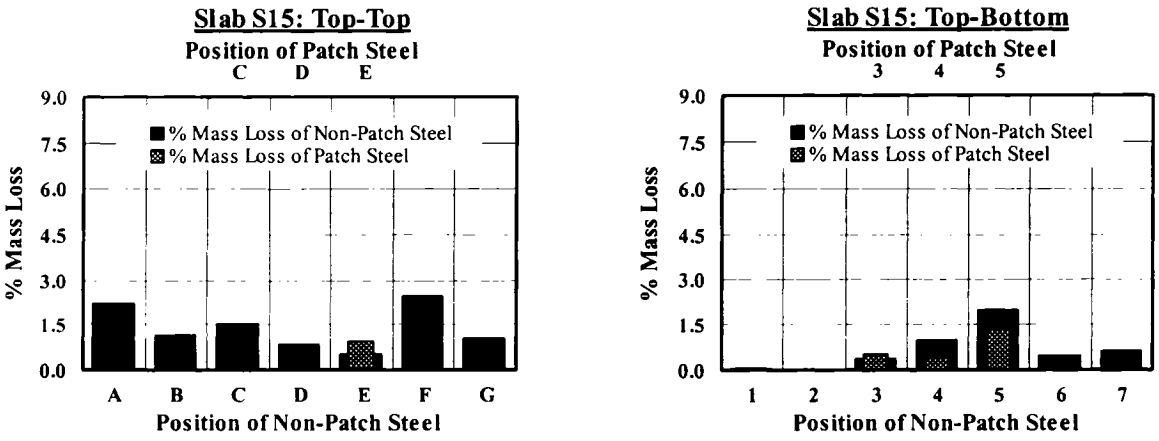

Figure D.15: Percent Mass-Loss of Top Mesh Bars of Slab S15